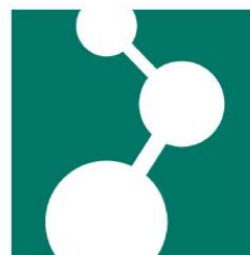


Near-infrared-sensitive materials based on photoresponsive ruthenium(II) polypyridyl complexes-functionalized lanthanide-doped upconverting nanoparticles

Dissertation
Zur Erlangung des Grades
Doktor der Naturwissenschaften
am Fachbereich Chemie, Pharmazie und Geowissenschaften
der Johannes Gutenberg-Universität Mainz



von
Zhijun CHEN
geboren in Anhui, China
Mainz, April 2017

Table of Contents

Abstract:	1
Chapter 1: Introduction and motivation	5
1.1 Ruthenium(II) polypyridyl complexes	5
1.2 Photochemical property of Ru complexes.....	5
1.3 Photosensitive Ru complexes	7
1.4 Bio-medical applications of photoresponsive Ru complexes.....	8
1.4.1 Photorelease of neurochemical molecules	8
1.4.2 Light-activated enzyme inhibition	9
1.4.3 Regulating gene expression	10
1.4.4 Anti-cancer reagent.....	11
1.5 Strategies for red-shifting responsive wavelength of Ru complexes.....	13
1.6 Lanthanide-doped upconverting nanoparticles (UCNPs).....	14
1.7 Mechanism of UCNPs	15
1.7.1 Mechanism of excited-state absorption (ESA)	15
1.7.2 Mechanism of energy transfer upconversion (ETU)	16
1.7.3 Mechanism of cooperative sensitization upconversion (CSU).....	17
1.7.4 Mechanism of cross-relaxation (CR).....	17
1.7.5 Mechanism of photon avalanche (PA).....	18
1.8 Development of NIR-sensitive molecules assisted by UCNPs	18
1.8.1 UCNP-assisted photolytic compounds	19
1.8.2 UCNP-assisted photoswitching compounds	20
1.8.3. UCNP-assisted photoinitiators.....	22
1.9 Bio-medical applications based on UCNP-assisted photosensitive compounds	24
1.9.1 NIR-controlled drug delivery.....	24

1.9.2 NIR-modulated biocatalysis.....	25
1.9.3 NIR-light-curable dental materials	26
1.9.4 NIR-light-controlled biointerfaces.....	27
1.9.5 NIR-light-activated enzyme.....	28
1.10 Challenges and motivation	29
1.10.1 Safe intensity for for bio-medical application	29
1.10.2 Challenge of patterning biomaterials	30
1.10.3 Challenge of pH manipulation	31
1.10.4 Challenge of photoinhibition of enzyme activities	31
1.10.5 Challenge of photocoupling technology for bio-medical application.....	31
Abbreviations	38
Chapter 2: Upconverting-nanoparticle-assisted photochemistry induced by low-intensity near-infrared light: how low can we go?.....	39
2.1 Statement of contribution	39
2.2 Abstract.....	39
2.3 Introduction	40
2.4 Results and Discussion	42
2.5 Conclusions	51
2.6 Experimental Section.....	51
2.7 Acknowledgements	52
2.8 References	53
2.9 Supporting information.....	55
Chapter 3: Photon upconversion lithography: patterning of biomaterials using near-infrared light.....	63
3.1 Statement of contribution	63
3.2 Introduction	63
3.3 Results and discussion	66

3.4 Conclusion	68
3.5 Acknowledgements	69
3.6 References	70
3.7 Supporting information.....	72
Chapter 4: Manipulating pH using near-infrared light assisted by upconverting nanoparticles .	79
4.1 Statement of contribution	79
4.2 Abstract.....	79
4.3 Introduction	79
4.4 Results and disscussion	81
4.5 Conclusion	86
4.6 Acknowledgements	86
4.7 Notes and references.....	87
4.8 Supporting information.....	89
Chapter 5: Near-infrared photoinhibition of enzyme activities in living cells enabled by upconverting nanoparticles.....	97
5.1 Statement of contribution	97
5.2 Introduction	97
5.3 Results and discussion	99
5.4 Conclusion	104
5.5 Acknowledgements	104
5.6 References	105
5.7 Supporting information.....	107
Chapter 6: Near infrared photoinduced coupling reactions assisted by upconversion nanoparticles.....	118
6.1 Statement of contribution	119
6.2 Abstract.....	119
6.3 Introduction	120

6.4 Results and discussion	122
6.5 Conclusion	127
6.6 Acknowledgements	127
6.6 References	128
6.7 Supporting information.....	130
Curriculum Vitae	145

Abstract

Photosensitive ruthenium(II) polypyridyl complexes (Ru complexes) show lots of applications in bio-medical area as they can be photocleaved to release a ligand by low-intensity visible/red light. However, visible/red light cannot penetrate deep tissue, which will hinder its further application *in vivo*. NIR light is preferred for bio-medical applications as it can penetrate through the deep tissue. Thus, construction of near-infrared (NIR)-sensitive Ru complexes for bio-medical use is necessary. For this purpose, lanthanide-doped upconverting nanoparticles (UCNPs) are introduced. UCNPs can convert NIR light to UV/visible light, which can be used by Ru complexes. As a result, NIR-sensitive Ru complexes assisted by UCNPs (UCNP-assisted Ru complexes) are developed through combination of UCNPs and Ru complexes. UCNP-assisted Ru complexes is systematically studied in this thesis and it shows lots of priorities for bio-medical applications in our study. Firstly, it can low the excitation intensity for traditional NIR-sensitive biomaterials assisted by UCNPs, which can reduce the overheating problem of high-intensity NIR irradiation (**Chapter 2**). Secondly, developing biomaterials based on UCNP-assisted Ru complexes can solve several challenges in bio-medical area including patterning biomaterials (**Chapter 3**), pH manipulation in biological systems (**Chapter 4**) and cellular enzyme photoinhibition (**Chapter 5**). Besides demonstrating application of UCNP-assisted Ru complexes in bio-medical area, a new type of NIR-triggered photocoupling technology for bio-medical use is also developed in this thesis (**Chapter 6**).

In the chapter 2, we demonstrate UCNP-assisted Ru complexes can be triggered by low-intensity NIR light. We synthesized five photosensitive compounds including two Ru complexes with different absorption bands. A 974-nm laser was used to induce photoreactions of these photosensitive compounds in the presence of the UCNPs. The excitation thresholds of the photoreactions induced by 974-nm light were measured. Our results indicate that the threshold for UCNP-assisted Ru complexes can be reduced to 0.5 W/cm^2 , which is lower than the maximum permissible exposure of skin (0.726 W/cm^2). Low excitation intensity in UCNP-assisted Ru complexes is important for biomedical applications because it minimizes the overheating problems of NIR light and causes less photodamage to biomaterials.

In the chapter 3, we demonstrate that NIR light can be used for photolithography of biomaterials via UCNP-assisted Ru complexes. A blue-lightcleavable Ru complex (Ru1) and polyethylene glycol (PEG) were co-grafted onto the UCNP-decorated substrate. Proteins were

adsorbed onto the surface via electrostatic interactions between the negatively charged proteins and the positively charged Ru complexes. For the patterning of proteins, a photomask was positioned between the NIR light and the proteins. In the exposed areas, UCNPs convert NIR light into blue light that induces cleavage of the Ru complexes and the local release of proteins. Protein patterns can be fabricated in this manner.

In the chapter 4, pH manipulation is also developed based on UCNP-assisted Ru complexes. NIR light can be used to manipulate the pH of aqueous solutions by using upconverting nanoparticle-assisted photocleavage of a ruthenium complex photobase. Upconverting nanoparticles and the photobase were also introduced into a pH-responsive hydrogel, in which NIR irradiation induced swelling of the hydrogel.

In the chapter 5, NIR photoinhibition of enzyme activities in living cells is developed using UCNP-assisted Ru complexes. To construct a platform for PUEI, a NaYF₄:TmYb@NaYF₄ UCNP and caged enzyme inhibitors (RuEI) are encapsulated in a hollow mesoporous silica nanoparticle (hmSiO₂). UCNPs can convert NIR light to blue light, which can uncage enzyme inhibitor (EI) from RuEI upon NIR irradiation. After NIR photoactivation, the released EI can inhibit the activities of the cathepsin K enzyme in cells.

In the chapter 6, a new type of NIR-triggered photocoupling technology assisted by UCNPs is developed. We report nitrile imine-mediated tetrazole-ene cycloadditions (NITEC) in the presence of UCNPs. The combination of NITEC and UCNPs technology was exploited for small molecule cycloadditions, polymer end-group modification and the formation of block copolymers from functional macromolecular precursors, constituting the first example of a NIR-induced cycloaddition. As the technique was attractive for potential in vivo applications, through-tissue experiments in the presence of a biologically relevant biotin coupling species were carried out. Quantitative cycloadditions and retention of biological activity of the biotin units were possible at 974 nm irradiation.

Zusammenfassung

Lichtempfindliche Ruthenium(II)-Polypyridyl-Komplexe (Ru-Komplexe) zeigen viele Anwendungen im biomedizinischen Bereich, da sie durch Licht gespalten werden können, um einen Liganden durch geringe Intensität sichtbaren/roten Lichts freizusetzen. Allerdings kann sichtbares/rotes Licht nicht in tiefes Gewebe eindringen, was seine Anwendung in vivo behindern wird. NIR-Licht wird für biomedizinische Anwendungen bevorzugt, da es in tiefes Gewebe eindringen kann. Somit ist die Darstellung von nahinfrarot (NIR)-sensitiven Ru-Komplexen für die biomedizinische Verwendung notwendig. Zu diesem Zweck werden lanthanoiddotierte aufkonvertierende Nanopartikel (UCNPs) eingeführt. UCNPs können NIR-Licht in UV/sichtbares Licht umwandeln, das von Ru-Komplexen verwendet werden kann. Als Ergebnis werden NIR-empfindliche Ru-Komplexe, die durch UCNPs unterstützt werden (UCNP-unterstützte Ru-Komplexe), durch Kombination von UCNPs und Ru-Komplexen entwickelt. UCNP-unterstützte Ru-Komplexe werden in dieser Arbeit systematisch untersucht und zeigen in unserer Studie viele Prioritäten für biomedizinische Anwendungen. Erstens kann es die Anregungsintensität für traditionelle NIR-empfindliche Biomaterialien, die von UCNPs unterstützt werden, verringern, was das Überhitzungsproblem der hochintensiven NIR-Bestrahlung reduzieren kann (Kapitel 2). Zweitens kann die Entwicklung von Biomaterialien auf der Basis von UCNP-unterstützten Ru-Komplexen mehrere Herausforderungen im biomedizinischen Bereich lösen, einschließlich der Strukturierung von Biomaterialien (Kapitel 3), der pH-Manipulation in biologischen Systemen (Kapitel 4) und der zellulären Enzym-Photoinhibition (Kapitel 5). Eine neue Art der NIR-getriggerten Photokupplungstechnologie für den biomedizinischen Einsatz entwickelt (Kapitel 6).

In Kapitel 2 zeigen wir, dass UCNP-unterstützte Ru-Komplexe durch NIR-Licht mit geringer Intensität getriggert werden können. Wir synthetisierten fünf lichtempfindliche Verbindungen, darunter zwei Ru-Komplexe mit unterschiedlichen Absorptionsbanden. Ein 974-nm-Laser wurde verwendet, um Photoreaktionen dieser lichtempfindlichen Verbindungen in Gegenwart der UCNPs zu induzieren. Die Anregungsschwellen der durch 974-nm-Licht induzierten Photoreaktionen wurden gemessen. Unsere Ergebnisse zeigen, dass die Schwelle für UCNP-unterstützte Ru-Komplexe auf $0,5 \text{ W/cm}^2$ reduziert werden kann, was niedriger ist als die maximal zulässige Exposition der Haut ($0,726 \text{ W/cm}^2$). Niedrige Anregungsintensität in UCNP-unterstützten Ru-Komplexen ist für biomedizinische Anwendungen wichtig, da sie die Überhitzungsprobleme von NIR-Licht minimiert und weniger Schaden an Biomaterialien hervorruft.

In Kapitel 3 zeigen wir, dass NIR-Licht für Photolithographie von Biomaterialien durch UCNP-unterstützte Ru-Komplexe verwendet werden kann. Ein durch blaues Licht spaltbarer Ru-Komplex (Ru1) und Polyethylenglykol (PEG) wurden auf das mit UCNP ausgestattete Substrat co-gefropft. Proteine wurden auf der Oberfläche durch elektrostatische Wechselwirkungen zwischen den negativ geladenen Proteinen und den positiv geladenen Ru-Komplexen adsorbiert. Für die Oberflächenstrukturierung mit Proteinen wurde eine Photomaske zwischen dem NIR-Licht und den Proteinen positioniert. In den exponierten Bereichen konvertieren UCNPs NIR-Licht in blaues Licht, das die Spaltung der Ru-Komplexe und die lokale Freisetzung von Proteinen induziert. Auf diese Weise können Proteinmuster hergestellt werden.

In Kapitel 4 wird die pH-Manipulation auf Basis von UCNP-unterstützten Ru-Komplexen entwickelt. NIR-Licht kann verwendet werden, um den pH-Wert von wässrigen Lösungen zu manipulieren, indem eine Rutheniumkomplexphotobase unterstützt durch UCNPs gespalten wird. Aufkonvertierende Nanopartikel und die Photobase wurden ebenfalls in ein pH-reagierendes Hydrogel eingeführt, in dem die NIR-Bestrahlung eine Schwellung des Hydrogels induzierte.

In Kapitel 5 wird die NIR-Photoinhibition von Enzymaktivitäten in lebenden Zellen unter Verwendung von UCNP-unterstützten Ru-Komplexen entwickelt. Um eine Plattform für RUEI darzustellen, werden ein NaYF₄:TmYb@NaYF₄ UCNP und Enzyminhibitoren (RuEI) in einem hohlen mesoporösen Siliciumdioxid-Nanopartikel (hmSiO₂) eingekapselt. UCNPs können NIR-Licht in blaues Licht umwandeln, das bei NIR-Bestrahlung den Enzym-Inhibitor (EI) aus RuEI befreien kann. Nach der NIR-Photoaktivierung kann der freigesetzte EI die Aktivitäten des Kathepsin-K-Enzyms in Zellen hemmen.

In Kapitel 6 wird eine neue Art von NIR-getriggerte Photokupplungstechnologie entwickelt, die von UCNPs unterstützt wird. Wir berichten über Nitrilimin-vermittelte Tetrazol-En-Cycloadditionen (NITEC) in Gegenwart von UCNPs. Die Kombination von NITEC- und UCNPs-Technologie wurde für Cycloadditionen von kleinen Molekülen, Polymer-Endgruppen-Modifikation und die Bildung von Blockcopolymeren aus funktionellen makromolekularen Vorstufen ausgenutzt, das erste Beispiel NIR-induzierter Cycloadditionen. Da die Technik für potentielle *in-vivo*-Anwendungen attraktiv war, wurden Experimente durch Gewebe in Gegenwart einer biologisch relevanten Biotin-Kopplungsart durchgeführt. Quantitative Cycloadditionen und Retention der biologischen Aktivität der Biotineinheiten waren möglich bei Bestrahlung mit Licht der Wellenlänge 974 nm.

Chapter 1: Introduction and motivation

1.1 Ruthenium(II) polypyridyl complexes

Recently, ruthenium(II) polypyridyl complexes (Ru complexes) have been well studied and demonstrated tremendous applications in catalyst,^[1] photosensitizers,^[2] solar sensitive dyes^[3] and biomaterials.^[4] These Ru complexes consist of ruthenium metal center and polypyridyl ligands via six coordination bonds. Ru complexes can be classified into three main types on the basis of the denticity of their ligands (**Figure 1.1a, b, c**). 1. ruthenium center + three bidentate pyridyl ligands (**Figure 1.1a**);^[5] 2. ruthenium center + two bidentate pyridyl ligands + two monodentate ligands (X, Y can be the same or different, **Figure 1.1b**);^[6] 3. ruthenium center + one tridentate pyridyl ligand + one bidentate pyridyl ligand + one monodentate ligand (**Figure 1.1c**).^[6]

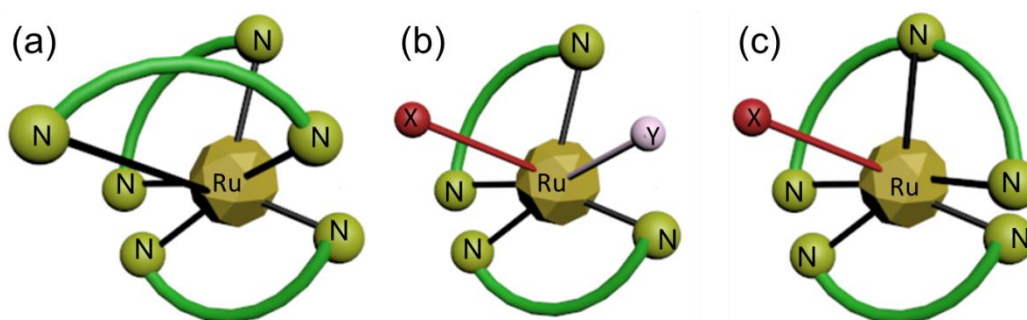


Figure 1.1. a) Ru complexes with three bidentate pyridyl ligands; b) Ru complexes with two bidentate pyridyl ligands and two monodentate ligands; c) Ru complexes with one tridentate pyridyl ligand, one bidentate pyridyl ligand and one monodentate ligand.

1.2 Photochemical property of Ru complexes

The photochemical property of Ru complexes was studied deeply in past several years.^[7] $[\text{Ru}(\text{bpy})_2\text{XY}]^{n+}$ ^[8] and $[\text{Ru}(\text{terpy})(\text{bpy})\text{X}]^{n+}$ ^[9] are two kinds of classic Ru complexes for photochemical research (**Figure 1.2a, b**). Their photochemistry is determined by photo dissociation of one or two monodentate ligands.^[6, 9-10] Dwyer et al firstly reported the photoreactivity of $[\text{Ru}(\text{bpy})_2\text{XY}]^{n+}$ in 1963.^[11] Then, Pinnick & Durham systematically studied photochemistry of these Ru complexes including quantum yield of photoreaction, redox potential ($E_{1/2}$) of the Ru(II)/Ru(III) couple.^[7]

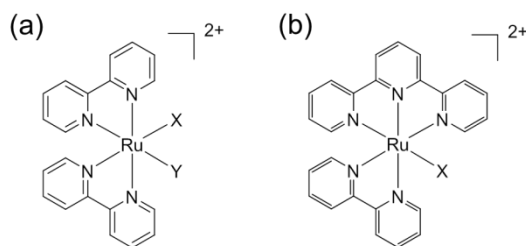


Figure 1.2. a) The Ru complexes bearing two bipyridines and two monodentate ligands ($[\text{Ru}(\text{bpy})_2\text{XY}]^{n+}$). b) The Ru complexes bearing one tripyridine, one bipyridine and one monodentate ligand ($[\text{Ru}(\text{terpy})(\text{bpy})\text{X}]^{n+}$).

The mechanism of photochemistry of $[\text{Ru}(\text{bpy})_2\text{XY}]^{n+}$ and $[\text{Ru}(\text{terpy})(\text{bpy})\text{X}]^{n+}$ is explained in the state diagram (**Figure 1.3**).^[6] The maximum absorption of metal-to-ligand charge transfer band is located in visible/red region of UV-Vis spectra.^[6] Thus, singlet metal-to-ligand charge transfer ($^1\text{MLCT}$) can be excited by visible or red light. Subsequently, efficient intersystem crossing of $^1\text{MLCT}$ triggers population of triplet $^3\text{MLCT}$. The triplet $^3\text{MLCT}$ band can be deactivated through non-irradiative routes, emission, and populating non-bonding d-d state. Populating non-bonding d-d state results in release of the monodentate ligand. The d-d state has a higher energy than that of $^3\text{MLCT}$, which indicates the final transition is thermally activated. For efficiency of photodissociation, energy of $^1\text{MLCT}$ is positively correlated. At a given temperature, efficiency of photo dissociation can be improved with the blue-shifted $^1\text{MLCT}$. Specifically, blue-shifted $^1\text{MLCT}$ band means $^1\text{MLCT}$ with higher energy, which corresponds to higher energy $^3\text{MLCT}$ band. $^3\text{MLCT}$ with higher energy can transfer more energy to populate the anti-bonding d-d state, which triggers a higher photo dissociation yield. Quantum yield of photosubstitution of $[\text{Ru}(\text{bpy})_2\text{XY}]^{n+}$, $[\text{Ru}(\text{terpy})(\text{bpy})\text{X}]^{n+}$ complexes is also correlated with the redox potential ($E_{1/2}$) of Ru(II)/Ru(III) couple. High redox potential ($E_{1/2}$) of the Ru(II)/Ru(III) couple can enhance a higher quantum yield of photosubstitution.^[12]

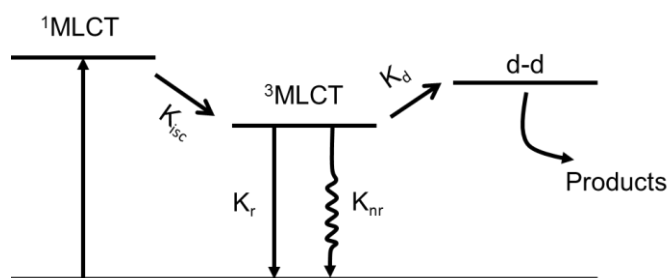


Figure 1.3. Basic structure and electronic states diagram of the family of $[\text{Ru}(\text{bpy})_2\text{XY}]^{n+}$, $[\text{Ru}(\text{terpy})(\text{bpy})\text{X}]^{n+}$.^[6]

1.3 Photosensitive Ru complexes

Generally, Ru complexes ($[\text{Ru}(\text{bpy})_2\text{XY}]^{n+}$ and $[\text{Ru}(\text{terpy})(\text{bpy})\text{X}]^{n+}$) are sensitive to visible/red light. Irradiation of visible/red light can trigger photocleavable reaction of $[\text{Ru}(\text{bpy})_2\text{XY}]^{n+}$, $[\text{Ru}(\text{terpy})(\text{bpy})\text{X}]^{n+}$.^[6, 10, 12-13] The monodentate ligand will be photocleaved and corresponding ruthenium aqueous byproduct will be generated upon irradiation of light (**Figure 1.4a**). There are several types of photocleavable monodentate ligands reported including ligands with methylthiol,^[14] cyan,^[15] amine^[12] and pyridine moieties.^[16] The photolytic reaction of $[\text{Ru}(\text{bpy})_2\text{XY}]^{n+}$ and $[\text{Ru}(\text{terpy})(\text{bpy})\text{X}]^{n+}$ has three priorities.^[6, 17] Firstly, most of them can be activated by visible light due to their ¹MLCT bands in visible region. Secondly, monodentate ligands are photocleaved as entire molecules, without any other unwanted reactions. Finally, due to the weak-energy coordination bond between the Ru center and monodentate ligand, Ru complexes have high photosensitivity values and can be photocleaved by low-intensity visible light. As visible light can penetrate deeper in tissue and have low biological toxicity compared with the UV light, visible/red-light-responsive Ru complexes have more advantages as biomaterials than UV-responsive chromophores. Photoreactions of Ru complexes are partially summarized (**Figure 1.4a-e**).

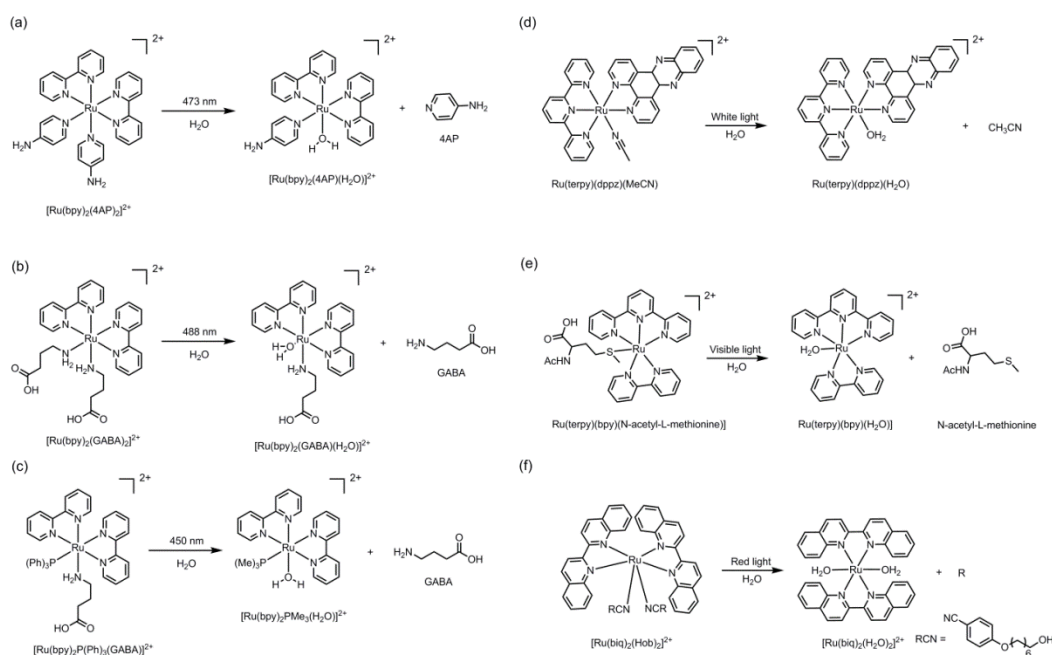


Figure 1.4. Photoreaction of a) $[\text{Ru}(\text{bpy})_2(4\text{AP})_2]^{2+}$,^[16] b) $[\text{Ru}(\text{bpy})_2(\text{GABA})_2]^{2+}$,^[8] c) $[\text{Ru}(\text{bpy})_2\text{P}(\text{Ph})_3(\text{GABA})_2]^{2+}$,^[18] d) $[\text{Ru}(\text{terpy})(\text{dppz})(\text{MeCN})]$,^[19] e) $[\text{Ru}(\text{terpy})(\text{bpy})(\text{N-acetyl-L-methionine})]$ ^[14] and f) $[\text{Ru}(\text{biq})_2(\text{Hob})_2]$.^[20]

1.4 Bio-medical applications of photoresponsive Ru complexes

1.4.1 Photorelease of neurochemical molecules

UV light was used to release neurocompounds from organic sensitive molecules during the past several years.^[16] In these reports, UV irradiation was used to photocleave a σ covalent bond. UV light may damage DNA, cells and tissues. Thus, visible-light-triggered release of neurocompounds should be developed. Etchenique's group firstly reported that visible-light-controlled release of 4-aminopyridine as a blocker for neuro potassium channel in the presence of Ru complex-based photocage (**Figure 1.5a**).^[16] Upon irradiation of 470-nm light, 4-aminopyridine was photocleaved from the Ru complex and an obvious neuro signal response was observed (**Figure 1.5b**). This is the first Ru complexes-based photocage for bio-medical application.^[21]

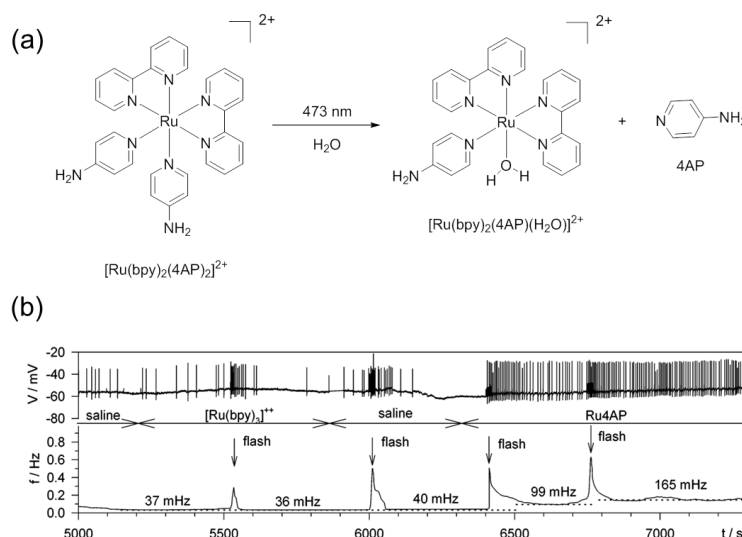


Figure 1.5. a) Photolysis of $[\text{Ru}(\text{bpy})_2(4\text{AP})_2]^{2+}$; b) Action potentials (spikes) recorded in a leech neuron in the presence of $[\text{Ru}(\text{bpy})_2(4\text{AP})_2]^{2+}$ without light irradiation (top) and upon light irradiation (down). Panel (b) reproduced with permission. Copyright 2003, American Chemical Society.^[16]

After this work, a new complex $[\text{Ru}(\text{bpy})_2(\text{PPh}_3)(\text{GABA})]^{2+}$ (bpy = bis(bipyridine), GABA = γ -aminobutyric acid) was also reported by the same group (**Figure 1.6a**).^[12] In order to increase quantum yield of photoreaction, they introduced a new ligand triphenylphosphine (PPh_3) in this work. The quantum yield of the complex at 450 nm was above 0.2. The γ -aminobutyric acid was released by 450-nm irradiation. To demonstrate the application, they also used the light-triggered release of GABA to adjust receptor-mediated Cl^- currents in frog

oocytes (**Figure 1.6b**). This kind of photocontrolled release showed the same effect as pure GABA to frog oocytes.

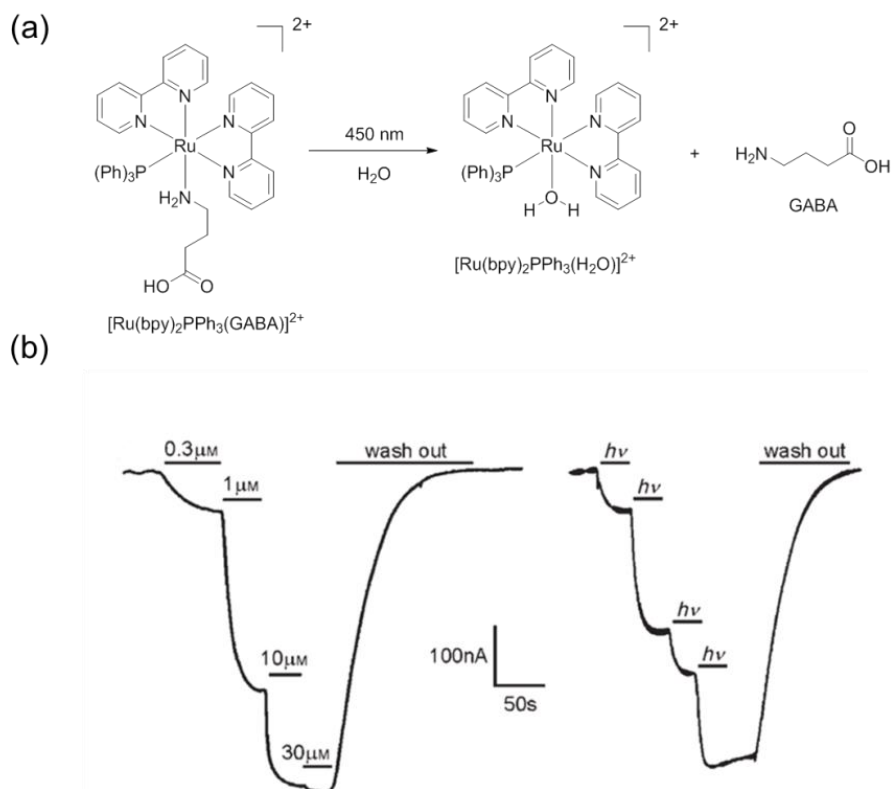


Figure 1.6. a) Photolysis of $[\text{Ru}(\text{bpy})_2\text{PPh}_3(\text{GABA})]^{2+}$. b) Membrane ionic currents recorded in frog oocytes in the presence of increasing concentration of free GABA (left) and with $[\text{Ru}(\text{bpy})_2\text{PPh}_3(\text{GABA})]^{2+}$ upon light excitation. Panel (b) reproduced with permission. Copyright 2016, WILEY-VCH Verlag GmbH & Co. KGaA.^[12]

1.4.2 Light-activated enzyme inhibition

Turro's and Kodanko's group reported a novel photoresponsive Ru complex for protease inhibition (**Figure 1.7**).^[13b] In their work, conventional enzyme inhibitor was coordinated to ruthenium center to form photosensitive pro-inhibitor. Upon irradiation of light ($\lambda_{\text{irr}} > 395$ nm), the coordinated inhibitor can be released to inhibit enzyme activity (**Figure 1.7a, b**). Moreover, another byproduct of this photoreaction, ruthenium aqueous compound, did not show a big influence on the enzyme activity. Following the same strategy, Kodanko's group synthesized three new photosensitive enzyme inhibitors based on Ru complexes and investigated their photochemical properties.^[13c] Cellular experiments confirmed that activity of cellular enzyme was inhibited in the presence of the synthesized Ru complex upon irradiation of visible light.

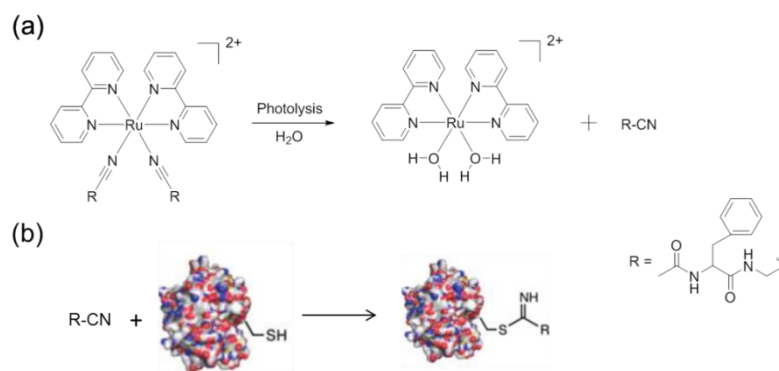


Figure 1.7. Caging strategy for nitrile-based cysteine protease inhibitors. a) Schematic illustration of light-triggered release of protease inhibitor. b) Inhibition mechanism of the released protease inhibitor and enzyme. Panel (b) reproduced with permission. Copyright 2011, American Chemical Society. ^[13b]

1.4.3 Regulating gene expression

Dmochowski's group reported that Ru complexes, as photolinks, were functionalized by morpholinos (MOs) oligonucleotide *via* Cu(I) mediated cycloaddition reactions (**Figure 1.8a**).^[22] One-cell-stage zebrafish embryos microinjected with MOs functionalized Ru complexes (Ru-MO) showed gene knockdown upon light irradiation at 450 nm (**Figure 1.8a**). The gene knockdown was due to dissociation of one 3-ethynylpyridine ligand and uncaged the MOs (**Figure 1.8 b4**), while gene expression was still observed in other control groups (**Figure 1.8 b1, 2, 3**).^[22]

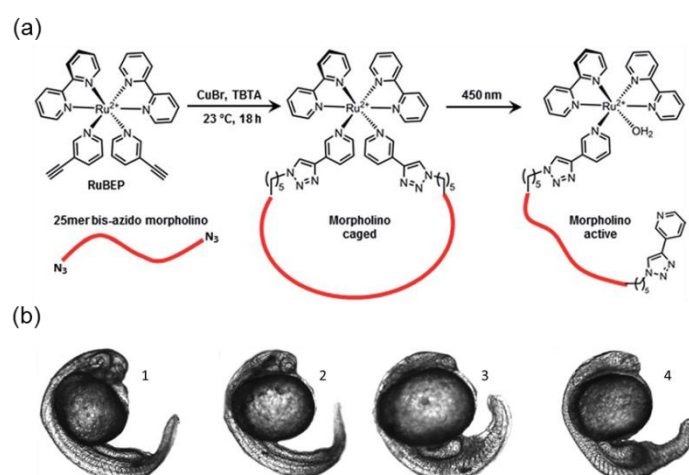


Figure 1.8. a) Synthesis and photolysis of Ru-MO. b) phenotypic response of zebrafish embryos upon irradiation at 450 nm. Panel (a) and (b) reproduced with permission. Copyright 2011, Royal Society of Chemistry. ^[22]

1.4.4 Anti-cancer reagent

Like Platinum complex, Ru complex was also be used as an anti-cancer reagent. The mechanism of cancer cell inhibition using ruthenium complex is thermal aquation of the coordinated ruthenium-chloride bonds, followed by coordination to DNA or proteins.^[14] However, as bond energy of Ru-Cl is too weak, thermal aquation of Ru-Cl bonds might happen anywhere in a human body without any control. Thus, ruthenium complexes both have antitumor activity and general toxicity. Bonnet's group solved the problem of general toxicity by coordinating a thioether ligand as a substitute for chloride to ruthenium center.^[14] The coordination bond between ruthenium and thioether ligand was stable and did not hydrolyze in the biological environment. Only when the complex was irradiated, did it release ruthenium aqueous compound to inhibit cancer cells (**Figure 1.9**).

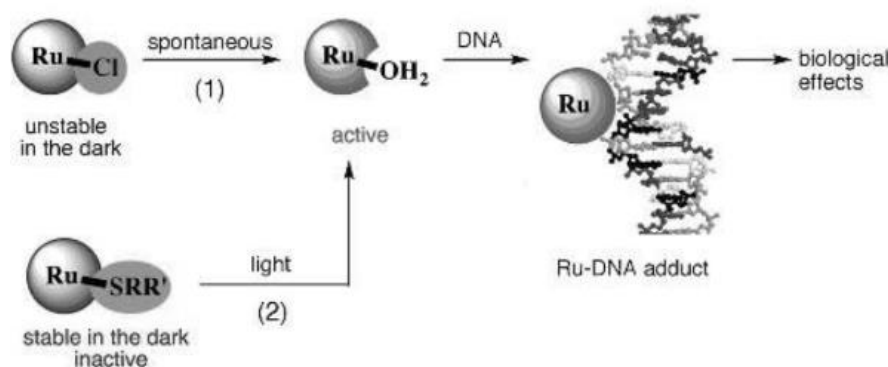


Figure 1.9. Reaction 1: schematic illustration of interaction between Ru complex (with Ru-Cl bond) and DNA in cancer cells. Reaction 2: schematic illustration of interaction between photosensitive Ru complex (with thioether ligand) and DNA in cancer cells. Reproduced with permission. Copyright 2011, WILEY-VCH Verlag GmbH & Co. KGaA.^[14]

Our group also reported to inhibit cancer cells using Ru complexes. We used self-assembled photoresponsive ruthenium-containing micelles/vesicles for anticancer phototherapy (**Figure 1.10a**).^[15] The Ru complexes in micelles/vesicles acted as a photoactivated prodrug. Irradiation of red light can generate ruthenium aqueous products as anti-cancer reagents and singlet oxygen in the presence of ruthenium-containing micelles/vesicles, which induced the apoptosis of cancer cells. The red-light-triggered release is a big progress as many of previous reports used blue light to trigger photoresponsive Ru complex-containing materials. After this work, our group synthesized a new amphiphilic Ru-

containing block copolymer. This new Ru-containing block copolymer formed self-assembly nanoparticles and accumulated at tumor sites (**Figure 1.10b**).^[20] The self-assembly nanoparticles of this Ru-containing released anticancer Ru complexes and generated singlet oxygen upon irradiation of red light. Thus, it could be used as a photoresponsive polymetallo drug for tumors treatment.^[20]

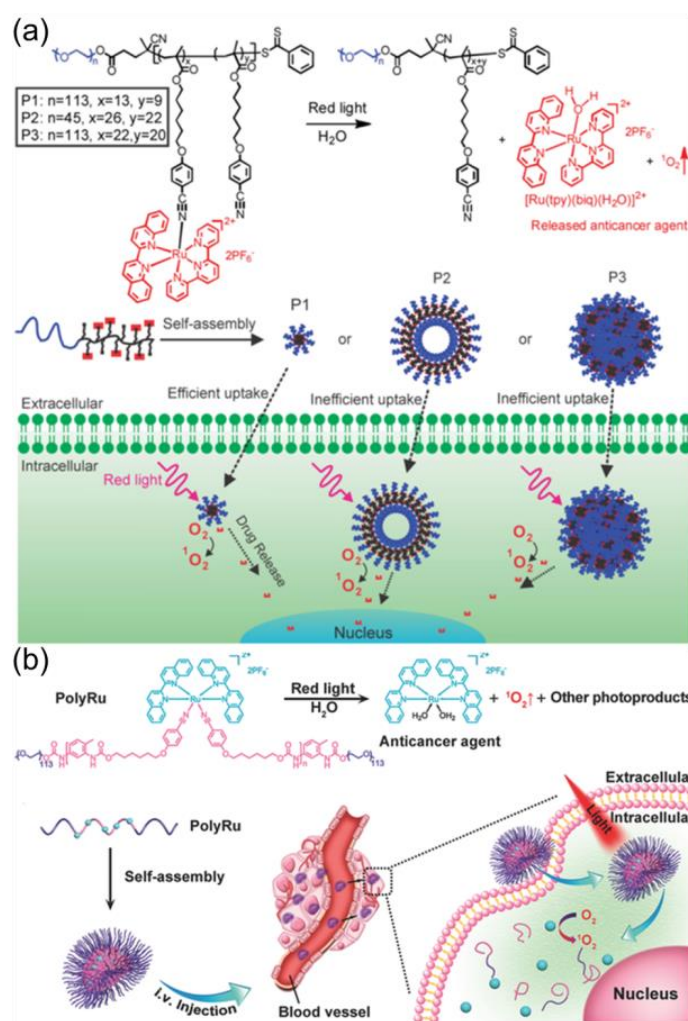


Figure 1.10. a) Schematic illustration of self-assembly of Ru-containing nanocarriers for drug delivery. Reproduced with permission. Copyright 2016, WILEY-VCH Verlag GmbH & Co. KGaA. b) Schematic illustration of self-assembly of Ru-containing nanocarriers for tumor treatment. Reproduced with permission. Copyright 2016, WILEY-VCH Verlag GmbH & Co. KGaA. ^[15, 20]

1.5 Strategies for red-shifting responsive wavelength of Ru complexes

Although photosensitive Ru complexes have been widely used in bio-medical area, there are still some problems. The main problem is that the responsive wavelength for Ru complexes is still in the visible or red region. Visible or red light cannot penetrate deep tissue to trigger photoreaction of Ru complexes, which will hinder its further application in vivo and practical clinics (**Figure 1.11**).^[17, 23] Compared to visible or red light, NIR source is preferred for bio-medical applications as it can penetrate through the deep tissue (**Figure 1.11**).^[23] One approach to constructing NIR-sensitive Ru complexes is based on simultaneous two-photon absorption.^[24] For example, 700-nm pulsed laser can be used to trigger the photoreaction of a photosensitive compound with an absorption band (350 nm) via simultaneous two-photon absorption. Etchenique's group and Campo's group developed NIR-responsive Ru complexes based on this two-photon absorption process.^[25] Nevertheless, two-photon absorption is inefficient for bio-medical applications. First, two-photon absorption only occurs at the focus of a laser because it requires high-intensity light, which means it cannot trigger the efficient reaction on a macroscopic scale.^[17] Moreover, as the femtosecond laser used for simultaneous two-photon absorption will defocus while passing through the tissue, the two-photon absorption strategy is impractical for deep tissue trials.^[26]

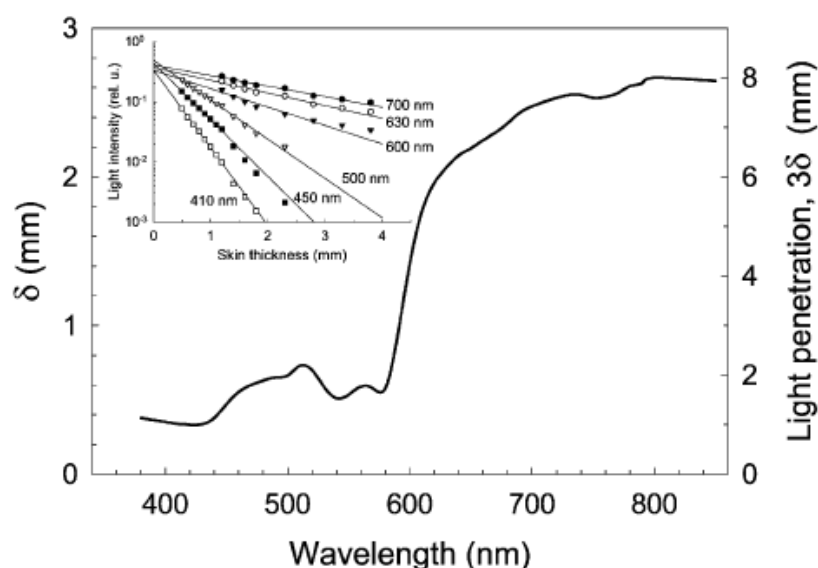


Figure 1.11. The penetration depth of the excitation light in the rat skin. Insert: light fluence presented for some of the wavelengths. Reproduced with permission. Copyright 2014, Royal Society of Chemistry.^[23]

In 2004, Bonnet's group firstly demonstrated Ru complexes could be photocleaved upon irradiation of 630 nm light assisted by triplet-triplet annihilation (TTA) upconverting materials.^[27] TTA was firstly reported by Parker and Hatchard in the mixture solution of phenanthrene/naphthalene and proflavin hydrochloride/anthracene.^[28] One sensitizer molecule and two annihilator molecules are involved in TTA upconverting materials.^[29] In the upconverting process of TTA, sensitizer absorbs low-energy photon. Then, the sensitizer will go to a triplet state via intersystem crossing. Meanwhile, the energy can transfer from sensitizer to an annihilator by triplet-triplet energy transfer process. Finally, photon upconversion is produced by collision of two triplet annihilator molecules. Lots of molecule couples have been reported for TTA photon upconversion in nanoparticles, polymers, solvents and ionic liquid.^[29a] Although the Ru complexes assisted by TTA photon upconversion materials cannot be responsive to NIR light in Bonnet's work, the strategy used here gives us lots of inspiration. Developing NIR-responsive Ru complexes for practical use may be achieved by combining Ru complexes and lanthanide-doped upconverting nanoparticles which can absorb NIR photons.

1.6 Lanthanide-doped upconverting nanoparticles (UCNPs)

UCNPs consist of three ingredients including activator, sensitizer and host matrices (**Figure 1.12**).^[30] UCNPs belong to guest-host systems where trivalent lanthanide ions (activators, sensitizers) are dispersed as a guest in a host matrices (**Figure 1.12**).^[30] Generally, dimension of UCNPs is about 50 nm.^[31] The lanthanide ions (activators, generally Tm^{3+} , Er^{3+} , Ho^{3+}) are active centers, which generate upconverted photons when they are excited.^[32] As most of activators have very low cross section at NIR wavelength region, another dopant (sensitizers, generally Yb^{3+}) with a large absorption coefficient of NIR light is co-dispersed in a host matrix as absorption assistant.^[33] Through reasonable combination of activators and sensitizers, UCNPs can show different emission wavelengths, ranging from UV to NIR emission. To date, many kinds of UCNPs have been developed. Most of them can absorb 980 nm/808 nm light. Among these reported UCNPs, Yb^{3+} -sensitized $\text{Tm}^{3+}/\text{Er}^{3+}$ systems in β -phase NaYF_4 crystal matrices are two of the most commonly used and efficient UCNPs.^[17]

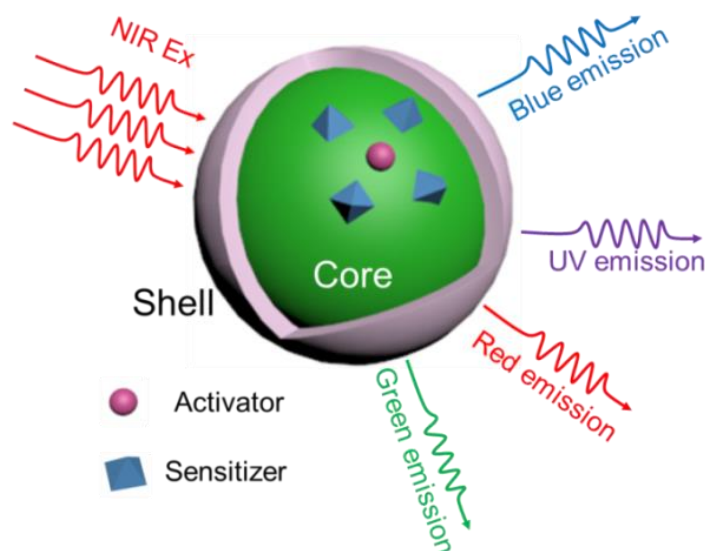


Figure 1.12. Schematic illustration of a core/shell structure and possible emission of UCNPs upon NIR irradiation.

1.7 Mechanism of UCNPs

Mechanisms involved in upconverted emission of UCNPs are mainly summarized in these five types, excited-state absorption (ESA), energy transfer upconversion (ETU), cooperative sensitization upconversion (CSU), cross-relaxation (CR), and photon avalanche (PA).^[30, 33]

1.7.1 Mechanism of excited-state absorption (ESA)

In the mechanism of ESA, a single ground-state photon absorbs pump photons successively (**Figure 1.13**). The ESA mechanism is a three-level system. Firstly, an activator ion migrates from the ground state to the E1 level upon excitation. Then, a second photon will promote the activator ion at E1 level to a higher state (E2). Subsequently, the activator ions at E2 level will decay to the ground state, which results in upconversion emission. Thus, the activator ion with ladder-like energy states is necessary for high energy transfer efficiency in the ESA. Thus, only a few lanthanide ions can be used as the activator ions for ESA, such as Er^{3+} , Ho^{3+} , Tm^{3+} , and Nd^{3+} . Also, the required excitation for these ions can well match the output of commercially available diode lasers (974 nm/808 nm).^[33]

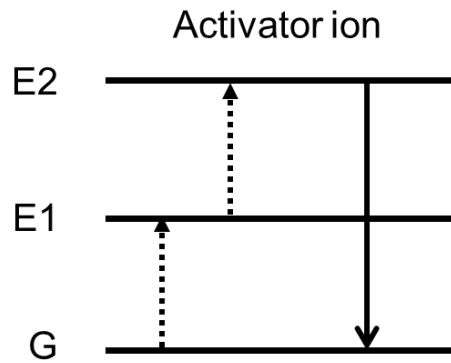


Figure 1.13. Principal UC processes of excited-state absorption for lanthanide-doped UCNPs

1.7.2 Mechanism of energy transfer upconversion (ETU)

In ETU, sequential absorption of two photons is also involved, which is similar to upconversion process in ESA. The main difference between ETU and ESA is two kinds of lanthanide ions (activator, sensitizer) are operated in the ETU while only one ion (activator) is used in the ESA (**Figure 1.14**). In the ETU, populated sensitizer ion migrates from ground state to metastable level (E1) upon excitation of NIR photons. Then, the populated sensitizer ion transfers its harvested energy to the activator ion at the ground state and E1 level. Activator ion will be excited to E2 level, meanwhile, sensitizer ion relaxes to the ground state. Finally, the activator ions at E2 level will decay to the ground state, which results in upconversion emission. Upconversion process via ETU mechanism can be significantly influenced by the distance of dopant activators and sensitizers determined by the dopant concentration. While, Upconversion process via ESA mechanism is independent of the dopant distance due to its single activator ion involved. ^[30, 34]

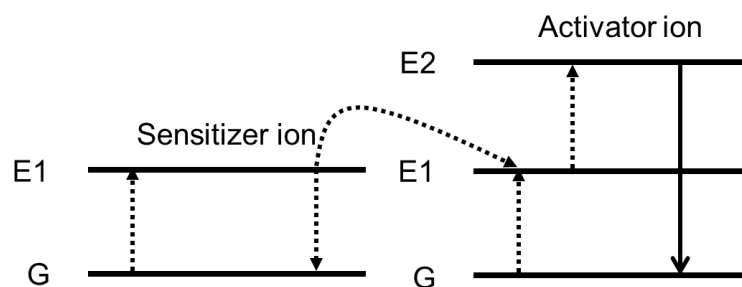


Figure 1.14. Principal UC processes of energy transfer upconversion for lanthanide-doped UCNPs.

1.7.3 Mechanism of cooperative sensitization upconversion (CSU)

Compared to the ETU and ESA, CSU is a process with energy transfer between three ions (**Figure 1.15**). Two of them are sensitizer ions and one is activator ion. Upon excitation of NIR photons, sensitizer ions can be populated to the higher-lying level (E1). Subsequently, the harvested energy of these two sensitizer ions will be transferred to an activator ion at ground state, which leads to the excitation of activator to E2 level. Finally, the activator ion at E2 level will decay to the ground state, which releases upconversion photon. The efficiency of CSU is much lower than the ESA or ETU process. Upconversion process of $\text{Yb}^{3+}/\text{Tb}^{3+}$, $\text{Yb}^{3+}/\text{Pr}^{3+}$ and $\text{Yb}^{3+}/\text{Eu}^{3+}$ ion pairs are reported via the CSU mechanism.^[30]

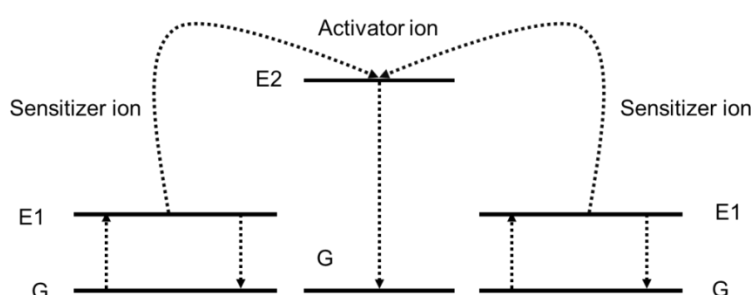


Figure 1.15. Principal upconverting processes of cooperative sensitization upconversion for lanthanide-doped UCNPs.

1.7.4 Mechanism of cross-relaxation (CR)

Typically, CR is considered as a main factor for “concentration quench” (**Figure 1.16**). Generally, the process happened between two ions. These two ions can be either the same or different. Specifically, when an ion was interacted with another, energy will transfer from one ion to another, $G(\text{ion } 2) + E2(\text{ion } 1) \rightarrow E1(\text{ion } 1) + E1(\text{ion } 2)$. However, this mechanism can be intentionally used for tuning emission spectra of UCNPs.^[30, 33-34]

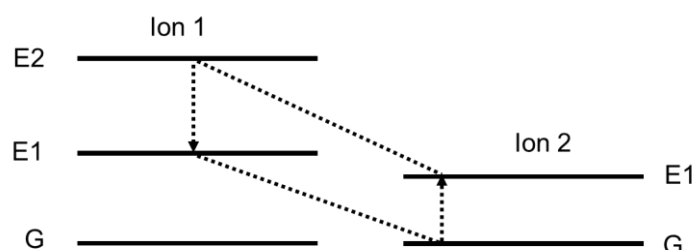


Figure 1.16. Principal upconverting processes of cross relaxation for lanthanide-doped UCNPs.

1.7.5 Mechanism of photon avalanche (PA)

Photon avalanche was first reported by Chivian's group. Obvious upconverted fluorescence can only be excited upon a certain excitation power, which is attributed to photon avalanche mechanism (**Figure 1.17**). Below the threshold value, very little upconverted photons generate. When the irradiation is above threshold value, intensity of upconverted light increases by orders of magnitude. Actually, PA is a looping process with ESA and CR as excitation light and feedback respectively. The Ion 2 was initially excited to level E1 by non-resonant weak ground-state absorption (NRA). Then, Ion 2 reaches E2 level via ESA process. An efficient CR process happened between Ion 1 and Ion 2 ($E2(\text{Ion } 1) + G(\text{Ion } 2) \rightarrow E1(\text{Ion } 1) + E1(\text{Ion } 2)$). Both of Ion 1 and Ion 2 are at E1 level as a result. This looping process can produce two Ion 2 at E1 state using one Ion 2 at the same state. Avalanche effect will happen when the looping process continues. Two Ion 2 at the E1 state will produce four Ion 2 at the same state, four will generate eight.^[34-35]

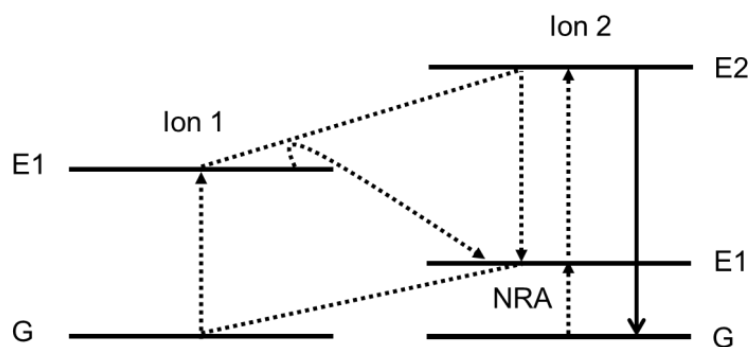


Figure 1.17. Principal upconverting processes of photon avalanche for lanthanide-doped UCNPs.

1.8 Development of NIR-sensitive molecules assisted by UCNPs

Conventional UV-/visible-sensitive molecules can be sensitive to NIR light in the presence of UCNPs. These kind of NIR-sensitive molecules is referred to as UCNP-assisted photosensitive molecules.^[32] UCNP-assisted photosensitive molecules consists of two components including UCNPs and photosensitive molecules.^[32] UCNP-assisted photosensitive molecules requires that upconverted light can be absorbed by the photosensitive compounds, that is, the emission bands of the UCNPs should overlap with the absorption bands of the photosensitive compounds.^[17] UCNP-assisted photosensitive

molecules was well developed since Branda and co-workers first demonstrated dithienylethene derivatives was sensitive to NIR light with assistance of UCNP in 2009.^[36] Recently, our group summarized that three main types of UCNP-assisted photosensitive compounds including photolytic compounds, photoswitching compounds, and photoinitiators in a review.^[32]

1.8.1 UCNP-assisted photolytic compounds

For UCNP-assisted photolytic compounds, UCNP are combined with photolytic molecules. Photocleavable reaction of photolytic molecules can be triggered by upconverted UV or visible emission. The reported photolytic reactions of UCNP-assisted photolytic compounds are summarized (**Figure 1.18**). The photolytic molecules used here can be divided into two types including organic molecules and coordinated metal complexes. Branda and co-workers reported the first UCNP-assisted photolytic reaction was reported (**Figure 1.18b**).^[37] In their report, 3',5'-di(carboxymethoxy)benzoin acetate grafted on UCNP was photocleaved by upconverted UV light as absorption band of 3',5'-di(carboxymethoxy)benzoin was overlapped with upconverted UV emission. After this work, photolysis of *o*-nitrobenzyl and coumarin assisted by UCNP was developed (**Figure 1.18c, d**).^[38] *o*-nitrobenzyl, coumarin and their derivatives are classic photocages, which has the absorption bands in UV region. The absorption of *o*-nitrobenzyl, coumarin and their derivatives overlaps with the emission of thulium/erbium-containing UCNP, which is the reason for the UCNP-assisted photolysis of *o*-nitrobenzyl, coumarin and their derivatives. Besides these organic molecules, some photosensitive metal complexes can also be used for UCNP-assisted photolytic compounds. For example, Pt complexes could be photocleaved upon excitation of upconverted UV photons, which can reduce Pt(IV) to Pt(II) (**Figure 1.18e**).^[39] Another metal complex for UCNP-assisted photolytic compounds is Mn complex (**Figure 1.18f**).^[40] After photolytic reaction triggered by the visible upconverted emission, the Mn complex can release CO. Ruthenium complex can also be combine with the UCNP for construction of photochemistry system (**Figure 1.18g**).^[17, 41] Upon excitation of NIR light, ruthenium complex can be photocleaved by upconverted visible photons and release a monodentate ligand.

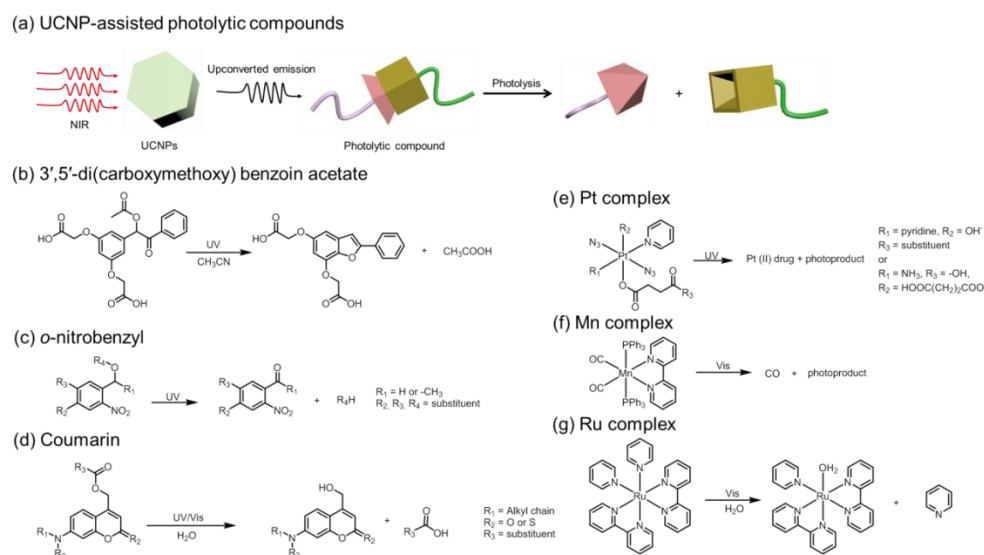


Figure 1.17. a) Schematic illustration of UCNP-assisted photolytic compounds. Photolytic reaction of b) 3',5'-di(carboxymethoxy)benzoic acetate,^[37] c) o-nitrobenzyl derivatives,^[38c] d) coumarin derivatives,^[38m] e) Pt complexes,^[39b] f) Mn complexes^[40] and g) Ru complex^[41b] can be triggered upon NIR excitation assisted by UCNPs.

1.8.2 UCNP-assisted photoswitching compounds

NIR-sensitive photoswitching compounds assisted by UCNPs can be achieved when the UCNPs and photoswitchable molecules are combined together (**Figure 1.19a**).^[32] The upconverted photons can trigger one-way or reversible isomerization of molecules upon excitation of NIR light. Dithienylethene derivatives, azobenzene derivatives, and spiropyran derivatives are the commonly used photoswitchable molecules for UCNP-assisted photoswitching compounds.^[32]

NIR-triggered one-way isomerization of dithienylethene derivatives was achieved by combining the molecules with UCNPs with UV emission or with green/red emission.^[36, 42] The UCNPs can emit UV light or green/red light upon NIR excitation, which can isomerize dithienylethene derivatives from open form to close form or close form to open form respectively (**Figure 1.19b**). NIR-induced reversible photoisomerization of dithienylethene derivatives assisted by UCNPs were also developed.^[43] UCNPs with multiple layers show excitation intensity-dependent emission. When the UCNPs are excited by low-intensity NIR light, the UCNPs can have green and red emission. While, high-intensity NIR irradiation can induce UV upconverted emission of the UCNPs. Thus, the reversible photoisomerization of

dithienylethene derivatives can be achieved assisted by this multiple-layer structured UCNPs upon excitation of NIR light at different intensity. After this work, UCNP-assisted reversible photoisomerization triggered by two different NIR wavelength was also reported.^[43] Novel UCNPs were developed, which can convert 800/974 nm NIR light to UV emission/green and red emission respectively. Thus, photoisomerization of dithienylethene derivatives triggered by the 800/974 nm light in the presence of this novel UCNPs was realized.

Azobenzene and its derivatives can be isomerized reversibly from trans to cis upon irradiation of UV and visible light (**Figure 1.19c**). Inspired by this, Yu's group used upconverted UV light to trigger the trans-cis isomerization of azotolane.^[44] However, the cis-trans isomerization was only achieved through thermal relaxation. Besides this one-way UCNP-assisted photoisomerization, continuous photoisomerization (trans to cis) of azobenzene derivatives assisted by UCNPs was also reported.^[45] Both trans and cis isomers of azobenzene derivatives can absorb the same upconverted emission, which can trigger the continuous photoisomerization. NIR light at different intensities can trigger the reversible photoisomerization of azobenzene derivatives assisted by UCNPs.^[46] At high intensity, NIR light can excite more UV photons, which trigger trans-cis isomerization. While, cis-trans isomerization can be achieved upon low-intensity NIR irradiation as more blue upconverted photons are generated.

NIR-sensitive spiropyran derivatives assisted by UCNPs were also demonstrated (**Figure 1.19d**). With the assistance of UCNPs, upconverted UV light can trigger one-way photoisomerization of spiropyran form (SP) to the merocyanine form (MC) upon excitation of NIR light. But in this report, MC-SP isomerization can only be manipulated by visible light. In another report, SP-MC photoisomerization was triggered by UV light.^[47] But, MC-SP isomerization in the presence of UCNPs was controlled by upconverted visible light upon irradiation of NIR light. In these examples, only one-way isomerization (SP-MC/MC-SP) was reported. After these work, NIR-triggered reversible photoisomerization of spiropyran derivatives assisted by UCNPs was reported.^[48] 980 nm and 808 nm light can excite visible and UV emission in the presence of multiple-layer-structured UCNPs. These upconverted UV/visible photons can trigger isomerization of SP-MC/MC-SP. Thus, reversible photoisomerization of spiropyran derivatives can be controlled using 980/808 nm light assisted by multiple-layer-structured UCNPs.

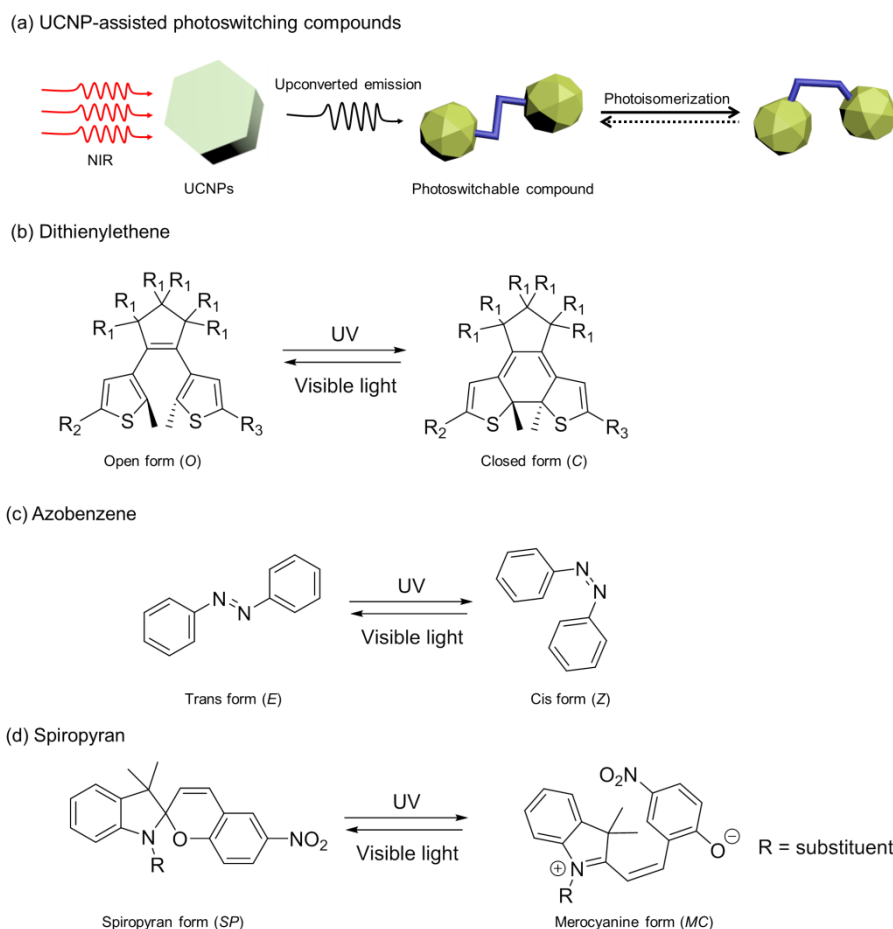


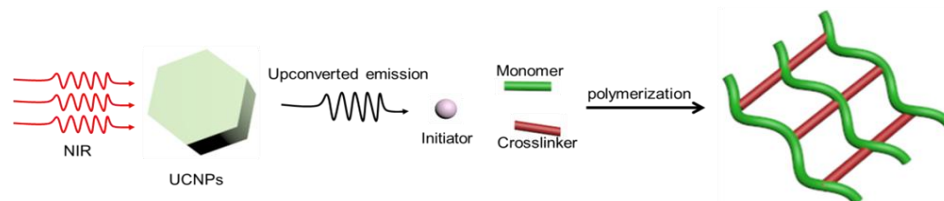
Figure 1.19. a) Schematic illustration of UCNP-assisted photoisomerization. Upconverted emission triggers photoisomerization of photoswitchable molecules. NIR-triggered Photoisomerization of b) dithienylethene derivatives,^[36] c) azobenzene derivatives,^[44] and d) spiropyran derivatives assisted by UCNPs.^[47b]

1.8.3. UCNP-assisted photoinitiators

UCNP-assisted photoinitiators consist of three main components including UCNPs, crosslinkers/monomers and photoinitiators/co-initiators.^[32] UCNP-assisted photoinitiators can be used for NIR-induced polymerization. Specifically, photoinitiators are excited by upconverted light. The excited photoinitiators can then initiate polymerization of crosslinkers and monomers (**Figure 1.20a**). Different conventional UV/visible-sensitive photoinitiators can be combined with different kinds of UCNPs which can upconvert UV/visible light for UCNP-assisted photoinitiators. Different crosslinkers/monomers, such as acrylates, methacrylates, acrylic acid and acrylamides, have been also used for NIR-induced

polymerization in the presence of UCNP-assisted photoinitiators. The reported NIR-induced polymerization in the presence of UCNP-assisted photoinitiators was summarized (**Figure 1.20b**).^[49] Compared to UCNP-assisted photolytic/photoswitching compounds, few studies on UCNP-assisted photoinitiators were reported. However, it should be noticed that these compounds have a great potential in deep photo-curable materials as NIR light has a good penetration capability.^[32]

(a) NIR-induced photopolymerization in the presence of UCNP-assisted photoinitiators



(b)

Initiator/Co-initiator	Monomer/Crosslinker
CQ	BiGMA
Eosin Y	TEGDMA
TEA	AA
BP	NVP
TEA	PEGDA
BDC	HEMA
DMPA	EbAM
MPPA	GA
Irgacure 784	AB
AMP	CEA
PXEP	PA
EXEP	oligomers
	BA
	VAc
	MMA

Figure 1.20. a) Schematic illustration of UCNP-assisted photopolymerization. The upconverted light induces photopolymerization of monomers and crosslinkers. b) Summarized structures of photoinitiators, co-initiators, crosslinkers and monomers for UCNP-assisted photopolymerization.^[49]

1.9 Bio-medical applications based on UCNP-assisted photosensitive compounds

Many NIR-responsive bio-medical materials are constructed based on UCNP-assisted photosensitive compounds. These materials can be responsive to NIR irradiation and some of them can functionalize in deep tissue. In the following, we will discuss some of their biomedical applications.^[32]

1.9.1 NIR-controlled drug delivery

Light-sensitive drug delivery system was explored for several years as using light as a stimuli source provides a temporal and spatial control method. Most of these drug delivery systems are triggered by UV/visible light. UV/visible light has several limitations in bio-medical application, such as biological toxicity of UV light, shallow tissue penetration depth, etc. Thus, it is desirable to use NIR to control drug delivery. UCNP-assisted photolytic compounds have been deployed for constructing NIR-controlled drug delivery systems.^[50] Zhao's group prepared photosensitive block copolymer micelles loaded with NaYF₄:Yb/Tm@NaYF₄ UCNPs and dyes as cargo models (**Figure 1.21a**).^[38a] Photolysis of o-nitrobenzyl groups can be triggered by upconverted UV photons upon excitation of 980 nm. The dyes loaded were then released due to dissociation of micelles caused by upconverted photolysis. Following the same strategy, NIR-triggered drug delivery was reported by Liu's group.^[38b] In their work, UCNPs and drugs were loaded in copolymer micelles. Cellular drug release can be controlled by NIR light assisted by UCNPs. Yan et al. also reported NIR-regulated release of protein from UCNP-loaded photodegradable hydrogel (**Figure 1.21b**).^[51] Specifically, upconverted UV light photocleaved o-nitrobenzyl groups grafted to the crosslinker of the hydrogel upon excitation of NIR light. Subsequently, the crosslinker was degraded and gel-sol transition was triggered. Finally, the proteins entrapped in the hydrogel were released.

In addition to polymeric carriers for drug delivery, inorganic drug nanocarriers were also combined with UCNPs for drug delivery. Liu et al. synthesized a core-shell nanocarriers for drug delivery by coating NaYF₄:Yb/Tm@NaYF₄ UCNPs with an mesoporous silica shell functionalized by azobenzene (**Figure 1.21c**).^[45] Doxorubicin was then loaded in the porous of shell. Continuous UCNP-assisted trans-cis-trans photoisomerization was triggered upon irradiation of 980 light, which led to the motion of azobenzene as an impeller. This impeller-like motion triggered release of doxorubicin. Our group also reported to use UCNP-assisted

photolysis of ruthenium complexes to control drug delivery.^[41d] UCNPs was coated with Ru complexes functionalized mesoporous silica. And doxorubicin was loaded in the mesoporous structures. Low-intensity NIR light could penetrate through a piece of tissue to trigger release of doxorubicin assisted by UCNPs. It should be noticed that thermal effect of NIR irradiation can also contribute to release of cargos from nanocarriers.^[52] Thus, to demonstrate that drug delivery is due to photochemical process rather than thermal effect, the cooling setup should be used and control experiments should be done.

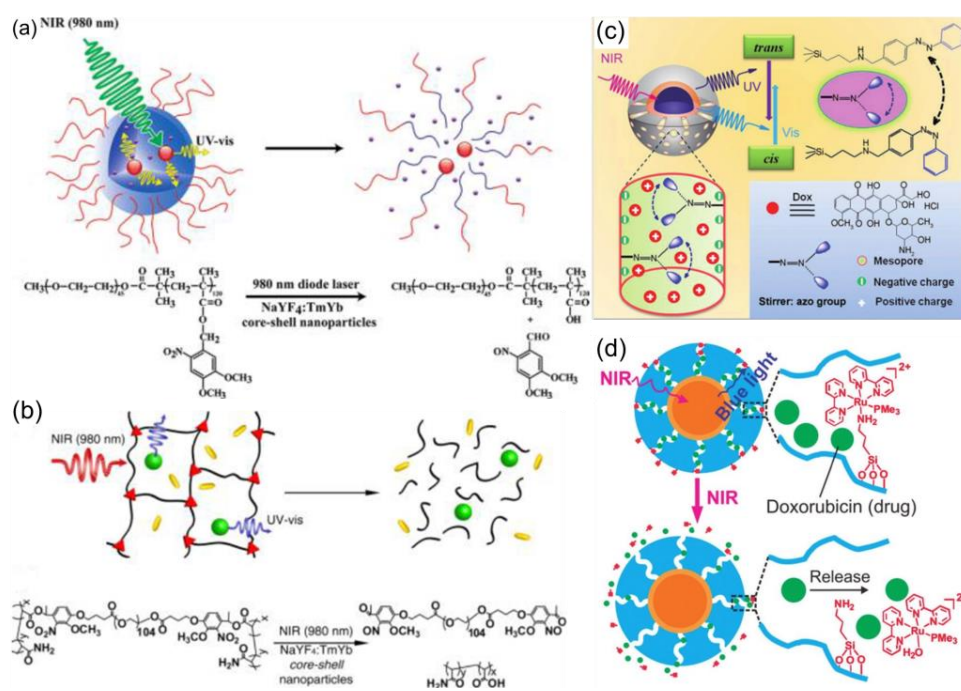


Figure 1.21. Drug delivery controlled by NIR light based on UCNP-assisted photolytic a,b) o-nitrobenzyl groups, c) azobenzene and d) ruthenium complex. Panel (a) reproduced with permission. Copyright 2009, American Chemical Society.^[38a] Panel (b) reproduced with permission. Copyright 2013, American Chemical Society.^[51] Panel (c) reproduced with permission. Copyright 2013, WILEY-VCH Verlag GmbH & Co. KGaA.^[45] Panel (d) reproduced with permission. Copyright 2015, Royal Society of Chemistry.^[41d]

1.9.2 NIR-modulated biocatalysis

Chemical and biological reactions can be catalyzed by biocatalysts, e.g., enzymes. Chen et al. demonstrated NIR-controlled biocatalysis assisted by UCNPs (**Figure 1.22**).^[47b] By utilizing photochromic spiropyrans conjugated upconversion nanophosphors, the one-way SP-

MC photoisomerization was triggered by NIR light and visible light was used for the MC-SP back photoisomerization. The reversible photoisomerization triggered by NIR light and visible light can alter wettability of the UCNP, which further triggered inversion of Pickering emulsions and induced the release of a biocatalyst in the aqueous phase.

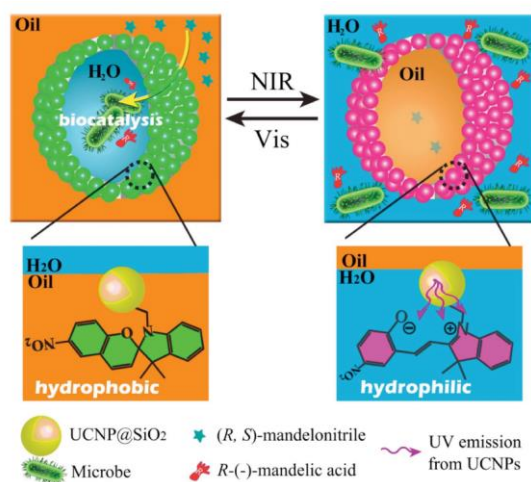


Figure 1.22. Schematic illustration of NIR-controlled reversible inversion of Pickering emulsions assisted by UCNP for biocatalysis. Reproduced with permission. Copyright 2014, American Chemical Society. ^[47b]

1.9.3 NIR-light-curable dental materials

UCNP-assisted photoinitiators were used for therapy of dental resins.^[53] Traditional way for treatment of caries lesions (**Figure 1.23a**) is to use UV or blue source. There were two shortages using UV/blue light therapy: (1) shallow penetration depth, which leads to a time-consuming layer-by-layer process; (2) problems of shrinkage and re-infection will be caused. To solve these problems, UCNP-assisted photopolymerization was used. UCNP can generate blue photons upon irradiation of NIR light, which facilitate polymerization of dental resins in a single step (**Figure 1.23b**). Moreover, it is possible to use this method to repair large and complex defects as NIR irradiation can pass through the tooth sides to trigger the UCNP-assisted photoinitiators for polymerization.

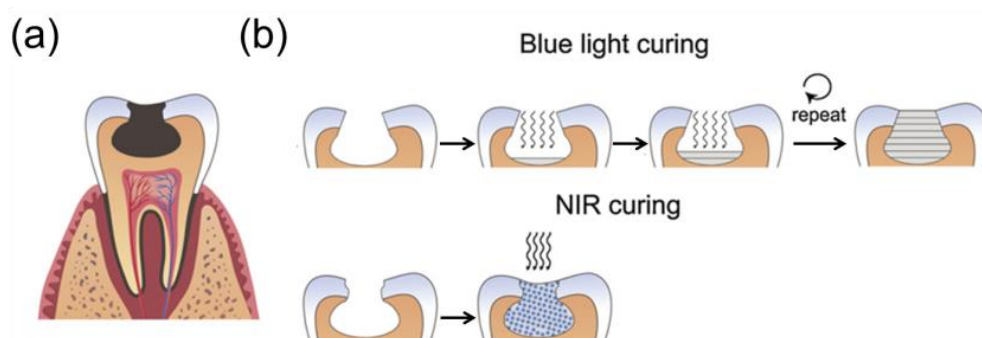


Figure 1.23. Schematic illustration of curing dental materials based on UCNP-assisted photoinitiators. a) caries lesions (dark area) in tooth. b) Blue light and NIR light curing process. Reproduced with permission. Copyright 2012, Elsevier. ^[53]

1.9.4 NIR-light-controlled biointerfaces

Photocontrol of implanted biomaterials surface is always achieved by UV light. But, UV light has biological toxicity and shallow penetration depth. Recently, Li et al. reported using NIR to control cell adhesion assisted by UCNPs.^[38d] Photocleavage of *o*-nitrobenzene modified RGD on the quartz surface was triggered by NIR light assisted by rod-shaped UCNP (**Figure 1.24a**). The photocleavage reaction triggered release of cells which were attached to RGD. In this work, the detachment is not reversible. Once photocleavage of *o*-nitrobenzene happened, the detached cells cannot be attached on the surface again. To solve this problem, the same group developed using UCNP-assisted photochemistry to dynamically regulate reversible cell adsorption and desorption (**Figure 1.24b**).^[54] Specifically, UCNPs have UV/visible emission at different excitation intensity. With the assistance of this UCNPs, reversible photoisomerization of spiropyrans was controlled by 980 nm light at different intensities. SP-MC isomerization can be triggered by NIR at high intensity and low-intensity NIR can trigger MC-SP isomerization assisted by UCNPs. Such reversible photoisomerization made a reversible cell adhesion and detachment on the substrate.

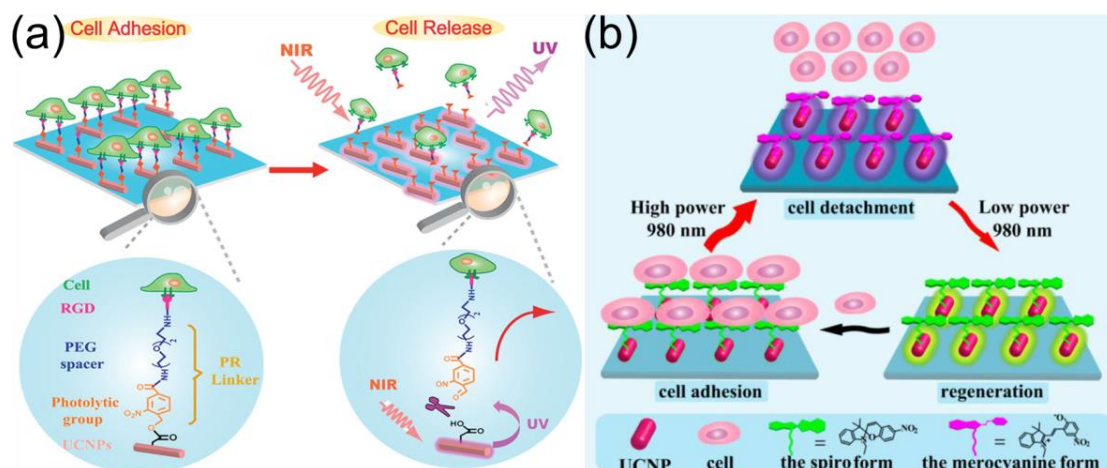


Figure 1.24. a) Schematic illustration of NIR-controlled cell release on the quartz surface assisted by UCNPs. b) Schematic illustration of regulating reversible cell adsorption and desorption dynamically by NIR light at different intensities assisted by UCNPs. Reproduced with permission. Panel (a) reproduced with permission. Copyright 2014, American Chemical Society. Panel (b) reproduced with permission. Copyright 2015, American Chemical Society. [38d, 54]

1.9.5 NIR-light-activated enzyme

Photoactivatable biomaterials provide a way to accurately remotely control biochemical processes in organisms. Most of photoactivatable biomaterials are triggered by UV light and visible light, but the phototoxicity of UV and the poor tissue penetration depth of UV/visible light limit their further applications *in vivo*. The group of Hsien-Ming Lee demonstrated using UCNP-assisted photochemistry to activate cellular enzymes (Figure 1.25).^[55] In their work, the activity of kinase A (PKA) enzyme was initially repressed by *o*-nitrobenzene. Upon irradiation with pulsed NIR light, *o*-nitrobenzene was photocleaved by upconverted UV light. The activity of the enzyme gradually increased with the photolysis of *o*-nitrobenzene.

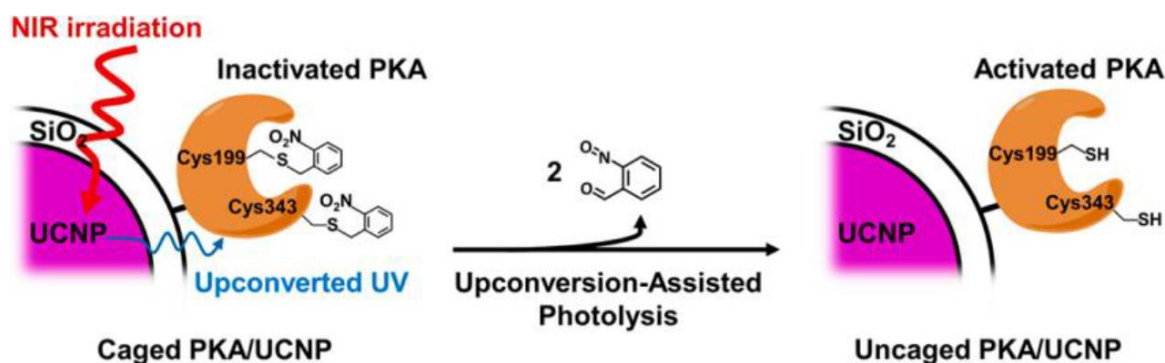


Figure 1.25. Caged PKA/UCNP complex design and the process of upconversion-assisted PKA uncaging. Reproduced with permission. Copyright 2015, American Chemical Society. [55]

1.10 Challenges and motivation

As introduced in previous part, compounds can be sensitive to NIR light with the assistance of UCNPs which can convert 974 nm/808 nm light to UV/visible emission. These UCNP-assisted compounds showed tremendous applications in bio-medical area. Also, our group and Salassa's group demonstrated NIR could trigger photolytic reaction of Ru complexes assisted by UCNPs.^[41b, 41d] Thus, UCNP-assisted Ru complexes for practical bio-medical use can be constructed through combination of UCNPs and Ru complexes. Although UCNP-assisted Ru complexes showed potential priorities for biomedical application,^[41d] it is not well studied and developed compared with other UCNP-assisted photosensitive compounds. Thus, UCNP-assisted UCNP-assisted Ru complexes is systematically studied in this thesis and some bio-medical challenges described as follows can be addressed based on UCNP-assisted Ru complexes developed by us. Besides these challenges, a new type of NIR-triggered photocoupling reaction assisted by UCNPs for bio-medical use was also developed in this thesis.

1.10.1 Safe intensity for for bio-medical application

Most of these UCNP-assisted photosensitive compounds for bio-medical application require high-intensity excitation source (more than 1 W/cm^2). Maximum permissible exposure of skin to continuous 980-nm laser is 0.726 W cm^{-2} , which is ruled in American national standard (**Figure 1.26**).^[17, 41d] Otherwise, the high-intensity laser irradiation will cause damages to cell, tissue and organisms. Thus, it is necessary to develop a UCNP-assisted

photosensitive compound triggered by low-intensity NIR light for bio-medical application. A good way to reduce required high-intensity irradiation for UCNP-assisted photosensitive compounds is to improve upconverting efficiency of UCNPs and photosensitive value of molecules in the system. Although lots of methods including changing host crystals,^[56] dye-sensitized methods^[57] and Li⁺/Mn²⁺ doping^[58] were used for improving the upconverting efficiency, the upconverting efficiency of these UCNPs is still low. Considering of this, to achieve a low-intensity-triggered UCNP-assisted photosensitive compound, more focus should be on developing responsive molecules with high photosensitive values. Thus, UCNP-assisted Ru complexes may solve the challenge.

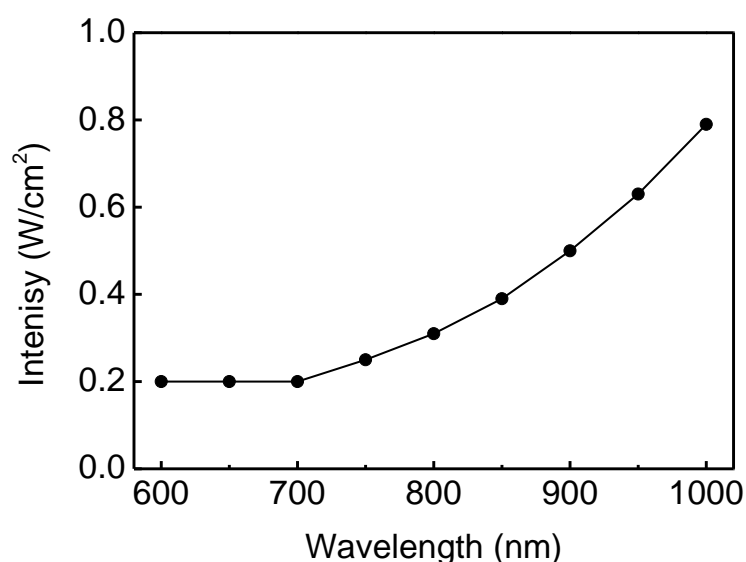


Figure 1.26. Maximum permissible exposure of skin to light irradiation ranging from 600 to 1000 nm.

1.10.2 Challenge of patterning biomaterials

Patterning biomaterials via photolithography is a very important technology in biological research.^[41a] In most cases, UV light is used for photo lithography.^[59] However, for patterning of biomaterials, the use of UV light is limited because it is not compatible with biomaterials, cannot penetrate deep into tissue, and lacks spatial resolution for in vivo applications. Compared to UV light, near-infrared (NIR) light is more suitable for photopatterning of biomaterials because NIR light causes less photodamage, scatters less and can penetrate deeper into tissues. One approach for the patterning of biomaterials using NIR light is based

on simultaneous two-photon absorption.^[25a] However, this method is inefficient as typical chromophores have small two-photon absorption cross-sections. Also, two-photon absorption can only occur at the focus of the femtosecond laser.^[17] Patterning biomaterials can only be produced by time-consuming spot-by-spot process. Thus, it is necessary to develop an efficient NIR-induced photolithography for patterning biomaterials

1.10.3 Challenge of pH manipulation

pH manipulation has been proposed as a powerful technique to control several diseases.^[60] However, most photoacids/bases are sensitive to only UV/visible light.^[61] UV light can damage DNA, cells and tissues and visible light has a poor tissue penetration depth. NIR light is better suited for biomedical applications. Therefore, pH manipulation for bio-medical use should be controlled by NIR light. Thus, controlling pH using NIR is necessary.

1.10.4 Challenge of photoinhibition of enzyme activities

Controlling the activities of enzymes is very important as they can regulate metabolism, manipulate cell functions, kill pathogens, and treat diseases.^[62] Light is a very ideal way to control the activity of enzyme as light provides high spatiotemporal resolution for controlling enzyme activities. However, only UV and NIR light via two-photon process can be used to control the enzyme activities.^[63] UV has biological toxicity and NIR light-sensitive materials via two-photon process required expensive setups and have low efficiency. NIR-triggered photoinhibition of enzyme activity via simultaneous two-photon absorption has the typical disadvantages of two-photon system demonstrated in the previous part. As a result, efficient NIR-induced photoinhibition of enzyme activity should be developed.

1.10.5 Challenge of photocoupling technology for bio-medical application

Photoinducible click chemistry is a powerful technique for visualizing protein perturbation in live cells, which is important for tracing protein dynamics and function in cells.^[64] Essentially, click reaction is a kind of photocoupling reaction. Fluorescent molecules can be covalently coupled to modified protein for the visualization of protein upon light irradiation based on biorthogonal reaction.^[65] As a typical photo-triggered click chemistry, tetrazole-alkene cycloaddition reaction, was well developed for visualizing protein.^[66] However, most of these photocycloadditions were only triggered by UV, visible light, which hindered its further application in vivo.^[67] NIR light is an ideal source for photoinducible biorthogonal reaction.^[66] Currently, only two-photon process can be used to achieve a NIR-sensitive click

reaction. However, the two-photon process required expensive lase and had low efficiency.^[17] Thus, developing a new NIR-triggered photocoupling technology for bio-medical application is of great importance.

To solve these challenges, UCNPs and Ru complexes were combined together to develop UCNP-assisted Ru complexes. The UCNP-assisted Ru complexes can be responsive to low-intensity NIR light (**Chapter 2**). Then, NIR light was used to pattern biomaterials based on UCNP-assisted Ru complexes in the presence of a photomask (**Chapter 3**). After this work, NIR-triggered pH manipulation was reported by us based on UCNP-assisted Ru complexes (**Chapter 4**). Also, we demonstrated how to realize NIR-controlled enzyme activity based on UCNP-assisted Ru complexes (**Chapter 5**). Besides these applications demonstrated in this thesis, a new efficient NIR-induced photocoupling technology assisted by UCNPs was also developed here for bio-medical application (**Chapter 6**).

References

- [1] J. A. Love, J. P. Morgan, T. M. Trnka, R. H. Grubbs, *Angew. Chem. Int. Ed.* **2002**, *41*, 4035.
- [2] P. V. Kamat, I. Bedja, S. Hotchandani, L. K. Patterson, *J. Phys. Chem.* **1996**, *100*, 4900.
- [3] P. Wang, S. M. Zakeeruddin, J. E. Moser, M. K. Nazeeruddin, T. Sekiguchi, M. Grätzel, *Nat. Mater.* **2003**, *2*, 402.
- [4] S. Laïb, B. H. Fellah, A. Fatimi, S. Quillard, C. Vinatier, O. Gauthier, P. Janvier, M. Petit, B. Bujoli, S. Bohic, *Biomaterials* **2009**, *30*, 1568.
- [5] P. A. Anderson, G. B. Deacon, K. H. Haarmann, F. R. Keene, T. J. Meyer, D. A. Reitsma, B. W. Skelton, G. F. Strouse, N. C. Thomas, J. A. Treadway, *Inorg. Chem.* **1995**, *34*, 6145.
- [6] L. Zayat, O. Filevich, L. M. Baraldo, R. Etchenique, *Philos. Trans. A Math. Phys. Eng. Sci.* **2013**, *371*, 20120330.
- [7] D. V. Pinnick, B. Durham, *Inorg. Chem.* **1984**, *23*, 1440.
- [8] L. Zayat, M. Salierno, R. Etchenique, *Inorg. Chem.* **2006**, *45*, 1728.
- [9] R. E. Goldbach, I. Rodriguez-Garcia, J. H. van Lenthe, M. A. Siegler, S. Bonnet, *Chem-Eur J.* **2011**, *17*, 9924.
- [10] S. Bonnet, J.-P. Collin, *Chem.Soc. Rev.* **2008**, *37*, 1207.
- [11] F. Dwyer, H. Goodwin, E. Gyarfas, *Aust. J. Chem.* **1963**, *16*, 544.
- [12] L. Zayat, M. G. Noval, J. Campi, C. I. Calero, D. J. Calvo, R. Etchenique, *ChemBioChem* **2007**, *8*, 2035.
- [13] a S. Bonnet, B. Limburg, J. D. Meeldijk, R. J. M. K. Gebbink, J. A. Killian, *J. Am. Chem. Soc.* **2011**, *133*, 252; b T. Respondek, R. N. Garner, M. K. Herroon, I. Podgorski, C. Turro, J. J. Kodanko, *J. Am. Chem. Soc.* **2011**, *133*, 17164; c T. Respondek, R. Sharma, M. K. Herroon, R. N. Garner, J. D. Knoll, E. Cueny, C. Turro, I. Podgorski, J. J. Kodanko, *Chemmedchem* **2014**, *9*, 1306.
- [14] R. E. Goldbach, I. Rodriguez-Garcia, J. H. van Lenthe, M. A. Siegler, S. Bonnet, *Chem-Eur J.* **2011**, *17*, 9924.
- [15] W. Sun, M. Parowatkin, W. Steffen, H. J. Butt, V. Mailänder, S. Wu, *Adv. Healthc. Mater.* **2016**, *5*, 467.
- [16] L. Zayat, C. Calero, P. Alborés, L. Baraldo, R. Etchenique, *J. Am. Chem. Soc.* **2003**, *125*, 882.

- [17] Z. Chen, W. Sun, H. J. Butt, S. Wu, *Chem-Eur J.* **2015**, *21*, 9165.
- [18] L. Zayat, M. G. Noval, J. Campi, C. I. Calero, D. J. Calvo, R. Etchenique, *Chembiochem* **2007**, *8*, 2035.
- [19] M. Frascioni, Z. Liu, J. Lei, Y. Wu, E. Strelakova, D. Malin, M. W. Ambrogio, X. Chen, Y. Y. Botros, V. L. Cryns, *J. Am. Chem. Soc.* **2013**, *135*, 11603.
- [20] W. Sun, S. Li, B. Häupler, J. Liu, S. Jin, W. Steffen, U. S. Schubert, H. J. Butt, X. J. Liang, S. Wu, *Adv. Mater.* **2016**. DOI: 10.1002/adma.201603702.
- [21] O. Filevich, L. Zayat, L. M. Baraldo, R. Etchenique, in *Luminescent and Photoactive Transition Metal Complexes as Biomolecular Probes and Cellular Reagents*, Springer, **2014**, 47.
- [22] J. C. Griepenburg, T. L. Rapp, P. J. Carroll, J. Eberwine, I. J. Dmochowski, *Chem. Sci.* **2015**, *6*, 2342.
- [23] P. Juzenas, A. Juzeniene, O. Kaalhus, V. Iani, J. Moan, *Photoch. Photobio. Sci.* **2002**, *1*, 745.
- [24] a Q. Lin, Q. Huang, C. Li, C. Bao, Z. Liu, F. Li, L. Zhu, *J. Am. Chem. Soc.* **2010**, *132*, 10645-10647; b N. Kandoth, V. Kirejev, S. Monti, R. Gref, M. B. Ericson, S. Sortino, *Biomacromolecules* **2014**, *15*, 1768.
- [25] a V. n. San Miguel, M. Álvarez, O. Filevich, R. Etchenique, A. n. del Campo, *Langmuir* **2011**, *28*, 1217; b L. Zayat, M. Salierno, R. Etchenique, *Inorg. chem.* **2006**, *45*, 1728.
- [26] P. Lederhose, Z. Chen, R. Müller, J. P. Blinco, S. Wu, C. Barner-Kowollik, *Angew. Chem. Int. Ed.* **2016**, *55*, 12195.
- [27] S. H. Askes, A. Bahreman, S. Bonnet, *Angew. Chem. Int. Ed.* **2014**, *53*, 1029.
- [28] C. Parker, C. Hatchard, T. A. Joyce, *Analyst* **1965**, *90*, 1.
- [29] a T. N. Singh-Rachford, F. N. Castellano, *Coordin. Chem. Rev.* **2010**, *254*, 2560; b F. Deng, Bowling Green State University **2014**.
- [30] G. Chen, H. Qiu, P. N. Prasad, X. Chen, *Chem. rev.* **2014**, *114*, 5161.
- [31] J. Zhou, Z. Liu, F. Li, *Chem. Soc. Rev.* **2012**, *41*, 1323.
- [32] S. Wu, H. J. Butt, *Adv. Mater.* **2016**, *28*, 1208.
- [33] M. Haase, H. Schäfer, *Angew. Chem. Int. Ed.* **2011**, *50*, 5808.
- [34] F. Zhang, *Photon upconversion nanomaterials*, Springer, **2015**.
- [35] X. Liu, C.-H. Yan, J. A. Capobianco, *Chem. Soc. Rev.* **2015**, *44*, 1299.
- [36] C.-J. Carling, J.-C. Boyer, N. R. Branda, *J. Am. Chem. Soc.* **2009**, *131*, 10838.

- [37] C. J. Carling, F. Nourmohammadian, J. C. Boyer, N. R. Branda, *Angew. Chem. Int. Ed.* **2010**, *122*, 3870.
- [38] a B. Yan, J.-C. Boyer, N. R. Branda, Y. Zhao, *J. Am. Chem. Soc.* **2011**, *133*, 19714; b G. Liu, L. Zhou, Y. Su, C.-M. Dong, *Chem. Commun.* **2014**, *50*, 12538; c B. Yan, J.-C. Boyer, D. Habault, N. R. Branda, Y. Zhao, *J. Am. Chem. Soc.* **2012**, *134*, 16558; d W. Li, J. Wang, J. Ren, X. Qu, *J. Am. Chem. Soc.* **2014**, *136*, 2248; e M. L. Viger, M. Grossman, N. Fomina, A. Almutairi, *Adv. Mater.* **2013**, *25*, 3733; f Y. Yang, B. Velmurugan, X. Liu, B. Xing, *Small* **2013**, *9*, 2937; g M. K. G. Jayakumar, N. M. Idris, Y. Zhang, *Proc. Natl. Acad. Sci. U S A.* **2012**, *109*, 8483; h J. Shen, G. Chen, T. Y. Ohulchanskyy, S. J. Kesseli, S. Buchholz, Z. Li, P. N. Prasad, G. Han, *Small* **2013**, *9*, 3213; i Y. Yang, Q. Shao, R. Deng, C. Wang, X. Teng, K. Cheng, Z. Cheng, L. Huang, Z. Liu, X. Liu, *Angew. Chem. Int. Ed.* **2012**, *51*, 3125; j Y.-H. Chien, Y.-L. Chou, S.-W. Wang, S.-T. Hung, M.-C. Liau, Y.-J. Chao, C.-H. Su, C.-S. Yeh, *Acs Nano* **2013**, *7*, 8516; k L. Zhao, J. Peng, Q. Huang, C. Li, M. Chen, Y. Sun, Q. Lin, L. Zhu, F. Li, *Adv. Funct. Mater.* **2014**, *24*, 363; l Z. Chen, W. Sun, H. J. Butt, S. Wu, *Chem-Eur J.* **2015**, *21*, 9165; m L. Z. Zhao, J. J. Peng, Q. Huang, C. Y. Li, M. Chen, Y. Sun, Q. N. Lin, L. Y. Zhu, F. Y. Li, *Adv. Funct. Mater.* **2014**, *24*, 363.
- [39] a Y. Dai, H. Xiao, J. Liu, Q. Yuan, P. a. Ma, D. Yang, C. Li, Z. Cheng, Z. Hou, P. Yang, *J. Am. Chem. Soc.* **2013**, *135*, 18920; b Y. Min, J. Li, F. Liu, E. K. Yeow, B. Xing, *Angew. Chem. Int. Ed.* **2014**, *126*, 1030; c E. Ruggiero, J. Hernández-Gil, J. C. Mareque-Rivas, L. Salassa, *Chem. Commun.* **2015**, *51*, 2091.
- [40] A. E. Pierri, P.-J. Huang, J. V. Garcia, J. G. Stanfill, M. Chui, G. Wu, N. Zheng, P. C. Ford, *Chem. Commun.* **2015**, *51*, 2072.
- [41] a Z. J. Chen, S. Q. He, H. J. Butt, S. Wu, *Adv. Mater.* **2015**, *27*, 2203; b E. Ruggiero, A. Habtemariam, L. Yate, J. C. Mareque-Rivas, L. Salassa, *Chem. Commun.* **2014**, *50*, 1715; c Z. Chen, Y. Xiong, R. Etchenique, S. Wu, *Chem. Commun.* **2016**, *52*, 13959; d S. Q. He, K. Krippes, S. Ritz, Z. J. Chen, A. Best, H. J. Butt, V. Mailander, S. Wu, *Chem. Commun.* **2015**, *51*, 431.
- [42] T. Wu, M. Barker, K. M. Arafteh, J. C. Boyer, C. J. Carling, N. R. Branda, *Angew. Chem. Int. Ed.* **2013**, *52*, 11106.
- [43] L. Wang, H. Dong, Y. Li, R. Liu, Y. F. Wang, H. K. Bisoyi, L. D. Sun, C. H. Yan, Q. Li, *Adv. Mater.* **2015**, *27*, 2065.
- [44] W. Wu, L. Yao, T. Yang, R. Yin, F. Li, Y. Yu, *J. Am. Chem. Soc.* **2011**, *133*, 15810.

- [45] J. Liu, W. Bu, L. Pan, J. Shi, *Angew. Chem. Int. Ed.* **2013**, *52*, 4375.
- [46] L. Wang, H. Dong, Y. Li, C. Xue, L.-D. Sun, C.-H. Yan, Q. Li, *Angew. Chem. Int. Ed.* **2014**, *136*, 4480.
- [47] a B. F. Zhang, M. Frigoli, F. Angiuli, F. Vetrone, J. A. Capobianco, *Chem. Commun.* **2012**, *48*, 7244; b Z. Chen, L. Zhou, W. Bing, Z. Zhang, Z. Li, J. Ren, X. Qu, *J. Am. Chem. Soc.* **2014**, *136*, 7498.
- [48] J. Lai, Y. Zhang, N. Pasquale, K. B. Lee, *Angew. Chem. Int. Ed.* **2014**, *53*, 14419.
- [49] a A. Stepuk, D. Mohn, R. N. Grass, M. Zehnder, K. W. Krämer, F. Pellé, A. Ferrier, W. J. Stark, *Dent. Mater.* **2012**, *28*, 304; b S. Beyazit, S. Ambrosini, N. Marchyk, E. Palo, V. Kale, T. Soukka, B. Tse Sum Bui, K. Haupt, *Angew. Chem. Int. Ed.* **2014**, *53*, 8919; c Q. Xiao, Y. Ji, Z. Xiao, Y. Zhang, H. Lin, Q. Wang, *Chem. Commun.* **2013**, *49*, 1527; d C. Ding, J. Wang, W. Zhang, X. Pan, Z. Zhang, W. Zhang, J. Zhu, X. Zhu, *Polym. Chem.* **2016**, *7*, 7370; e R. Liu, H. Chen, Z. Li, F. Shi, X. Liu, *Polym. Chem.* **2016**, *7*, 2457.
- [50] A. Bagheri, H. Arandiyan, C. Boyer, M. Lim, *Adv. Sci.* **2016**, *3*, 1500437.
- [51] B. Yan, J. C. Boyer, D. Habault, N. R. Branda, Y. Zhao, *J. Am. Chem. Soc.* **2012**, *134*, 16558.
- [52] J. Dong, J. I. Zink, *Small* **2015**, *11*, 4165.
- [53] A. Stepuk, D. Mohn, R. N. Grass, M. Zehnder, K. W. Kramer, F. Pelle, A. Ferrier, W. J. Stark, *Dent. Mater.* **2012**, *28*, 304.
- [54] W. Li, Z. Chen, L. Zhou, Z. Li, J. Ren, X. Qu, *J. Am. Chem. Soc.* **2015**, *137*, 8199.
- [55] H. D. Gao, P. Thanasekaran, C. W. Chiang, J. L. Hong, Y. C. Liu, Y. H. Chang, H. M. Lee, *Acs Nano* **2015**, *9*, 7041.
- [56] G. Chen, J. Shen, T. Y. Ohulchanskyy, N. J. Patel, A. Kutikov, Z. Li, J. Song, R. K. Pandey, H. Ågren, P. N. Prasad, *ACS nano* **2012**, *6*, 8280.
- [57] a G. Chen, J. Damasco, H. Qiu, W. Shao, T. Y. Ohulchanskyy, R. R. Valiev, X. Wu, G. Han, Y. Wang, C. Yang, *Nano letters* **2015**, *15*, 7400; b X. Wu, Y. Zhang, K. Takle, O. Bilsel, Z. Li, H. Lee, Z. Zhang, D. Li, W. Fan, C. Duan, *ACS nano* **2016**, *10*, 1060.
- [58] a W. Yin, L. Zhao, L. Zhou, Z. Gu, X. Liu, G. Tian, S. Jin, L. Yan, W. Ren, G. Xing, *Chem-Eur J.* **2012**, *18*, 9239; b S. Zeng, Z. Yi, W. Lu, C. Qian, H. Wang, L. Rao, T. Zeng, H. Liu, H. Liu, B. Fei, *Adv. Funct. Mater.* **2014**, *24*, 4051.
- [59] W. Wang, Z. Cheng, P. Yang, Z. Hou, C. Li, G. Li, Y. Dai, J. Lin, *Adv. Funct. Mater.* **2011**, *21*, 456.

-
- [60] N. Abeyrathna, Y. Liao, *J. Am. Chem. Soc.* **2015**, *137*, 11282.
- [61] M. Shirai, H. Okamura, *Prog. Org. Coat.* **2009**, *64*, 175.
- [62] J. M. Berg, J. L. Tymoczko, L. Stryer, New York: WH Freeman, **2002**.
- [63] a A. Leonidova, C. Mari, C. Aebersold, G. Gasser, *Organometallics* **2016**, *35*, 851; b H. Kaufman, Vratsano.Sm, B. F. Erlanger, *Science* **1968**, *162*, 1487.
- [64] R. Nussinov, *Chem. Rev.* **2016**, *116*, 6263,.
- [65] A. Herner, Q. Lin, *Top. Curr. Chem.* **2016**, *374*, 1.
- [66] J. Li, P. R. Chen, *Nat. Chem. Biol.* **2016**, *12*, 129.
- [67] P. Lederhose, K. N. Wüst, C. Barner-Kowollik, J. P. Blinco, *Chem. Commun.* **2016**, *52*, 5928.

Abbreviations

UCNPs	upconverting nanoparticles
Ru complexes	ruthenium(II)polypyridyl complexes
NIR	near-infrared light
UV	ultraviolet
AA	acrylic acid
W	Watt
APS	3-aminopropyltriethoxysilane
CLSM	confocal laser scanning microscopy
CVD	chemical vapor deposition
μm	micrometer
nm	nanometer
PAA	poly(acrylic acid)
rpm	round per minute
SEM	scanning electron microscopy
TEM	transmission electron microscopy
NMR	Nuclear magnetic resonance
THF	tetrahydrofuran
M	mol/L

Chapter 2: Upconverting-nanoparticle-assisted photochemistry induced by low-intensity near-infrared light: how low can we go?

Zhijun Chen, Wen Sun, Hans-Jürgen Butt, and Si Wu*

Max Planck Institute for Polymer Research, Ackermannweg 10, D-55128, Mainz (Germany)

Published in *Chem. Eur. J.*, 2015, **21**, 9165.

Reproduced from *Chem. Eur. J.*, 2015, **21**, 9165 with permission from the WILEY-VCH Verlag GmbH & Co. KGaA.

2.1 Statement of contribution

Si Wu conceived the idea and led the project. Si Wu and Hans-Jürgen Butt led the project.

Zhijun CHEN synthesized all the materials (UNCNPs, NB-1, CM-2, CM-3, Ru-4) and conducted the measurements

Wen Sun synthesized Ru-5.

2.2 Abstract: Upconverting nanoparticles (UCNPs) convert near-infrared (NIR) light into UV or visible light that can trigger photoreactions of photosensitive compounds. In this paper, we demonstrate how to reduce the intensity of NIR light for UCNP-assisted photochemistry. We synthesized two types of UCNPs with different emission bands and five photosensitive compounds with different absorption bands. A 974-nm laser was used to induce photoreactions in all of the investigated photosensitive compounds in the presence of the UCNPs. The excitation thresholds of the photoreactions induced by 974-nm light were measured. The lowest threshold was 0.5 W/cm^2 , which is lower than the maximum permissible exposure of skin (0.726 W/cm^2). We demonstrate that low-intensity NIR light can induce photoreactions after passing through a piece of tissue without damaging the tissue. Our results indicate that the threshold for UCNP-assisted photochemistry can be reduced using highly photosensitive compounds that absorb upconverted visible light. Low excitation intensity in UCNP-assisted photochemistry is important for biomedical applications because it minimizes the overheating problems of NIR light and causes less photodamage to biomaterials.

2.3 Introduction

Photochemistry has numerous biomedical applications, including photoinduced drug delivery,^[1] photo-controlled cell adhesion and migration,^[2] and photopatterning of extracellular matrices.^[3] Photoreactions are usually induced by UV light because only UV light can be efficiently absorbed by most photosensitive compounds. However, UV light is problematic in biomedical applications because it may damage biomaterials such as DNA and because it cannot penetrate deeply into tissue. Compared with UV light, near-infrared (NIR) light is better suited for biomedical applications. NIR light causes less photodamage, and it can penetrate deeper into tissue. One approach to inducing photoreactions by NIR light is based on simultaneous two-photon absorption.^[4] For example, to induce the photoreaction of a photosensitive compound with an absorption band at 400 nm, the photosensitive compound may absorb two 800-nm photons simultaneously. However, two-photon absorption is inefficient even when pulsed lasers are used because photosensitive compounds typically have small two-photon absorption cross-sections. Two-photon absorption only occurs at the focus of a laser because it requires high-intensity light. To induce photoreactions on a macroscopic scale by two-photon absorption, photosensitive compounds must be exposed to high-intensity light via a time-consuming spot-by-spot process. The development of new methods that can efficiently induce photoreactions by NIR light is therefore desirable.

An alternative approach to achieving NIR-light-induced photochemistry is based on photon upconversion by lanthanide-doped upconverting nanoparticles (UCNPs). UCNPs convert NIR light into UV and visible light that can induce photoreactions of normal photosensitive compounds.^[5] This process is referred to as UCNP-assisted photochemistry. Photoreactions, including photoisomerization,^[6] photocleavage,^[7] and photopolymerization reactions,^[8] have been induced by NIR light via UCNP-assisted photochemistry. UCNP-assisted photochemistry also has biomedical applications such as drug delivery^[7a, 9] and controlled cell adhesion.^[10] One advantage of photon upconversion is that it does not require high-intensity pulsed lasers. UCNPs can be excited by continuous-wave NIR laser diodes with relatively low intensity, thereby enabling photoreactions to be conducted on a macroscopic scale via UCNP-assisted photochemistry. Photon upconversion is a nonlinear optical process^[11] that requires the excitation intensity to exceed a certain threshold. The reported excitation intensity for UCNP-assisted photochemistry is typically between several hundred mW/cm² to several hundred W/cm².^[5-10] However, according to the “American National Standard for Safe Use of

Lasers,” the maximum permissible exposure of skin to NIR light with wavelengths from 650 to 980 nm ranges from 0.2 to 0.726 W/cm².^[12] The relatively high-intensity NIR light required by UCNP-assisted photochemistry may damage cells,^[13] tissue (**Figure 1**), and other biomaterials.^[14] Therefore, the reduction of the excitation intensity for UCNP-assisted photochemistry to a medically harmless level is an important objective. However, methods for achieving such a reduction of excitation intensity have not been systematically studied. Such a study is essential for advancing the biomedical applications of UCNP-assisted photochemistry.

Here, we investigated the design of suitable combinations of UCNPs and photosensitive compounds to reduce the excitation intensity for UCNP-assisted photochemistry. UCNP-assisted photochemistry requires that photosensitive compounds absorb upconverted light from UCNPs (**Figure 2a**); i.e., the emission bands of the UCNPs should overlap with the absorption bands of the photosensitive compounds. We prepared two types of UCNPs with different emission bands and five photosensitive compounds with different absorption bands. We systematically studied the UCNP-assisted photochemistry of the photosensitive compounds in the presence of the UCNPs. This study provides insights into the design of materials that are sensitive to low-intensity NIR light.

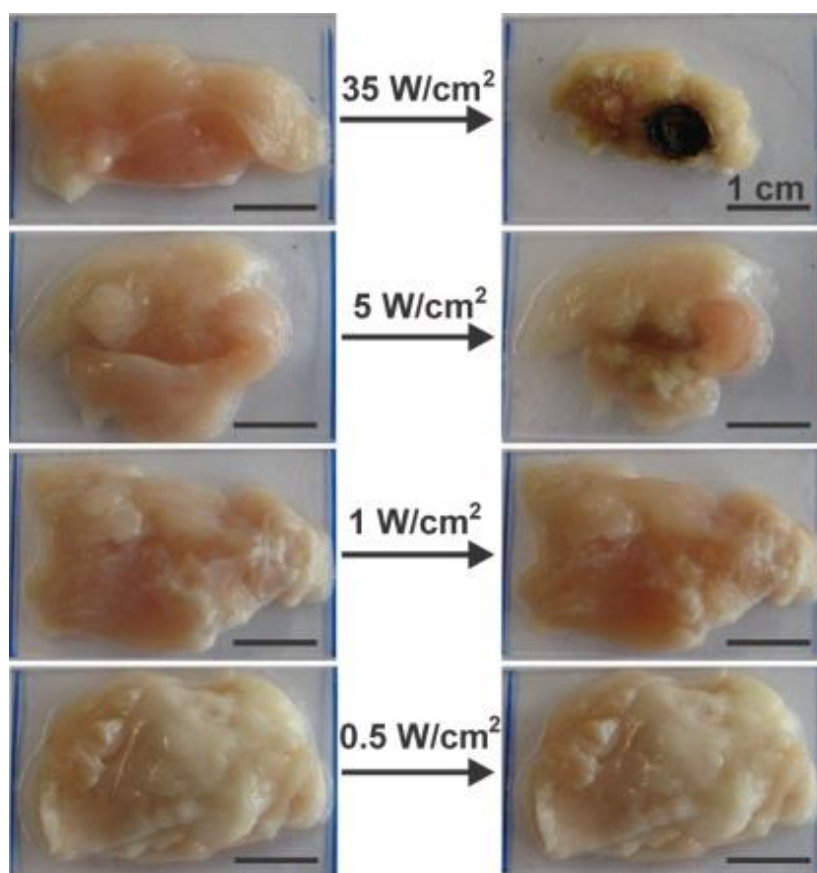


Figure 1. Chicken tissue before and after 974-nm light irradiation for 20 min. 974-nm light with intensities of 35 W/cm^2 and 5 W/cm^2 caused burn wounds and shrinking of the tissue. 974-nm light with an intensity less than 1 W/cm^2 did not cause observable burn wounds. The scale bars represent 1 cm.

2.4 Results and discussion

To construct systems for UCNP-assisted photochemistry, we used five photocleavable compounds (**Figure 2b**); their photoreactions are shown in **Figure S1**. Because their absorption bands are located at different wavelengths (**Figure 3a** and **Table 1**), these photocleavable compounds are sensitive to light of different wavelengths. The nitrobenzyl derivative NB-1 and the coumarin derivative CM-2 are sensitive to 365-nm light (**Figure S2, S3**). The coumarin derivative CM-3 and the Ru complex Ru-4 are sensitive to 365-nm, 470-nm and 530-nm light (**Figure S4, S5**). The Ru complex Ru-5 is sensitive to 365-nm, 470-nm, 530-nm and 656-nm light (**Figure S6**). Several photochemical properties of the photocleavable compounds, such as their absorption maximum (λ_{max}), absorption coefficient (ϵ), quantum yield (Φ), and photosensitivity ($\epsilon\Phi$), were measured (**Figure S2–S6** and **Table S1**); the results are listed in **Table 1**.

UCNPs are the other component used to construct systems for UCNP-assisted photochemistry. We prepared Tm-UCNP (core = NaYF₄: 0.5 mol % Tm³⁺: 30 mol % Yb³⁺; shell = NaYF₄) and Er-UCNP (core = NaYF₄: 2 mol % Er³⁺: 30 mol % Yb³⁺; shell = NaYF₄). These UCNPs are two of the most efficient UCNPs reported to date.^[5b,15] The average diameters of both UCNPs, as measured by TEM, were ~50 nm (**Figure 2c,d**).

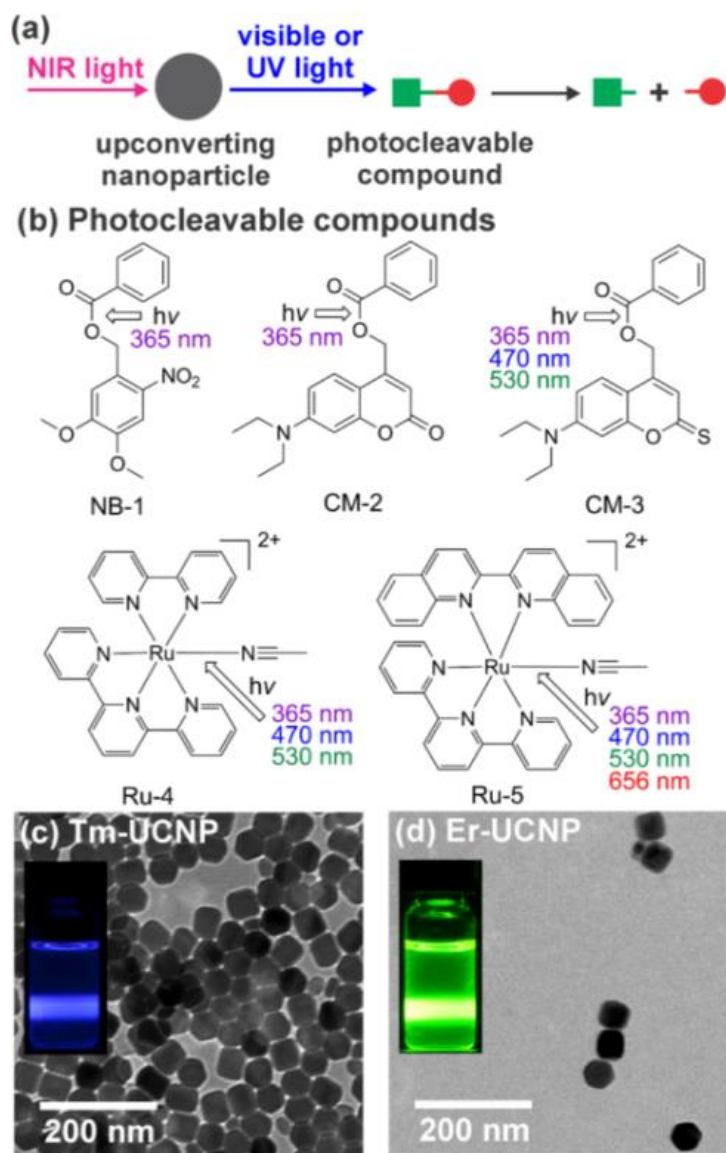


Figure 2. (a) Schematic of UCNP-assisted photochemistry. UCNPs convert NIR light into UV or visible light that induces photoreactions of photocleavable compounds. (b) Chemical structures of five photocleavable compounds. The photocleavable bonds are indicated by the arrows. (c), (d) TEM images of Tm-UCNP and Er-UCNP. The insets show photographs of the UCNPs after 974-nm laser exposure.

We measured the emission spectra of the Tm-UCNPs at different excitation intensities with a 974-nm laser (**Figure 3b, S7**). The Tm-UCNPs emitted both blue and UV light at excitation intensities greater than 2.2 W/cm². When the excitation intensity was between 0.19 and 2.2 W/cm², only blue light was emitted. The relative intensity of the emissions depends on the excitation intensity.^[6a,11,16] The excitation thresholds for the ¹I₆-³F₄ transition (340 nm, five-photon process^[16,17]), ¹D₂-³H₆ transition (360 nm, four-photon process^[16,17]), ¹D₂-³F₄ transition (450 nm, four-photon process^[16,17]), and ¹G₄-³H₆ transition (470 nm, three-photon process^[16,17]) were 5.5, 2.2, 0.64 and 0.19 W/cm², respectively (**Table 2**). Thus, at relatively low excitation intensities (0.19-2.2 W/cm²), the blue emission remains and the UV emission completely vanishes. The photoreactions of NB-1 and CM-2 can be induced by the four-photon NIR-to-UV upconversion that requires greater excitation intensity. The photoreactions of CM-3, Ru-4 and Ru-5 can be induced by either the four-photon NIR-to-UV upconversion that requires greater excitation intensity or the three-photon NIR-to-blue light upconversion that requires lower excitation intensity. Therefore, assisted by Tm-UCNP, the photoreactions of CM-3, Ru-4 and Ru-5 might require lower excitation intensities than those required for the photoreactions of NB-1 and CM-2.

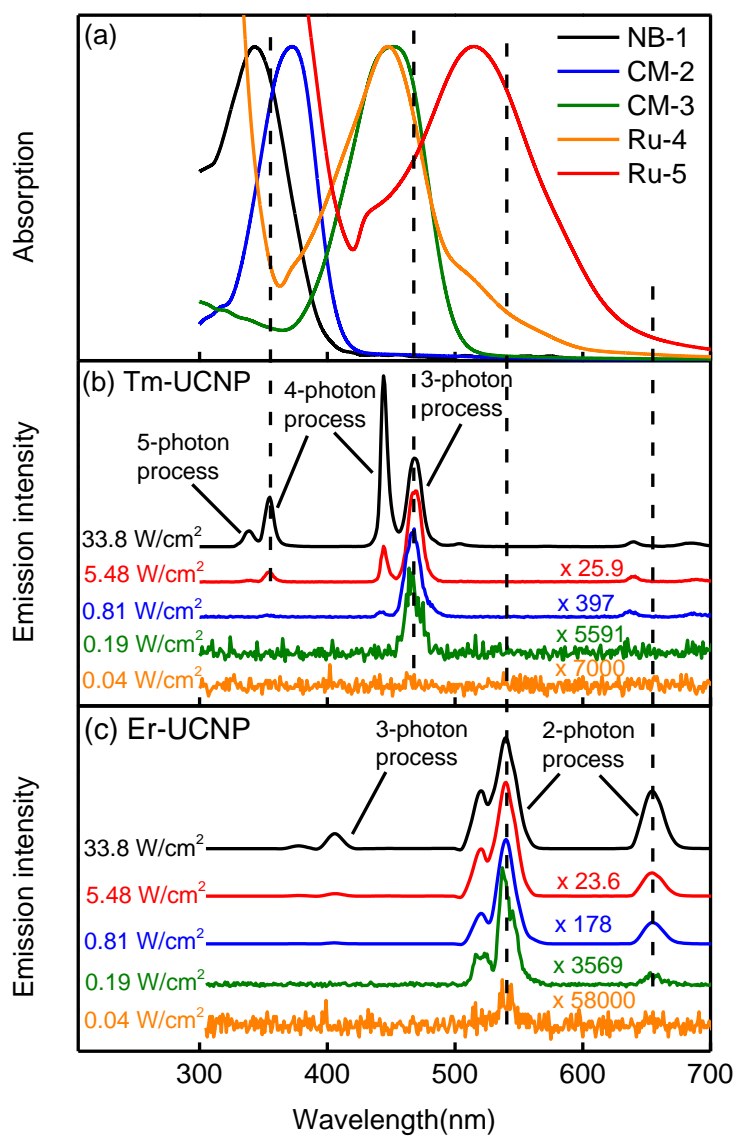


Figure 3. (a) UV-vis absorption spectra of five photocleavable compounds. (b), (c) Emission spectra of Tm-UCNP and Er-UCNP excited by a 974-nm laser with different excitation intensities. The excitation intensity was controlled by a laser driver. The emission intensities of Tm-UCNP and Er-UCNP are normalized at 470 nm and 540 nm, respectively.

Table 1. Summary of the photochemical properties of photocleavable compounds.^[a]

Compound	λ_{max} (nm)	$\epsilon@_{\lambda_{max}}$ (M ⁻¹ cm ⁻¹)	$\epsilon\Phi@365$ nm (M ⁻¹ cm ⁻¹)	$\epsilon\Phi@470$ nm (M ⁻¹ cm ⁻¹)	$\epsilon\Phi@530$ nm (M ⁻¹ cm ⁻¹)	$\epsilon\Phi@656$ nm (M ⁻¹ cm ⁻¹)
NB-1	343	5333	19.4	0	0	0
CM-2	373	32266	47.5	0	0	0
CM-3	453	26666	9.4	33.4	0.7	0
Ru-4	448	8000	35.8	56.5	23.1	0
Ru-5	515	6933	53.8	71.4	138.8	42.7

[a] Symbols and abbreviations: λ_{max} , absorption maximum; ϵ , absorption coefficient; Φ , quantum yield; $\epsilon\Phi$, photosensitivity.

We also studied the photon upconversion of Er-UCNPs at different excitation intensities with a 974-nm laser (**Figure 3c, S8**). Er-UCNPs emitted UV, blue, green and red light at excitation intensities greater than 33.8 W/cm². When the excitation intensity was between 0.09 and 2.2 W/cm², only green and red light were emitted. The excitation thresholds for the ²H_{9/2}-⁴I_{15/2} transition (409 nm, three-photon process^[17]), ²H_{11/2}-⁴I_{15/2} transition (520 nm, two-photon process^[17]), ⁴S_{3/2}-⁴I_{15/2} (540 nm, two-photon process^[17]), and ⁴F_{9/2}-⁴I_{15/2} transition (653 nm, two-photon process^[17]) were 2.2, 0.09, 0.04 and 0.09 W/cm², respectively (**Table 2**). Thus, at low excitation intensities (0.09-2.2 W/cm²), the green and red emissions remain and the blue emission completely vanishes. Among the five investigated photocleavable compounds, the photoreactions of NB-1 and CM-2 cannot be induced by the two-photon NIR-to-green light upconversion and the photoreaction of CM-3 induced by this upconversion should be inefficient because of the low photosensitivity of CM-3 in the green-light wavelength region (**Table 1**); however, the photoreactions of Ru-4 and Ru-5 can be induced by the two-photon NIR-to-green light upconversion. Therefore, the required excitation intensities for the photoreactions of Ru-4 and Ru-5 assisted by Er-UCNP should be lower than those for the photoreactions of the other compounds.

Table 2. Summary of photon upconversion in Tm-UCNP and Er-UCNP.

Nanoparticle	Transition ($\lambda^{[a]}$)	Upconversion threshold (W/cm^2)
Tm-UCNP	$^1I_6-^3F_4$ (340 nm)	5.5
	$^1D_2-^3H_6$ (360 nm)	2.2
	$^1D_2-^3F_4$ (450 nm)	0.64
	$^1G_4-^3H_6$ (470 nm)	0.19
Er-UCNP	$^2G_{9/2}-^4H_{15/2}$ (409 nm)	2.2
	$^2H_{11/2}-^4I_{15/2}$ (520 nm)	0.09
	$^4S_{3/2}-^4I_{15/2}$ (540 nm)	0.04
	$^4F_{9/2}-^4I_{15/2}$ (653 nm)	0.09

[a] Emission wavelength.

To study UCNP-assisted photochemistry, dispersions of UCNPs were mixed with solutions of photocleavable compounds. The concentrations of UCNPs (360 $\mu\text{g/mL}$) and photocleavable compounds (3.7×10^{-6} mol/L) in the mixtures were constant. To measure the apparent threshold for UCNP-assisted photochemistry, the mixtures were exposed to 974-nm light with different intensities for 1 h. The mixtures were then analyzed by UV-vis absorption spectroscopy (**Figure 4, 5**). The lowest excitation intensity that induced a spectral change was defined as the apparent threshold of UCNP-assisted chemistry for a given photocleavable compound/UCNP mixture.

The apparent thresholds for mixtures of photocleavable compound/Tm-UCNP were measured (**Figure 4**). Exposure of NB-1/Tm-UCNP and CM-2/Tm-UCNP to 974-nm light ($35 W/cm^2$, 1 h) did not induce any spectral change, indicating that their apparent thresholds were greater than $35 W/cm^2$. Their apparent thresholds are high because photocleavage of NB-1 and CM-2 can only be triggered by the four-photon NIR-to-UV upconversion, which requires high-intensity NIR light. The apparent thresholds for CM-3/Tm-UCNP, Ru-4/Tm-UCNP and Ru-5/Tm-UCNP were 35, 5, and $1 W/cm^2$, respectively. Photoreactions of these three compounds can be triggered by the three-photon NIR-to-blue light upconversion, which requires relatively low-intensity NIR light. A comparison of the apparent thresholds with the

photosensitivities of these three compounds at 470 nm (**Table 1**) suggests that the apparent threshold is lower if the compound is more photosensitive at the emission wavelength of the UCNPs.

The apparent thresholds of photocleavable compounds with Er-UCNP were also measured (**Figure 5**). The apparent thresholds for NB-1/Er-UCNP, CM-2/Er-UCNP, and CM-3/Er-UCNP were greater than 35 W/cm^2 . The apparent thresholds for Ru-4/Er-UCNP and Ru-5/Er-UCNP were 10 and 0.5 W/cm^2 , respectively. Ru-4/Er-UCNP and Ru-5/Er-UCNP exhibit lower apparent thresholds because their photoreactions can be triggered by the two-photon NIR-to-green light upconversion, which requires relatively low-intensity NIR light. A comparison of the apparent thresholds with the photosensitivities of Ru-4 and Ru-5 at 530 and 656 nm (**Table 1**) suggests that the apparent threshold is lower if the compound is more photosensitive at the emission wavelengths of the UCNPs. Exposure of all photocleavable compounds to 974-nm light in the absence of UCNPs did not change the compounds' absorption spectra (**Figure S9–S13**). This control experiment confirms that the photoreactions shown in Figure 4 and 5 were induced by upconversion.

The apparent thresholds of UCNP-assisted photochemistry (**Figure 4f, 5f**) are higher than the thresholds of the corresponding upconverted emissions that can induce the photoreactions (**Table 2**). This phenomenon is understandable. For example, exposure of Ru-4/Tm-UCNP to 974-nm light with an intensity of 5 W/cm^2 for 1 h induced an observable photoreaction (**Figure 4d**). 974-nm light at an intensity of 0.19 W/cm^2 is sufficient to excite the NIR-to-blue light upconversion (**Figure 3b**), which may induce the photoreaction of Ru-4. However, the intensity of blue light upconverted from 974-nm light at an intensity of 0.19 W/cm^2 is only ~0.4% that of blue light upconverted from 974-nm light at an intensity of 5 W/cm^2 (**Figure S7**). Thus, achieving the same effect of blue light upconverted from 974-nm light at 5 W/cm^2 for 1 h requires 250 h at 0.19 W/cm^2 . Therefore, no influence of 974-nm light at 0.19 W/cm^2 on the absorption spectrum of Ru-4/Tm-UCNP was observed within our experimental timeframe. Additionally, 974-nm light at 5 W/cm^2 also excites 450-nm and 360-nm emissions that contribute to photocleavage of Ru-4.

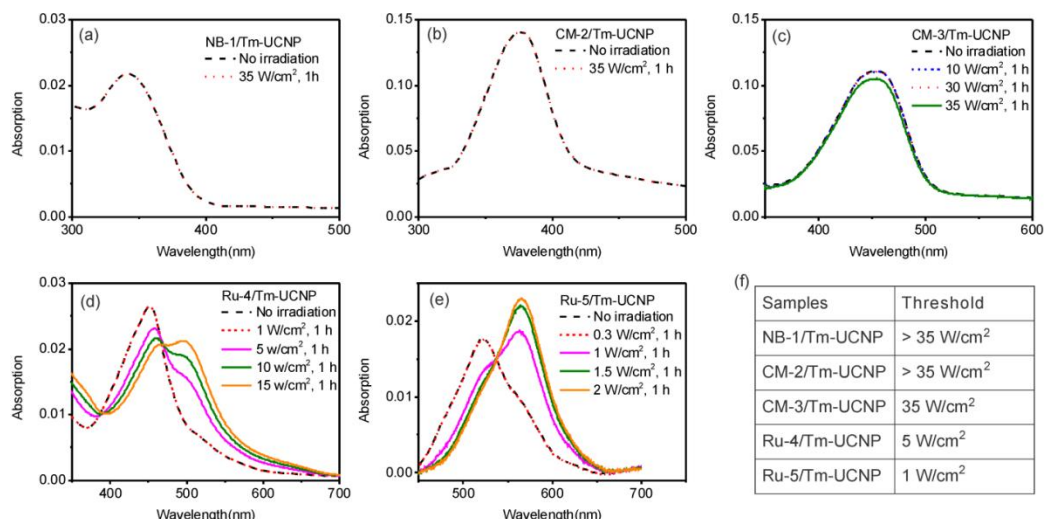


Figure 4. UV-vis absorption spectra of (a) NB-1/Tm-UCNP, (b) CM-2/Tm-UCNP, (c) CM-3/Tm-UCNP, (d) Ru-4/Tm-UCNP, and (e) Ru-5/Tm-UCNP before and after irradiation with 974-nm light. The irradiation time was fixed at 1 h. The light intensity was systematically changed to determine the apparent threshold of UCNP-assisted photochemistry. (f) Apparent thresholds of UCNP-assisted photochemistry for photocleavable compound/Tm-UCNP.

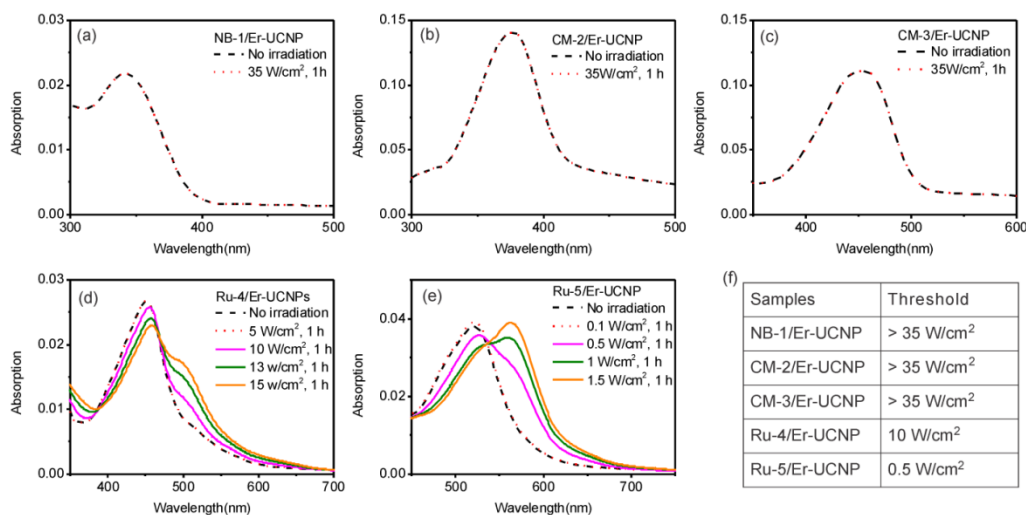


Figure 5. UV-vis absorption spectra of (a) NB-1/Er-UCNP, (b) CM-2/Er-UCNP, (c) CM-3/Er-UCNP, (d) Ru-4/Er-UCNP, and (e) Ru-5/Er-UCNP before and after irradiation with 974-nm light. The irradiation time was fixed at 1 h. The light intensity was systematically changed to determine the apparent threshold of UCNP-assisted photochemistry. (f) Apparent thresholds of UCNP-assisted photochemistry for photocleavable compound/Er-UCNP.

The irradiation time and UCNP concentration may influence the measured apparent threshold of UCNP-assisted photochemistry. The irradiation time in our experiments was 1 h, which is comparable to the irradiation time for photo-controlled drug delivery and cell adhesion based on UCNP-assisted photochemistry.^[5b,7a,9,10] The concentration of UCNPs in our experiments was 360 $\mu\text{g/mL}$, which is comparable to the concentrations of UCNPs used in drug delivery.^[5b,7a,9a-c,9e,f] Higher concentrations of UCNPs in biomedical applications may result in toxicity.^[5b] Moreover, the photocleavable chromophores used in this work exhibit numerous potential biomedical applications.^[2a,c,3,4,5b,7a,9f,18] Thus, we believe our results can provide guidance for the design of materials that are sensitive to low-intensity NIR light for biomedical applications.

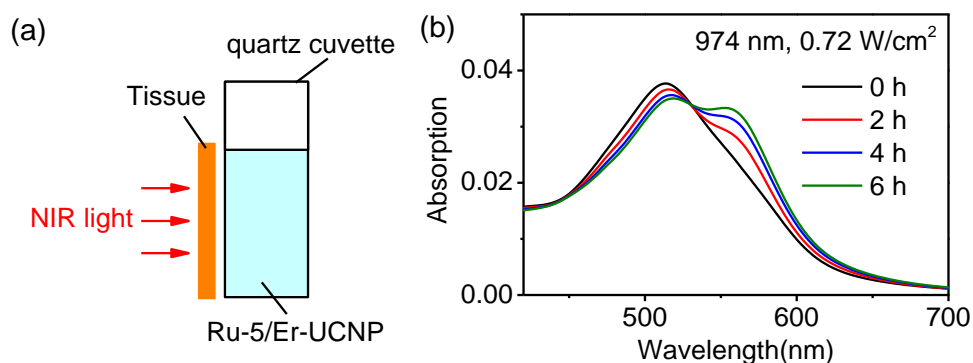


Figure 6. (a) Schematic model and (b) UV-vis absorption spectra of Ru-5/Er-UCNP when 0.5-mm-thick tissue is placed between 974-nm light (0.72 W/cm^2) and Ru-5/Er-UCNP.

Among the studied samples, Ru-5/Er-UCNP exhibited the lowest apparent threshold (0.5 W/cm^2); its threshold is lower than the maximum permissible exposure of skin (0.726 W/cm^2). Thus, the use of 974-nm light with an intensity of 0.5 W/cm^2 can minimize photodamage to tissue (**Figure 1**). Moreover, we studied the feasibility of using low-intensity NIR light to induce photocleavage of Ru-5 in deep tissue in the presence of Er-UCNP. For this purpose, a piece of tissue was inserted between a 974-nm laser and Ru-5/Er-UCNP (**Figure 6a**). The 974-nm light at an intensity of 0.72 W/cm^2 was still able to cleave Ru-5 after passing through the tissue (**Figure 6b**). Thus, we envision that UCNP-assisted photochemistry with low excitation intensity can be used in deep-tissue biomedical applications.

2.5 Conclusions

We measured the thresholds of UCNP-assisted photochemistry for five different photocleavable compounds combined with Tm-UCNP or Er-UCNP. The threshold of UCNP-assisted photochemistry depends on the emissive properties of the UCNP and on the photochemical properties of the photocleavable compounds. To design photosensitive materials that are sensitive to low-intensity NIR light using UCNP, our results suggest that: (1) the absorption wavelengths of the photosensitive compounds should overlap the wavelengths of upconverted emissions that can be excited by low-intensity NIR light; and (2) the photosensitive compounds should be highly photosensitive at the emission wavelengths of UCNP. The threshold of UCNP-assisted photochemistry for Ru-5/Er-UCNP (0.5 W/cm^2) is lower than the maximum permissible exposure of skin (0.726 W/cm^2). We expect that not only the compounds used in this work but also other visible-light-sensitive compounds^[19] should be suitable for UCNP-assisted photochemistry induced by low-intensity NIR light. The excitation intensity for UCNP-assisted photochemistry can be reduced even further by (1) grafting photosensitive compounds onto the surface of UCNP, (2) using UCNP with improved upconversion efficiency, and (3) using surface plasmons to enhance upconversion. Low excitation intensity in UCNP-assisted photochemistry can prevent photodamage to biomaterials, which is important in biomedical applications.

2.6 Experimental section

Materials

Ytterbium(III) acetate hydrate (99.9%), thulium(III) acetate hydrate (99.9%), yttrium(III) acetate hydrate (99.9%), erbium(III) acetate hydrate (99.9%), 2,2'-bipyridine (98%), 1-octadecene (technical grade, 90%), oleic acid (technical grade, 90%), ammonium fluoride (99.99%), ruthenium(III) chloride trihydrate (technical grade), 2,2'-biquinoline (98%), and 2,2':6',2''-terpyridine (98%) were purchased from Sigma-Aldrich. All solvents and other chemicals were purchased from Sigma-Aldrich or Fisher Scientific. The synthesis of Tm-UCNP was reported in our previous work.^[7a] Er-UCNP,^[6a] NB-1,^[20] CM-2,^[21] CM-3,^[21] Ru-4,^[22] and Ru-5^[23] were synthesized according to the procedures described in the literature. Mixtures of photocleavable compounds/UCNP were prepared by adding dispersions of UCNP (20 μL , 45 mg/mL in cyclohexane) to solutions of photosensitive compounds (2.5 mL, $3.75 \times 10^{-6} \text{ M}$ in THF/H₂O (99:1, v/v)).

General Methods

UV-vis absorption spectra were recorded on a Lambda 900 spectrophotometer (Perkin Elmer). TEM images were collected on a JEOL JEM1400 transmission electron microscope. Upconversion photoluminescence measurements were performed on a Spex Fluorolog II (212) spectrometer. A diode laser with a wavelength of 974 nm (device type P976MF, PhotonTec Berlin GmbH) coupled with a 105- μm (core) fiber was used as the excitation source. The diode laser was equipped with an adjustable fiber collimator (Changchun New Industries Optoelectronics Technology). The output power of the diode laser was controlled by a tabletop laser driver (device type ds11-la12v08-pa08v16-t9519-254-282, OsTech GmbH i.G.). The output power density of the diode laser was measured using an optical power meter (model 407A, Spectra-Physics Corporation) and an NIR indicator (model F-IRC1, Newport). To measure the apparent threshold of UCNP-assisted photochemistry, photocleavable compound/UCNP mixtures were exposed to 974-nm light with a given intensity for 1 h. The UV-vis absorption spectrum of the photocleavable compound/UCNP mixture was then measured to determine if the light intensity was sufficient to induce the photoreaction. To measure the photosensitivity, the solutions of photocleavable compounds (3.7×10^{-6} mol/L) were irradiated by LEDs at 365 nm, 470 nm, 530 nm and 656 nm (device types LCS-0365-07-22, LCS-0470-03-22, LCS-0530-15-22, and LCS-0656-03-22, Mightex Systems). The photoreactions were studied by UV-vis absorption spectroscopy (Figure S2-S6), and the photosensitivities of the reactions were calculated (Table S1). The output power densities of the LEDs were controlled by an LED controller (device type SLC-MA04-MU, Mightex Systems).

2.7 Acknowledgements

Z.C. and W.S. were supported by the CSC program. We thank H. Menges for measuring the upconverting luminescence spectra.

Keywords: photochemistry • nanoparticles • upconversion • near infrared • photocages

2.8 References

- [1] R. Tong, D. S. Kohane, *Wiley Interdiscip. Rev. Nanomed. Nanobiotechnol.* **2012**, *4*, 638-662.
- [2] a) A. M. Kloxin, A. M. Kasko, C. N. Salinas, K. S. Anseth, *Science* **2009**, *324*, 59-63; b) J. Robertus, W. R. Browne, B. L. Feringa, *Chem. Soc. Rev.* **2010**, *39*, 354-378; c) M. Wirkner, J. M. Alonso, V. Maus, M. Salierno, T. T. Lee, A. J. Garca, A. del Campo, *Adv. Mater.* **2011**, *23*, 3907-3910.
- [3] a) B. D. Fairbanks, M. P. Schwartz, A. E. Halevi, C. R. Nuttelman, C. N. Bowman, K. S. Anseth, *Adv. Mater.* **2009**, *21*, 5005-5010; b) C. Rodriguez-Emmenegger, C. M. Preuss, B. Yameen, O. Pop-Georgievski, M. Bachmann, J. O. Mueller, M. Bruns, A. S. Goldmann, M. Bastmeyer and C. Barner-Kowollik, *Adv. Mater.* **2013**, *25*, 6123-6127.
- [4] T. Furuta, S. S. H. Wang, J. L. Dantzker, T. M. Dore, W. J. Bybee, E. M. Callaway, W. Denk, R. Y. Tsien, *Proc. Natl. Acad. Sci. U.S.A.* **1999**, *96*, 1193-1200.
- [5] a) C. J. Carling, J. C. Boyer, N. R. Branda, *J. Am. Chem. Soc.* **2009**, *131*, 10838-10839; b) D. Yang, P. a. Ma, Z. Hou, Z. Cheng, C. Li, J. Lin, *Chem. Soc. Rev.* **2015**, DOI: 10.1039/C4CS00155A.
- [6] a) J. C. Boyer, C. J. Carling, B. D. Gates, N. R. Branda, *J. Am. Chem. Soc.* **2010**, *132*, 15766-15772; b) W. Wu, L. M. Yao, T. S. Yang, R. Y. Yin, F. Y. Li, Y. L. Yu, *J. Am. Chem. Soc.* **2011**, *133*, 15810-15813.
- [7] a) S. He, K. Krippes, S. Ritz, Z. Chen, A. Best, H.-J. Butt, V. Mailander, S. Wu, *Chem. Commun.* **2015**, *51*, 431-434; b) Y. M. Yang, Q. Shao, R. R. Deng, C. Wang, X. Teng, K. Cheng, Z. Cheng, L. Huang, Z. Liu, X. G. Liu, B. G. Xing, *Angew. Chem. Int. Edit.* **2012**, *51*, 3125-3129; c) J. Shen, G. Chen, T. Y. Ohulchanskyy, S. J. Kesseli, S. Buchholz, Z. Li, P. N. Prasad, G. Han, *Small* **2013**, *9*, 3213-3217.
- [8] a) S. Beyazit, S. Ambrosini, N. Marchyk, E. Palo, V. Kale, T. Soukka, B. T. S. Bui and K. Haupt, *Angew. Chem. Int. Edit.* **2014**, *53*, 8919-8923; b) A. Stepuk, D. Mohn, R. N. Grass, M. Zehnder, K. W. Kramer, F. Pelle, A. Ferrier, W. J. Stark, *Dent. Mater.* **2012**, *28*, 304-311.
- [9] a) Y. Dai, H. Xiao, J. Liu, Q. Yuan, P. Ma, D. Yang, C. Li, Z. Cheng, Z. Hou, P. Yang, J. Lin, *J. Am. Chem. Soc.* **2013**, *135*, 18920-18929; b) X. Li, L. Zhou, Y. Wei, A. M. El-Toni, F. Zhang, D. Zhao, *J. Am. Chem. Soc.* **2014**, *136*, 15086-15092; c) J. Liu, W. Bu, L. Pan and J. Shi, *Angew. Chem. Int. Edit.* **2013**, *52*, 4375-4379; d) B. Yan, J. C. Boyer, N. R. Branda, Y. Zhao, *J. Am. Chem. Soc.* **2011**, *133*, 19714-19717; e) Y. Min, J. Li, F. Liu, E. K. Yeow, B.

- Xing, *Angew. Chem. Int. Edit.* **2014**, *53*, 1012-1016; f) L. Zhao, J. Peng, Q. Huang, C. Li, M. Chen, Y. Sun, Q. Lin, L. Zhu, F. Li, *Adv. Funct. Mater.* **2014**, *24*, 363-371.
- [10] W. Li, J. Wang, J. Ren, X. Qu, *J. Am. Chem. Soc.* **2014**, *136*, 2248-2251.
- [11] F. Auzel, *Chem. Rev.* **2004**, *104*, 139-173.
- [12] a) *American National Standard for Safe Use of Lasers; Laser Institute of America: Orlando, FL, 2000*; b) *Laser safety handbook, Northwestern University, 2011*.
- [13] X. Xie, N. Gao, R. Deng, Q. Sun, Q. H. Xu, X. Liu, *J. Am. Chem. Soc.* **2013**, *135*, 12608-12611.
- [14] R. Steiner in *Laser-Tissue Interactions*, (Eds.: C. Raulin and S. Karsai), Springer Berlin Heidelberg, **2011**, pp. 23-36.
- [15] F. Wang, X. G. Liu, *Chem. Soc. Rev.* **2009**, *38*, 976-989.
- [16] G. F. Wang, W. P. Qin, L. L. Wang, G. D. Wei, P. F. Zhu, R. J. Kim, *Opt. Exp.* **2008**, *16*, 11907-11914.
- [17] J. F. Suyver, J. Grimm, M. K. van Veen, D. Biner, K. W. Kramer, H. U. GÜdel, *J. Lumin.* **2006**, *117*, 1-12.
- [18] a) S. Bonnet, B. Limburg, J. D. Meeldijk, R. J. M. K. Gebbink, J. A. Killian, *J. Am. Chem. Soc.* **2011**, *133*, 252-261; b) M. Frasconi, Z. Liu, J. Lei, Y. Wu, E. Strelakova, D. Malin, M. W. Ambrogio, X. Chen, Y. Y. Botros, V. L. Cryns, J.-P. Sauvage, J. F. Stoddart, *J. Am. Chem. Soc.* **2013**, *135*, 11603-11613; c) M. A. Sgambellone, A. David, R. N. Garner, K. R. Dunbar, C. Turro, *J. Am. Chem. Soc.* **2013**, *135*, 11274-11282.
- [19] a) Z. Shi, P. Peng, D. Strohecker, Y. Liao, *J. Am. Chem. Soc.* **2011**, *133*, 14699-14703; b) V. K. Johns, P. Peng, J. Dejesus, Z. Wang, Y. Liao, *Chem.-Eur. J.* **2014**, *20*, 689-692; c) Z. Wang, V. K. Johns, Y. Liao, *Chem.-Eur. J.* **2014**, *20*, 14637-14640.
- [20] F. Bley, K. Schaper and H. Görner, *Photochem. Photobiol.* **2008**, *84*, 162-171.
- [21] L. Fournier, I. Aujard, T. Le Saux, S. Maurin, S. Beaupierre, J. B. Baudin, L. Jullien, *Chem.-Eur. J.* **2013**, *19*, 17494-17507.
- [22] C. R. Hecker, P. E. Fanwick, D. R. Mcmillin, *Inorg. Chem.* **1991**, *30*, 659-666.
- [23] a) J. D. Knoll, B. A. Albani, C. B. Durr, C. Turro, *J. Phys. Chem. A.* **2014**, *118*, 10603-10610; b) N. Kaveevivitchai, R. Zong, H.-W. Tseng, R. Chitta, R. P. Thummel, *Inorg. Chem.* **2012**, *51*, 2930-2939.

2.9 Supporting information

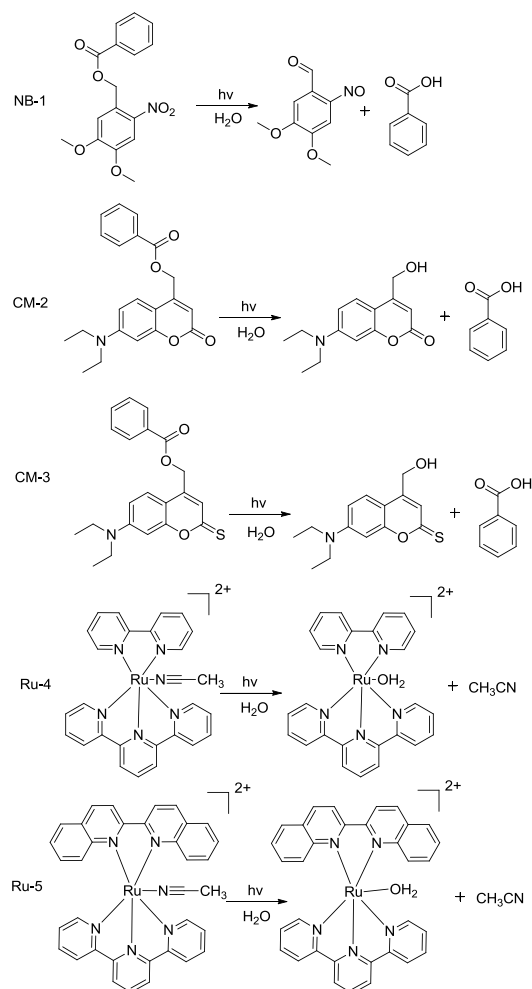


Figure S1. The photoreactions of the photocleavable compounds used in this work.

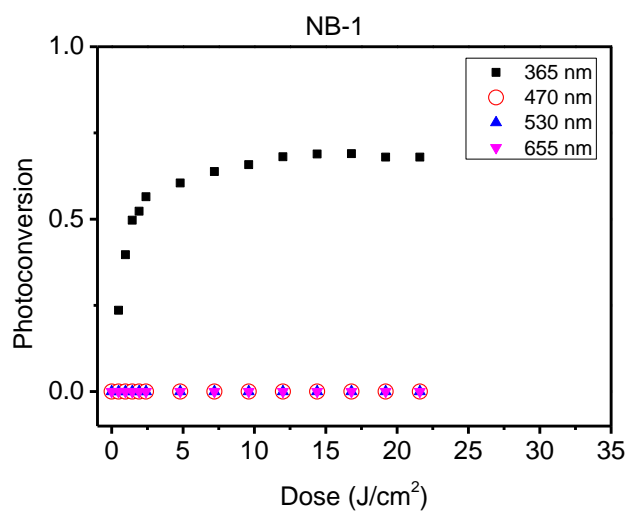


Figure S2. Photoconversion of NB-1 under the irradiation of light at 365 nm, 470 nm, 530 nm and 655 nm.

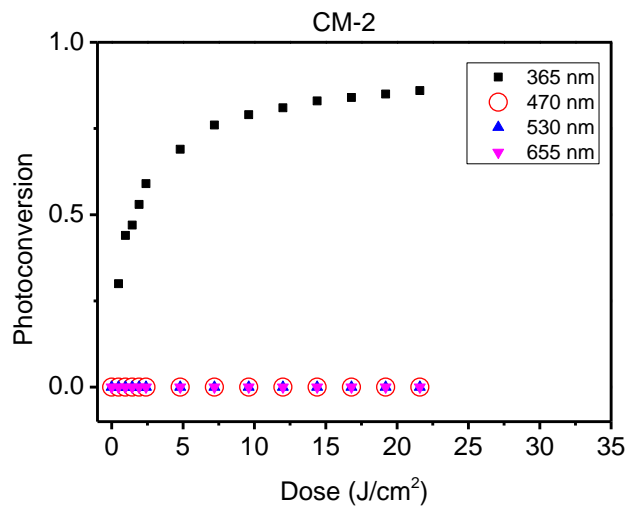


Figure S3. Photoconversion of CM-2 under the irradiation of light at 365 nm, 470 nm, 530 nm and 655 nm.

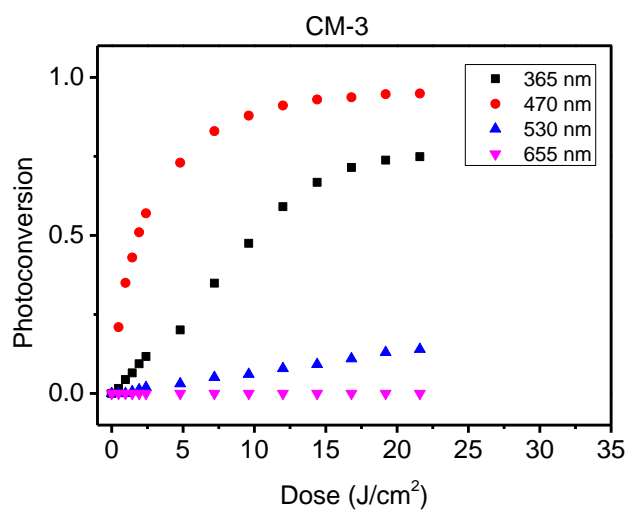


Figure S4. Photoconversion of CM-3 under the irradiation of light at 365 nm, 470 nm, 530 nm and 655 nm.

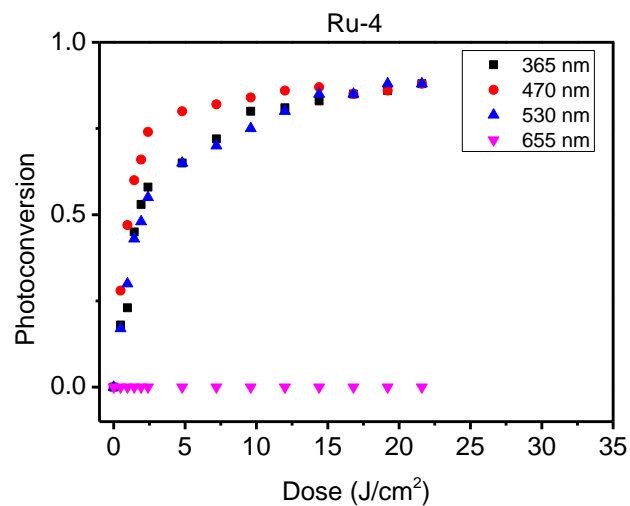


Figure S5. Photoconversion of Ru-4 under the irradiation of light at 365 nm, 470 nm, 530 nm and 655 nm.

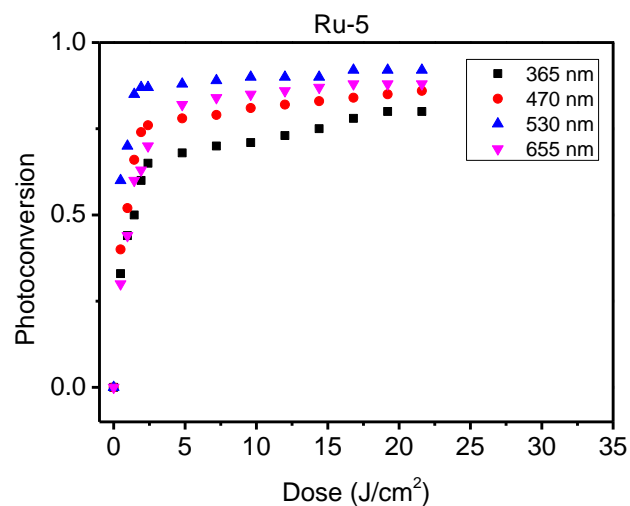


Figure S6. Photoconversion of Ru-5 under the irradiation of light at 365 nm, 470 nm, 530 nm and 655 nm.

Table S1. Calculation of the photosensitivity ($\epsilon\Phi$) of photocleavable compounds by fitting the experimental photoconversion following reference.^[1]

Compounds	Wavelength (nm)	$a_{dir}^{[a]}$ (J ⁻¹ cm ²)	$\epsilon\Phi^{[b]}$ (M ⁻¹ cm ⁻¹)
NB-1	365	0.31	19.4
	470	-	-
	530	-	-
	656	-	-
CM-2	365	0.35	47.5
	470	-	-
	530	-	-
	656	-	-
CM-3	365	0.06	9.4
	470	0.33	33.4
	530	0.006	0.7
	656	-	-
Ru-4	365	0.25	35.8
	470	0.56	56.5
	530	0.23	23.1
	656	-	-
Ru-5	365	0.37	53.8
	470	0.74	71.4
	530	1.38	138.8
	656	0.53	42.7

[a] Values extracted from the fits to the plots of photoconversion *versus* energy dose for the different photocleavable compounds and wavelengths with the equation $y = 1 - \exp(-a_{dir} x)$. The plots of photoconversion *versus* energy dose are shown in Figure S2-S6.

[b] Data calculated according to the equation $a_{dir} = 1/f_{EJ} [\ln(10) \epsilon\Phi]$, where f_{EJ} is the conversion factor from Einstein to Joule, as previously reported.^[1]

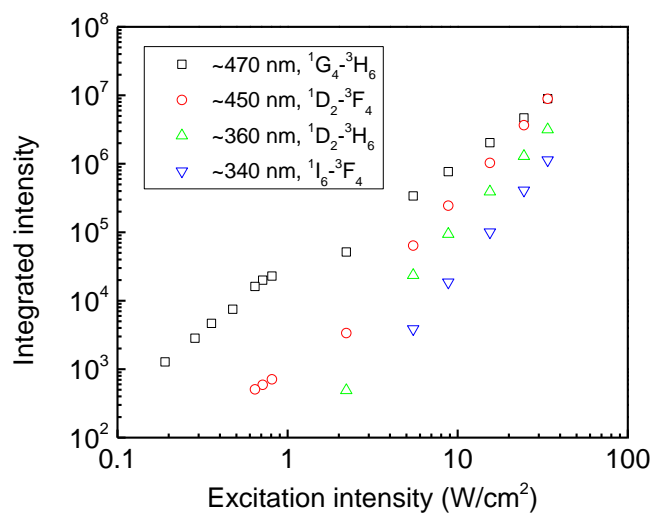


Figure S7. Double logarithmic plot of integrated emission intensity of Tm-UCNP upon 974 nm light excitation with different excitation intensities.

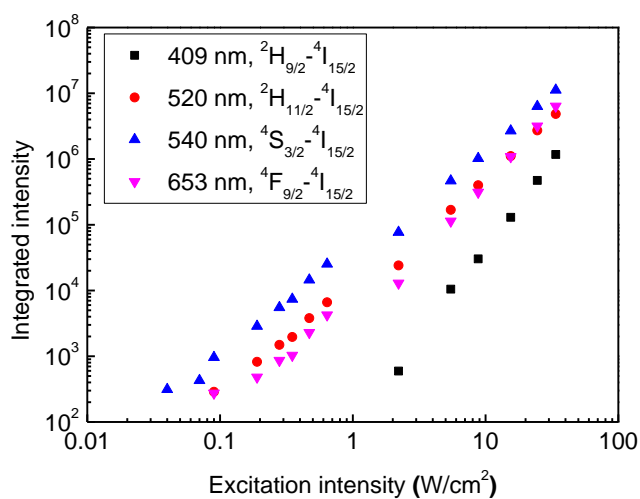


Figure S8. Double logarithmic plot of integrated emission intensity of Er-UCNP upon 974 nm light excitation with different excitation intensities.

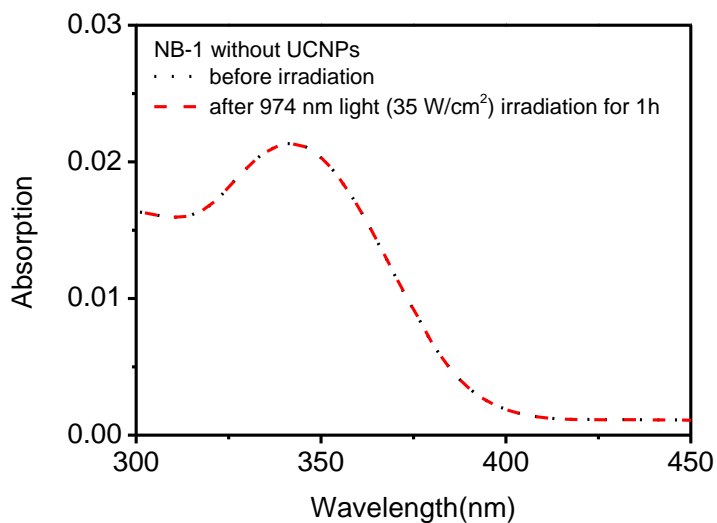


Figure S9. UV-vis absorption spectra of NB-1 before and after 974 nm light (35 W/cm²) irradiation for 1 h in the absence of UCNPs.

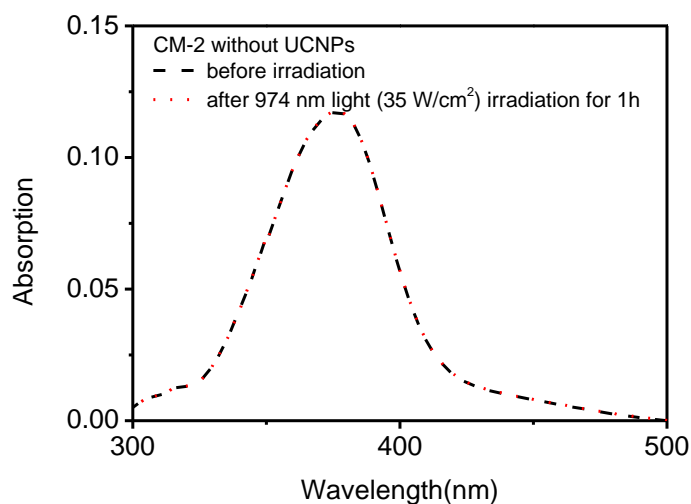


Figure S10. UV-vis absorption spectra of CM-2 before and after 974 nm light (35 W/cm²) irradiation for 1 h in the absence of UCNPs.

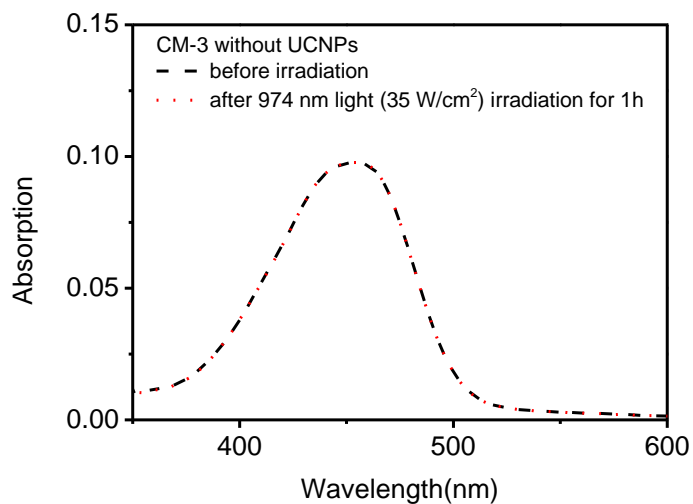


Figure S11. UV-vis absorption spectra of CM-3 before and after 974 nm light (35 W/cm²) irradiation for 1 h in the absence of UCNPs.

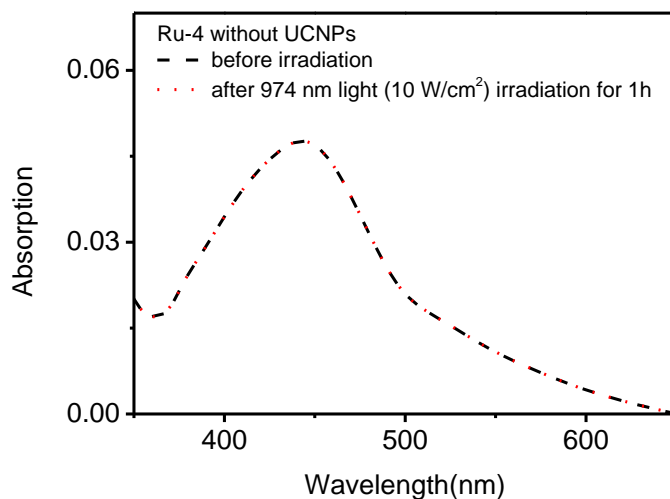


Figure S12. UV-vis absorption spectra of Ru-4 before and after 974 nm light (10 W/cm²) irradiation for 1 h in the absence of UCNPs.

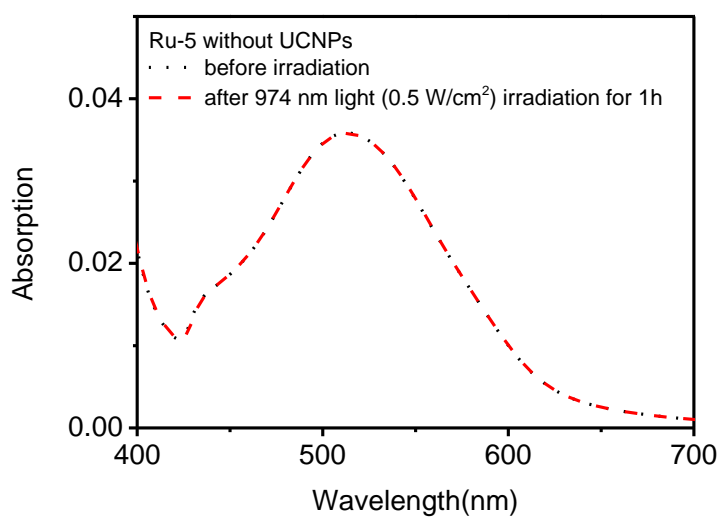


Figure S13. UV-vis absorption spectra of Ru-5 before and after 974 nm light (0.5 W/cm²) irradiation for 1 h in the absence of UCNPs.

References

- [1] D. Woll, S. Walbert, K. P. Stengele, T. J. Albert, T. Richmond, J. Norton, M. Singer, R. D. Green, W. Pfliderer, U. E. Steiner, *Helv. Chim. Acta.* **2004**, *87*, 28-45.

Chapter 3: Photon upconversion lithography: patterning of biomaterials using near-infrared light

Zhijun Chen, Shuqing He, Hans-Jürgen Butt, and Si Wu*

Max-Planck-Institut für Polymerforschung, Ackermannweg 10, 55128, Mainz, Germany

Published in *Adv. Mater.*, 2015, **27**, 2203.

Reproduced from *Adv. Mater.*, 2015, **27**, 2203 with permission from the WILEY-VCH Verlag GmbH & Co. KGaA.

3.1 Statement of contribution

Si Wu conceived the idea and led the project. Si Wu and Hans-Jürgen Butt led the project..

Zhijun CHEN performed the protein pattern

Shuqing He synthesized and characterized the materials.

Zhijun CHEN and Shuqing He contributed equally to this work.

Keywords: photopatterning, nanoparticles, upconversion, photocages, protein adsorption

3.2 Introduction

Photolithography is a photopatterning technique widely used in industry and academia. In photolithography, light transfers patterns from photomasks to photosensitive materials. For biomedical applications, photolithography has been used to pattern biomaterials such as proteins, cells and extracellular matrices.^[1] Patterned proteins, for example, can guide the development of neurons and control the adhesion and migration of cells.^[2] Compared to other patterning approaches,^[3] the advantage of photopatterning is that light provides high spatial and temporal resolution in a non-contact manner that can prevent contact contamination of biological systems. In most cases, UV light is used for photolithography^[1,4] because most photosensitive materials efficiently absorb UV light. However, for patterning of biomaterials, the use of UV light is limited because it is not compatible with biomaterials, cannot penetrate deep into tissue and lacks of spatial resolution for in vivo applications.^[5] Compared to UV light, near-infrared (NIR) light is more suitable for photopatterning of biomaterials because NIR light causes less photodamage, scatters less^[6] and can penetrate deeper into tissues. One approach for the patterning of biomaterials using NIR light is based on simultaneous two-photon absorption.^[7] However, this method is inefficient because of the small two-photon absorption cross-sections of typical chromophores. Because two-photon absorption requires

high-intensity light, two-photon absorption only occurs at the focus of a powerful pulsed laser. Patterns are generated using a spot-by-spot process that is time-consuming. As a result, the fabrication of large-area patterns via two-photon absorption is not practical. Solving these problems necessitates the development of alternative methods for the efficient patterning of biomaterials over large areas using NIR light.

Recently, NIR-light-induced photochemistry assisted by lanthanide-doped upconverting nanoparticles (UCNPs) has been developed.^[8-10] UCNPs convert NIR light into UV and visible light under the excitation of continuous-wave NIR laser diodes.^[11] The upconverted UV or visible light can induce photoreactions of normal UV- or visible-light-sensitive compounds.^[8-10] This process is called UCNP-assisted photochemistry. Assisted by UCNPs, NIR light has been successfully used to induce different photoreactions, such as photoisomerization,^[12] photocleavage^[10,13] and photopolymerization.^[14] NIR light has also been utilized to control drug delivery,^[15,16] cell adhesion,^[17] and bending of elastomers.^[18] However, no attention has been focused on using NIR light for photolithography via UCNP-assisted photochemistry.

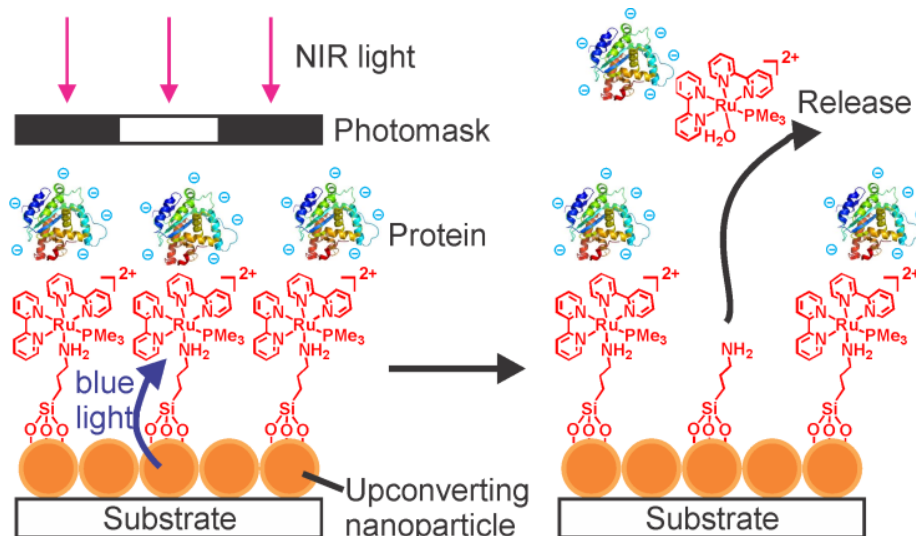


Figure 1. Schematic of photon upconversion lithography (PUCL) for the patterning of proteins. Note: Polyethylene glycol, which is co-grafted with Ru complexes on the upconverting nanoparticles (UCNPs), is not shown for clarity.

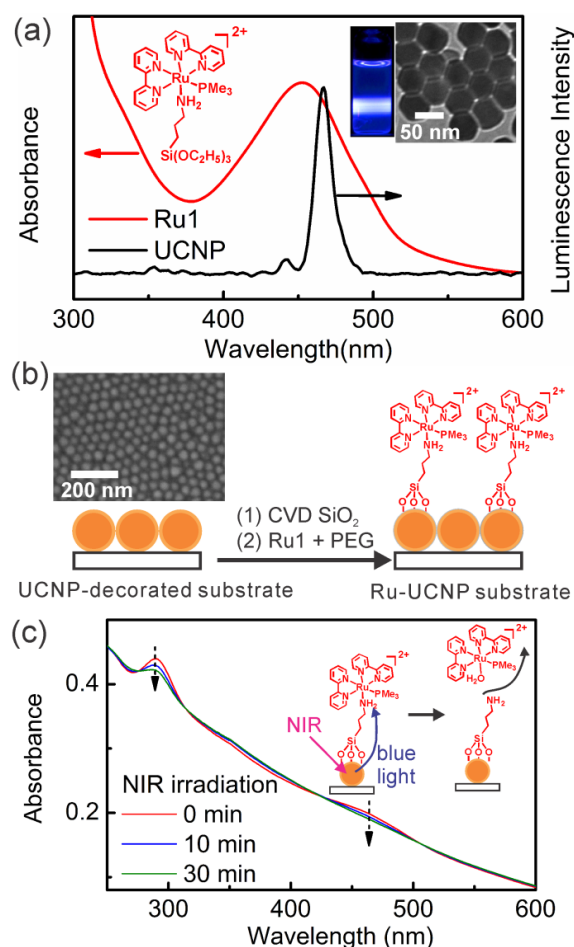


Figure 2. (a) Absorption spectrum of Ru1 (red line) and emission spectrum of UCNP (black line) under excitation by 974-nm light (0.64 W/cm^2). Insets: chemical structure of Ru1, photograph of UCNP under 974-nm light exposure and TEM image of UCNP. (b) Schematic of the fabrication the Ru-UCNP substrate. The co-grafted PEG is not shown for clarity. Inset: SEM image of a UCNP-decorated substrate. (c) UV-vis absorption spectra of the Ru-UCNP substrate upon exposure to 974-nm light (0.64 W/cm^2).

Here, we demonstrate that NIR light can be used for photolithography via UCNP-assisted photochemistry. We refer to this new method as photon upconversion lithography (PUCL). Figure 1 illustrates the patterning of proteins via PUCL. A blue-light-cleavable Ru complex (Ru1) and polyethylene glycol (PEG) were co-grafted onto the UCNP-decorated substrate. Proteins were adsorbed onto the surface via electrostatic interactions between the negatively charged proteins and the positively charged Ru complexes. For the patterning of proteins, a photomask was positioned between the NIR light and the proteins. In the exposed areas, UCNP convert NIR light into blue light that induces cleavage of the Ru complexes and the local release of proteins. Protein patterns can be fabricated in this manner.

3.3 Results and discussion

To construct the system for PUCL, β -phase NaYF₄:TmYb@NaYF₄ UCNPs (core = NaYF₄: 0.5 mol% Tm³⁺: 30 mol% Yb³⁺; shell = NaYF₄) were synthesized.^[16,19] The UCNPs emitted blue light under excitation by NIR light at 974 nm (Figure 2a). The transmission electron microscopy (TEM) image in the inset of Figure 2a shows that the average diameter of the UCNPs was 50 nm. For the preparation of the UCNP-decorated substrate, a self-assembled array of UCNPs at the air-water interface was transferred to a quartz substrate (Supporting Information).^[20] The UCNPs formed a close-packed array on the substrate (SEM image in Figure 2b). The UCNP-decorated substrate was subsequently coated with silica via the ammonia-catalyzed chemical vapor deposition (CVD) of tetraethoxysilane.^[21] Finally, the Ru-UCNP substrate was prepared via co-grafting of Ru1 and PEG in a 1:1 ratio on the UCNP-decorated substrate (Figure 2b). The successful grafting of Ru1 on the Ru-UCNP substrate was demonstrated using X-ray photoelectron spectroscopy (XPS, Figure S1).

The absorption band of Ru1 at 453 nm overlaps the blue emission band of the UCNPs (Figure 2a). Thus, Ru1 can absorb the upconverted blue light. Ru1 and similar Ru complexes are photocleavable.^[16,22,23] Ru-complex-modified substrates has been used for patterning via the conventional one-photon and two-photon processes.^[23] But patterning using the one-photon and two-photon processes cannot solve the general problems of photopatterning in biomedical applications. We therefore developed PCUL. In the dispersion of Ru1-functionalized UCNPs, we have demonstrated that the cleavage of Ru complexes can be induced using low-intensity NIR light that can minimize heating and prevent photodamage to biomaterials.^[16] To verify the feasibility of this photochemistry for photopatterning, we studied NIR-light-induced cleavage of Ru complexes from the Ru-UCNP substrate (Figure 2c). After the Ru-UCNP substrate was illuminated with NIR light (974 nm, 0.64 W/cm²), the absorption bands of the Ru complex indeed decreased in intensity, indicating that the Ru complex was cleaved from the substrate. This spectral change is identical to that observed for the Ru-complex-modified substrate that was exposed to blue light to directly trigger cleavage (Figure S2). The exposure of the Ru-complex-modified substrate to NIR light in the absence of UCNPs did not influence the absorption spectrum (Figure S3), which demonstrates that the cleavage of the Ru complex was induced by the photon upconversion process. Measurements using UV-vis absorption spectroscopy showed that 974-nm light (0.64 W/cm²) cleaved ~74% of the Ru complexes from the substrate after irradiation for 30 min (Figure S4).

To demonstrate PUCL, a photomasked Ru-UCNP substrate was irradiated with NIR light (Figure 3a). On the exposed part, the Ru complexes were cleaved and free amino groups were generated. An amine-reactive fluorescent dye was then used to stain the pattern. After being stained, the pattern was observed using confocal laser scanning microscopy. The clear fluorescent pattern demonstrates the successful patterning via photon upconversion (Figure 3b).

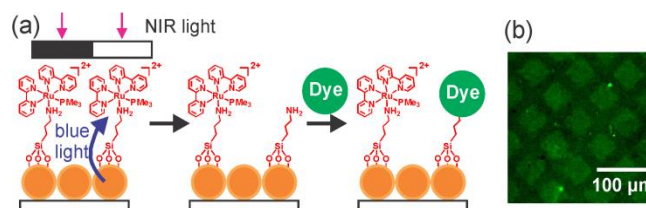


Figure 3. (a) Procedure for the fabrication of a fluorescent pattern using PUCL. (b) Confocal laser scanning microscopy image of the resulting pattern.

In the subsequent step, we used PUCL to pattern proteins. Fluorescently labeled bovine serum albumin (BSA) was adsorbed onto the Ru-UCNP substrate via electrostatic interactions. Before the substrate was irradiated with NIR light, the fluorescently labeled BSA on the substrate emitted bright red fluorescence (Figure 4a). After the substrate was irradiated with NIR light and washed with NaCl solution (Supporting Information), the fluorescence intensity decreased, suggesting that proteins were desorbed from the substrate. After 40 min of irradiation, the intensity decreased by ~90%. Exposure of the Ru-modified substrate without UCNP to NIR light did not induce protein desorption (Figure S5). This control experiment further confirms that the protein desorption was triggered by photon upconversion.

Encouraged by the success of NIR-light-controlled protein desorption, we used PUCL for the patterning of proteins. The patterning process led to a clear fluorescent pattern of proteins (Figure 4b). The light intensity for the patterning of proteins was 0.64 W/cm², which is a medically harmless dose.^[16,24] Moreover, we studied the feasibility of using PUCL for photopatterning in deep tissue, which is important for the *in vivo* applications of this technique. For this purpose, a piece of chicken tissue was placed between the NIR light and the sample (Figure 4c, left). The NIR light still generated a protein pattern after passing through the tissue (Figure 4c, right).

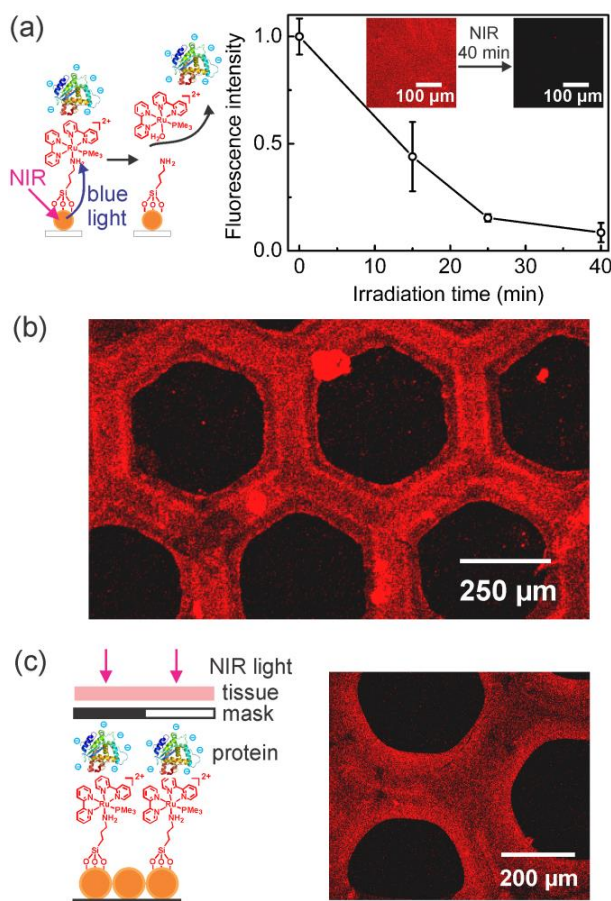


Figure 4. (a) NIR-light-triggered protein desorption from a Ru-UCNP substrate. Inset: confocal laser scanning microscopy images of the substrate before and after it was irradiated with 974-nm light (0.64 W/cm^2). (b) Confocal laser scanning microscopy image of a protein pattern fabricated using PUCL. The fabrication procedure is shown in Figure 1. (c) Fabrication of a protein pattern using 974-nm light passed through 0.5-mm-thick tissue.

3.4 Conclusion

In conclusion, PUCL, which was developed in this work, is a novel concept for the patterning of proteins using NIR light. In PUCL, NIR irradiation excited the UCNPs in the exposed areas through a photomask. The UCNPs converted the NIR light into local blue light that induced cleavage of the Ru complexes and desorption of the proteins. Different photoreactions might be triggered by NIR light via UCNPs-assisted photochemistry.^[9] Thus, not only photocleavable Ru complexes but also other photosensitive compounds^[25] could be used for PUCL. Moreover, PUCL could be an approach for the patterning of biomaterials other than proteins. The area of the pattern fabricated using PUCL is limited by the diameter of the laser beam and by the size of the photomask. The diameter of our laser beam can be

adjusted to 7 cm. The size of commercial photomasks is on the order of several inches. Therefore, PUCL enables the fabrication of large-area patterns. Additionally, the smallest line width obtained using PUCL was tens of microns under optimized irradiation conditions. This line width is comparable to the sizes of cells. Thus, we envision using PUCL to fabricate patterned extracellular matrices, control the migration of cells, guide the development of neurons, and regulate inflammation and vascularization of biomaterials.^[5]

3.5 Acknowledgements

S.H. was supported by the MPG-CAS Joint Doctoral Promotion Programme (DPP). Z.C. was supported by the CSC program. We thank H. Menges for upconverting luminescence spectra, A. Best for confocal laser scanning microscopy images, and Dr. K. Koynov and Dr. A. del Campo for helpful discussion.

3.6 References

- [1] a) A. M. Kloxin, A. M. Kasko, C. N. Salinas, K. S. Anseth, *Science* **2009**, *324*, 59; b) J. Robertus, W. R. Browne, B. L. Feringa, *Chem. Soc. Rev.* **2010**, *39*, 354; c) C. Rodriguez-Emmenegger, C. M. Preuss, B. Yameen, O. Pop-Georgievski, M. Bachmann, J. O. Mueller, M. Bruns, A. S. Goldmann, M. Bastmeyer, C. Barner-Kowollik, *Adv. Mater.* **2013**, *25*, 6123; d) M. J. Salierno, A. J. García, A. del Campo, *Adv. Funct. Mater.* **2013**, *23*, 5974; e) N. R. Gandavarapu, M. A. Azagarsamy, K. S. Anseth, *Adv. Mater.* **2014**, *26*, 2521; f) T. Tischer, C. Rodriguez-Emmenegger, V. Trouillet, A. Welle, V. Schueler, J. O. Mueller, A. S. Goldmann, E. Brynda, C. Barner-Kowollik, *Adv. Mater.* **2014**, *26*, 4087.
- [2] a) B. Kaehr, R. Allen, D. J. Javier, J. Currie, J. B. Shear, *Proc. Natl. Acad. Sci. U.S.A.* **2004**, *101*, 16104; b) X. Y. Chen, M. A. Brewer, C. P. Zou, P. J. Campagnola, *Integr. Biol.* **2009**, *1*, 469; c) B. P. Chan, J. N. Ma, J. Y. Xu, C. W. Li, J. P. Cheng, S. H. Cheng, *Adv. Funct. Mater.* **2014**, *24*, 277.
- [3] a) W. Wang, Z. Cheng, P. Yang, Z. Hou, C. Li, G. Li, Y. Dai, J. Lin, *Adv. Funct. Mater.* **2011**, *21*, 456; b) M. Yu, J. Lin, Z. Wang, J. Fu, S. Wang, H. J. Zhang, Y. C. Han, *Chem. Mater.* **2002**, *14*, 2224.
- [4] a) X. Q. Zhu, B. W. Wang, F. Shi, J. Nie, *Langmuir* **2012**, *28*, 14461; b) X. Q. Zhu, X. W. Fan, G. N. Ju, M. J. Cheng, Q. An, J. Nie, F. Shi, *Chem. Commun.* **2013**, *49*, 8093.
- [5] T. T. Lee, J. R. García, J. I. Paez, Ankur Singh, E. A. Phelps, S. Weis, Z. Shafiq, A. Shekaran, A. del Campo, A. J. García, *Nat. Mater.* **2014**, DOI:10.1038/nmat4157.
- [6] H. Ma, A. K.-Y. Jen, L. R. Dalton, *Adv. Mater.* **2002**, *14*, 1339.
- [7] M. Álvarez, A. Best, S. Pradhan-Kadam, K. Koynov, U. Jonas, M. Kreiter, *Adv. Mater.* **2008**, *20*, 4563.
- [8] C. J. Carling, J. C. Boyer, N. R. Branda, *J. Am. Chem. Soc.* **2009**, *131*, 10838.
- [9] D. Yang, P. Ma, Z. Hou, Z. Cheng, C. Li, J. Lin, *Chem. Soc. Rev.* **2015**, DOI: 10.1039/C4CS00155A.
- [10] C. J. Carling, F. Nourmohammadian, J. C. Boyer, N. R. Branda, *Angew. Chem. Int. Edit.* **2010**, *49*, 3782.
- [11] a) M. Haase, H. Schäfer, *Angew. Chem. Int. Edit.* **2011**, *50*, 5808; b) S. Gai, C. Li, P. Yang, J. Lin, *Chem. Rev.* **2014**, *114*, 2343.
- [12] J. C. Boyer, C. J. Carling, B. D. Gates, N. R. Branda, *J. Am. Chem. Soc.* **2010**, *132*, 15766.

- [13] a) Y. M. Yang, Q. Shao, R. R. Deng, C. Wang, X. Teng, K. Cheng, Z. Cheng, L. Huang, Z. Liu, X. G. Liu, B. G. Xing, *Angew. Chem. Int. Edit.* **2012**, *51*, 3125; b) M. L. Viger, M. Grossman, N. Fomina, A. Almutairi, *Adv. Mater.* **2013**, *25*, 3733.
- [14] a) A. Stepuk, D. Mohn, R. N. Grass, M. Zehnder, K. W. Krämer, F. Pellé, A. Ferrier, W. J. Stark, *Dent. Mater.* **2012**, *28*, 304; b) S. Beyazit, S. Ambrosini, N. Marchyk, E. Palo, V. Kale, T. Soukka, B. T. S. Bui, K. Haupt, *Angew. Chem. Int. Edit.* **2014**, *53*, 8919.
- [15] a) B. Yan, J. C. Boyer, N. R. Branda, Y. Zhao, *J. Am. Chem. Soc.* **2011**, *133*, 19714; b) Y. Dai, H. Xiao, J. Liu, Q. Yuan, P. Ma, D. Yang, C. Li, Z. Cheng, Z. Hou, P. Yang, J. Lin, *J. Am. Chem. Soc.* **2013**, *135*, 18920; c) J. Liu, W. Bu, L. Pan, J. Shi, *Angew. Chem. Int. Edit.* **2013**, *52*, 4375; d) Y. Min, J. Li, F. Liu, E. K. Yeow, B. Xing, *Angew. Chem. Int. Edit.* **2014**, *53*, 1012; e) L. Zhao, J. Peng, Q. Huang, C. Li, M. Chen, Y. Sun, Q. Lin, L. Zhu, F. Li, *Adv. Funct. Mater.* **2014**, *24*, 363.
- [16] S. He, K. Krippes, S. Ritz, Z. Chen, A. Best, H.-J. Butt, V. Mailänder, S. Wu, *Chem. Commun.* **2015**, *51*, 431.
- [17] W. Li, J. Wang, J. Ren, X. Qu, *J. Am. Chem. Soc.* **2014**, *136*, 2248.
- [18] W. Wu, L. M. Yao, T. S. Yang, R. Y. Yin, F. Y. Li, Y. L. Yu, *J. Am. Chem. Soc.* **2011**, *133*, 15810.
- [19] a) P. Ma, H. Xiao, X. Li, C. Li, Y. Dai, Z. Cheng, X. Jing, J. Lin, *Adv. Mater.* **2013**, *25*, 4898; b) Y. Dai, D. Yang, P. Ma, X. Kang, X. Zhang, C. Li, Z. Hou, Z. Cheng, J. Lin, *Biomaterials* **2012**, *33*, 8704.
- [20] A. G. Dong, J. Chen, P. M. Vora, J. M. Kikkawa, C. B. Murray, *Nature* **2010**, *466*, 474.
- [21] X. Deng, L. Mammen, H.-J. Butt, D. Vollmer, *Science* **2012**, *335*, 67.
- [22] S. Bonnet, B. Limburg, J. D. Meeldijk, R. J. M. K. Gebbink, J. A. Killian, *J. Am. Chem. Soc.* **2011**, *133*, 252;
- [23] V. S. Miguel, M. Álvarez, O. Filevich, R. Etchenique, A. del Campo, *Langmuir* **2012**, *28*, 1217.
- [24] a) American National Standard for Safe Use of Lasers, Laser Institute of America: Orlando, FL, **2000**; b) Laser Safety Handbook, Northwestern University, **2011**.
- [25] a) Z. Shi, P. Peng, D. Strohecker, Y. Liao, *J. Am. Chem. Soc.* **2011**, *133*, 14699; b) Z. Wang, V. K. Johns, Y. Liao, *Chem.-Eur. J.* **2014**, *20*, 14637.

3.7 Supporting information

Materials

Ytterbium(III) acetate hydrate (99.9%) and (3-aminopropyl)triethoxysilane (98%) were purchased from Alfa Aesar. ω -Trimethoxysilane-terminated poly(ethylene glycol) methyl ether (PEG, $M_n = 0.35$ kg/mol and $PDI = 1.10$) was purchased from Polymer Source. Thulium(III) acetate hydrate (99.9%), yttrium(III) acetate hydrate (99.9%), 2,2'-bipyridine (98%), Dowex® 22 Cl anion-exchange resin, trimethylphosphine solution (1.0 M in THF), lithium chloride ($\geq 99\%$), 1-octadecene (technical grade, 90%), oleic acid (technical grade, 90%), ammonium fluoride ($\geq 99.99\%$), ruthenium(III) chloride trihydrate (technical), and tetraethyl orthosilicate (98%) were purchased from Sigma-Aldrich. All other solvents were purchased from Sigma-Aldrich or Fisher Scientific. The fluorescent-labeled protein (Bovine Serum Albumin (BSA), Alexa Fluor® 680 conjugate) and amine-reactive fluorescent dye (Alexa Fluor 488 carboxylic acid, succinimidyl ester) were purchased from Life Technologies.

Characterization

UV-vis absorption spectra were collected using an Agilent Cary 4000 spectrometer. Confocal laser scanning microscopy images were collected using a confocal laser scanning microscope (Olympus IX70 microscope, FV300 laser scanning unit). SEM images were collected using a LEO Gemini 1530 system. The upconversion photoluminescence was measured using a Spex Fluorolog II (212) spectrometer. A diode laser with a wavelength of 974 nm (type P976MF, PhotonTec Berlin GmbH) coupled with a 105- μm (core) fiber was used as the excitation light source. The diode laser was equipped with an adjustable fiber collimator (Changchun New Industries Optoelectronics Technology). The output power of the diode laser was controlled by a tabletop laser driver (device type ds11-la12v08-pa08v16-t9519-254-282, OsTech GmbH i.G.). The output power density of the diode laser was measured using an optical power meter (model 407A, Spectra-Physics Corp.) and a NIR indicator (Newport, model F-IRC1).

Synthesis

The syntheses of β -NaYF₄:0.5 mol% Tm³⁺, 30 mol% Yb³⁺/ β -NaYF₄ core/shell UCNPs and the ruthenium complex Ru[(2,2'-bipyridine)₂(trimethylphosphine)((3-aminopropyl)triethoxysilane)](PF₆)₂ (Ru 1) are reported in our previous work.^[1]

Preparation of the Ru-UCNP substrate

First, we dropped a dispersion of UCNP in cyclohexane (2 mL, ~ 0.825 mg/mL) onto a water-air interface in a glass container (radius 25 mm). A quartz substrate (1 cm \times 1 cm) was placed at the bottom of the container. Cyclohexane was evaporated for 2 h. The UCNP formed an array at the air-water interface, and the water was subsequently extracted. The UCNP array was transferred to the quartz substrate underneath. The UCNP-decorated substrate was dried under vacuum at 40 °C for 6 h. The UCNP-decorated substrate was then coated with a silica layer via ammonia-catalyzed chemical vapor deposition (CVD) of tetraethoxysilane. For CVD, the array was placed into an exsiccator together with 2 vessels that contained TEOS (2 mL) and ammonia (2 mL) for 24 h. The array was then baked for 1 h at 90 °C in an oven under vacuum.

An aqueous solution of NaOH (20 μ L, 1 M NaOH) was added to an acetone solution (40 mL) of ω -trimethoxysilane-terminated poly(ethylene glycol) methyl ether (5×10^{-5} mol/L) and Ru1 (5×10^{-5} mol/L). The mixture was stirred for 30 min. The UCNP-decorated substrate was subsequently treated with oxygen plasma for 2 s and then placed into the mixture at 60 °C for 24 h. Afterwards, the substrate was rinsed with acetone and Milli-Q water three times. Finally, the Ru-UCNP substrate was baked for 1 h at 90 °C in an oven under vacuum. The Ru-UCNP substrate was stored in the absence of light before use.

NIR-light-induced cleavage of the Ru complexes from the Ru-UCNP substrate

The Ru-UCNP substrate was irradiated with 974-nm light (0.64 W/cm²). After being irradiated, the substrate was washed with acetone and Milli-Q water three times. After the substrate was dried under N₂, its absorption spectrum was measured using a UV-vis spectrometer (Figure 2c).

Fabrication of a fluorescent pattern using NIR light

A Ru-UCNP substrate was irradiated with 974-nm light while a photomask was placed between the light and the sample. After being irradiated for 1 h, the substrate was washed with acetone and Milli-Q water three times. Then, a DMSO solution (200 μ L) of Alexa Fluor 488 was dropped onto the irradiated area. The droplet was removed, and the substrate was washed using DMSO, THF and Milli-Q water. Finally, the sample was dried under N₂.

Protein adsorption on Ru-UCNP substrate and NIR-controlled protein release

The Ru-UCNP substrate was immersed in an aqueous solution of fluorescent-labeled BSA (0.5 mg/mL, pH 9) for 3 h and then washed with a 1 mM NaCl solution (pH = 9) three times. After drying under N₂, the substrate was stored in the absence of light.

To release the adsorbed proteins, the Ru-UCNP substrate with proteins was irradiated with 974-nm light (0.64 W/cm²). After being irradiated, the substrate was washed with a 1 mM NaCl solution (pH = 9) three times. After drying under N₂, the sample was imaged using a confocal laser scanning microscope.

Patterning of proteins by photon upconversion lithography

The Ru-UCNP substrate with proteins was irradiated with 974-nm light (0.64 W/cm², 40 min) while a photomask was placed between the light source and the sample. After being irradiated, the substrate was washed with a 1 mM NaCl solution (pH = 9) three times. After drying under N₂, the sample was imaged using a confocal laser scanning microscope.

The densities of Ru1 and BSA on the substrates

The grafting density of Ru1 (Γ) is measured according to the method reported in literature.^[2]

$$\Gamma = AN_A/2\varepsilon$$

where A is the absorbance of the monolayer of the Ru complex at λ_{\max} , ε is the molar extinction coefficient of the Ru complex in solution at λ_{\max} ($\sim 4000 \text{ M}^{-1}\text{cm}^{-1}$), N_A is Avogadro constant.

$$\Gamma = 7.5 \times 10^{13} \text{ molecule/cm}^2.$$

The small amount of the Ru complex will not cause toxicity for biomedical applications.

The number of binding sites of Ru complexes and BSA is about 0.6906-0.9159.^[3] The molecular weight of BSA is $\sim 66,000 \text{ g/mol}$. So, the density of BSA is $\sim 56.9 \sim 75 \text{ }\mu\text{g/cm}^2$.

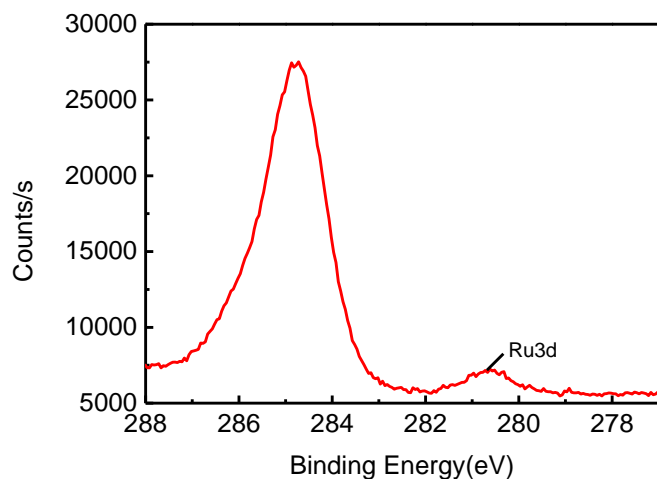


Figure S1. XPS spectrum of the Ru-UCNP substrate. The atomic percent of Ru on the surface measured by XPS is 0.08%.

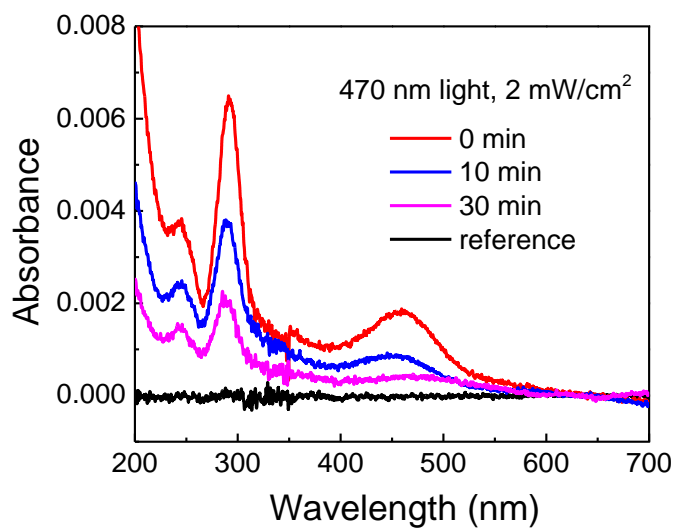


Figure S2. UV-vis absorption spectra of Ru1-modified quartz before and after irradiation with 470-nm light.

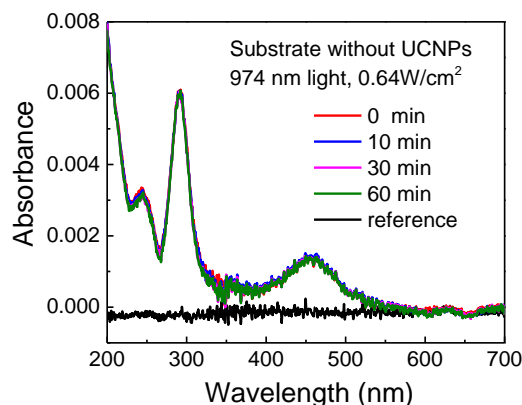


Figure S3. UV-vis absorption spectra of Ru1-modified quartz without UCNP before and after irradiation with NIR light.

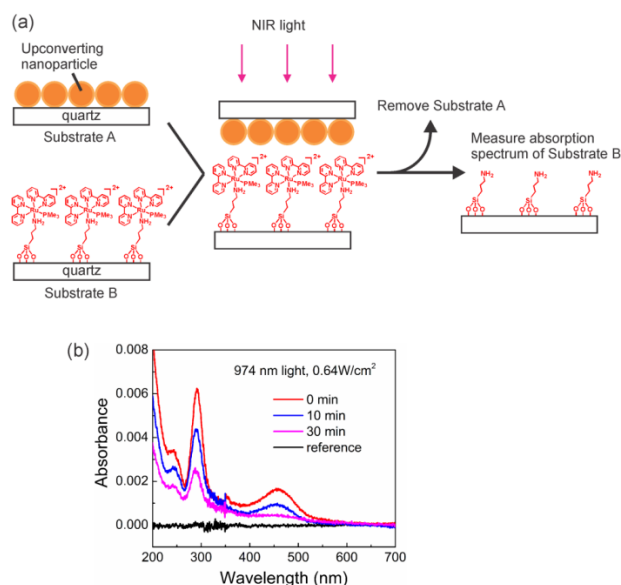


Figure S4. (a) Schematic of the release of Ru complexes and their quantification using UV-vis absorption spectroscopy. To make the energy transfer efficient, Substrate A directly contacted Substrate B. (b) UV-vis absorption spectra of Ru1-modified quartz (Substrate B) before and after irradiation with 974-nm light (0.64 W/cm^2) in the presence of the UCNP-decorated substrate (Substrate A).

In the spectra shown in Figure 2c, the substrate exhibits very strong scattering due to the UCNP. We were unable to calculate the amount of cleaved Ru complexes from Figure 2c. To avoid the influence of the strong scattering of the UCNP on the substrate, we used the procedure in Figure S4a to measure of the amount of released Ru using UV-vis absorption spectroscopy. On the basis of the decrease in the absorbance at 455 nm, $\sim 74\%$ of the Ru complexes were cleaved from the substrate after NIR irradiation for 30 min.

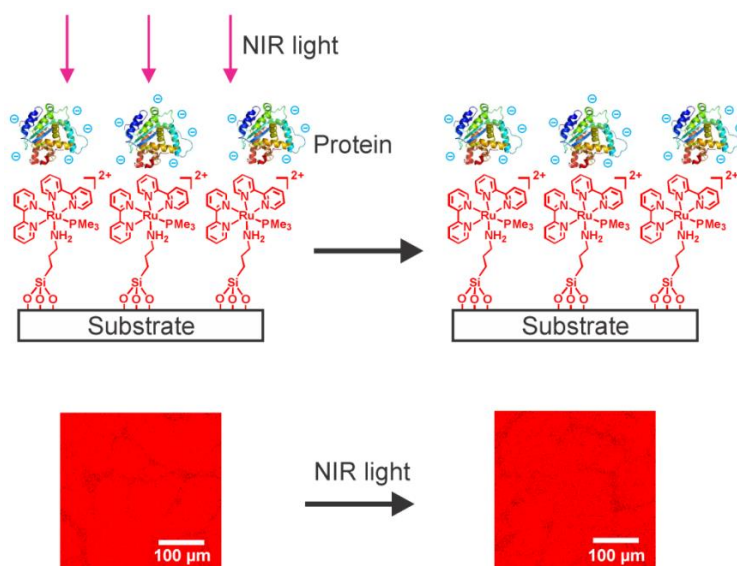


Figure S5. Schematic and confocal laser scanning microscopy images of Ru-modified substrates without UCNPs before and after NIR light exposure (0.64 W/cm^2 , 30 min). No desorption of proteins was observed.

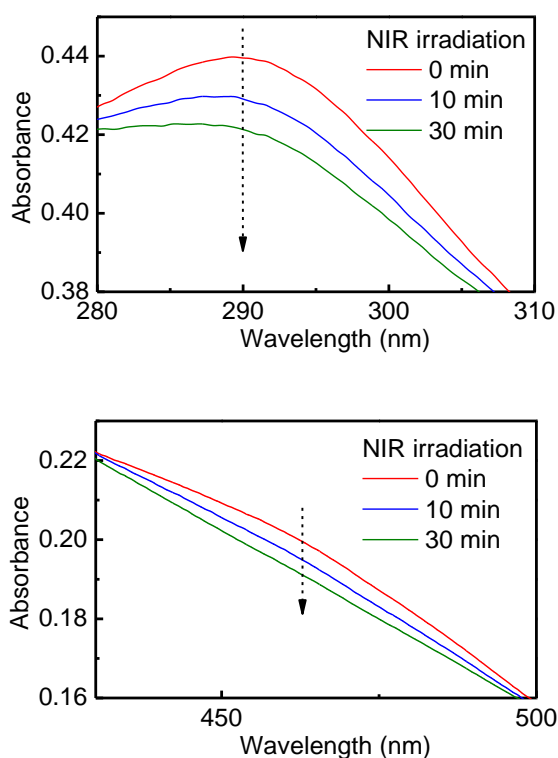


Figure S6. UV-vis absorption spectra of the Ru-UCNP substrate upon exposure to 974-nm light (0.64 W/cm^2). The upper and lower spectra are the enlarged spectra of Figure 2c at around 290 nm and 460 nm, respectively. They clearly show the photocleavage of the Ru complex.

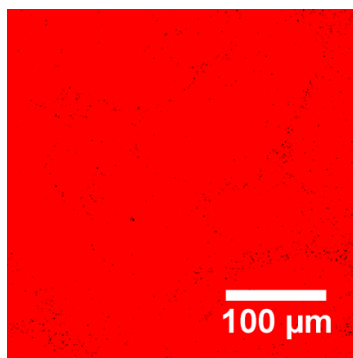


Figure S7. Confocal laser scanning microscopy image of a Ru-UCNP substrate with proteins after patterned blue light irradiation (470 nm, 40 min) when a piece of tissue was inserted between the light source and the sample. In this experiment, we only changed the NIR light source in Figure 4c to a 470-nm LED and kept all other conditions the same. No pattern was obtained.

References

- [1] S. He, K. Krippes, S. Ritz, Z. Chen, A. Best, H.-J. Butt, V. Mailänder, S. Wu, *Chem. Commun.* **2015**, 51, 431.
- [2] A. L. Bramblett, M. S. Boeck, K. D. Hauch, B. D. Ratner, T. Sasaki, J. W. Rogers, *Surf. Interface Anal.* **2002**, 33, 506.
- [3] a) P. Sathyadevi, P. Krishnamoorthy, N. S.P. Bhuvanesh, P. Kalaiselvi, V. V. Padma, N. Dharmaraj. *Eur. J. Med. Chem.* **2012**, 55, 420; b) P. Kalaivani, R. Prabhakaran, F. Dallemer, K. Natarajan, *RSC Adv.* **2014**, 4, 51850.

Chapter 4: Manipulating pH using near-infrared light assisted by upconverting nanoparticles

Zhijun Chen,^a Yubing Xiong,^a Roberto Etchenique,^b and Si Wu*^a

^aMax Planck Institute for Polymer Research, Ackermannweg 10, 55128 Mainz, Germany.

^bDepartamento de Química Inorgánica, Analítica y Química Física, INQUIMAE, Facultad de Ciencias Exactas y Naturales, Universidad de Buenos Aires, Ciudad Universitaria Pabellón 2, AR1428EHA Buenos Aires, Argentina.

Published in *Chem. Commun.*, **2016**, 52, 13959-13962.

Reproduced from *Chem. Commun.*, **2016**, 52, 13959-13962 with permission from the Royal Society of Chemistry

4.1 Statement of contribution

Si Wu conceived the idea and led the project.

Zhijun CHEN synthesized all the materials and conducted the measurements.

Roberto Etchenique analyzed the UV-Vis spectra of Ru-A.

Yubing Xiong drew the schematic figure.

4.2 Abstract: Near-infrared light can be used to manipulate the pH of aqueous solutions by using upconverting nanoparticle-assisted photocleavage of a ruthenium complex photobase. Upconverting nanoparticles and the photobase were also introduced into a pH-responsive hydrogel, in which near-infrared irradiation induced swelling of the hydrogel.

4.3 Introduction

pH is an important parameter in many chemical, physical and biological processes.^{1,2} Photoacids/bases, which can decrease/increase pH upon light irradiation, enable remote control of pH with high spatiotemporal resolution.³ Light-induced pH change can further control deformation of hydrogels,⁴ conductivity,⁵ polymerization,⁶ and host-guest interactions.⁷ pH manipulation has been proposed as a powerful technique to achieve control over relevant paths related to several diseases such as cancer, cardiovascular disease, Alzheimer's disease, etc.⁸ However, most photoacids/bases are sensitive to only UV light which can damage biological systems.⁹⁻¹¹ Recently, Liao et al. reported visible-light-responsive photoacids.^{4,8,12,13} Further, one of their photoacids

can be used in PBS buffer,⁸ which is desirable for biomedical applications. Nevertheless, visible light is still not able to deeply penetrate into tissue.¹⁴ Compared to UV and visible light, near-infrared (NIR) light is better suited for biomedical applications because NIR light causes less photodamage to biological systems and can penetrate much deeper into tissue.¹⁵ Therefore, developing NIR-manipulated pH represents significant progress for the biomedical field.

A promising approach to NIR-manipulated pH is based on photochemistry assisted by lanthanide-doped upconverting nanoparticles (UCNPs). UCNPs can convert NIR light into UV/visible light.^{16, 17} The upconverted UV/visible light can then induce photoreactions of conventional UV-/visible-light-sensitive compounds. This process is called UCNP-assisted photochemistry.¹⁸⁻²¹ UCNP-assisted photoisomerization,^{22,23} photocleavage,²⁴⁻²⁶ photopolymerization^{27,28}, and photo coupling reaction²⁹ have already been studied in the context of various applications.³⁰⁻³⁷ Additionally, a new type of UCNP-assisted photochemical process “UCNP-assisted photoinduced protonation/deprotonation” was proposed in the outlook of a recent review.³³ These previous works inspired us to use NIR light to control pH assisted by UCNPs.

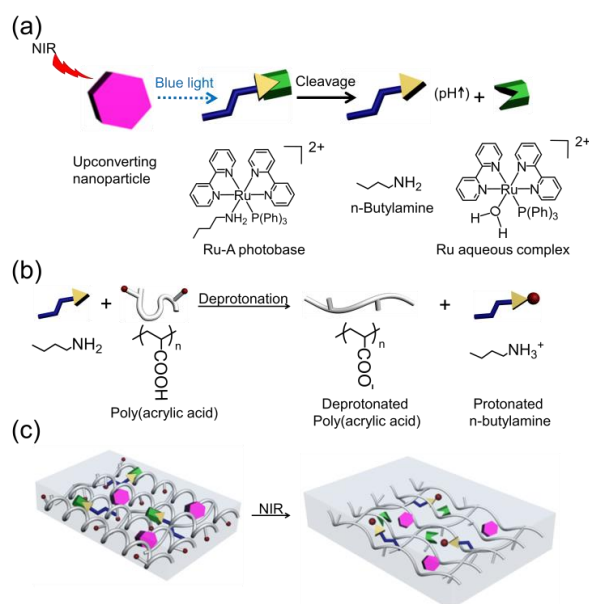


Fig. 1 Schematic illustration of photon upconversion pH manipulation and NIR light-induced swelling of the nanocomposite hydrogel. (a) The blue emission from UCNPs triggers the cleavage of the Ru photobase (Ru-A) and induces pH change; (b) The released butyl amine from Ru-A results in the deprotonation of poly(acrylic acid) (PAA); (c) NIR light-induced

swelling of the nanocomposite hydrogel, which was prepared by inducing UCNPs and Ru-A into crosslinked PAA. All the symbols are shown in (a) and (b).

Here, we experimentally demonstrate that the combination of UCNPs and a photobase enables the control of pH by NIR light (Figure 1a). We refer to this new combination as a photon upconversion pH manipulation. The complex $[\text{Ru}(\text{bpy})_2(\text{PPh}_3)(\text{BuNH}_2)]^{2+}$ (bpy=2,2' bipyridine; PPh_3 = triphenylphosphine, BuNH_2 = n-butylamine), hereafter Ru-A (Figure 1a), was used as the photobase because blue light irradiation on Ru-A can cause a pH change within nano to microseconds.³⁸ Moreover, we found that UCNPs can efficiently assist photocleavage of Ru complexes because of spectral overlap of Ru complex absorption³⁹⁻⁴¹ and UCNP emission.^{19, 42} Further, we have recently demonstrated the true sectioning power of the upconversion excitation,¹⁷ allowing precise z-axis manipulation of the downstream effects of NIR irradiation. On these bases, Ru-A was combined with UCNPs which would convert NIR light to blue light to enable the release of n-butylamine from Ru-A (Figure 1a). The released butyl amine would then increase the pH of an aqueous solution. When NIR light-induced release of n-butylamine occurs in the presence of poly(acrylic acid) (PAA), PAA can become more hydrophilic via deprotonation and thus swell due to electrostatic repulsion (Figure 1b). Thus, to demonstrate the potential application of NIR light-manipulated pH, we introduced UCNPs and Ru-A into a PAA hydrogel (Figure 1c).

4.4 Results and discussion

$\text{NaYF}_4:\text{TmYb}@ \text{NaYF}_4$ nanoparticles UCNPs (core = NaYF_4 : 0.5 mol% Tm^{3+} : 30 mol% Yb^{3+} ; shell = NaYF_4) with a diameter of 50 nm were synthesized as the upconverters (Figure 2a). These UCNPs emitted blue light under 974 nm NIR light excitation. The absorption band of the photobase Ru-A in the blue light region overlapped with the blue emission of the UCNPs (Figure 2a). To demonstrate absorption of upconverted blue light by the Ru-A, we compared upconversion luminescence spectra of UCNP in the presence and absence of Ru-A. The intensity of upconversion luminescence of UCNPs at 440 nm and 470 nm decreased significantly in the presence of Ru-A (Figure 2b). Additionally, Ru-A with higher concentration absorbed more upconverted blue light and resulted in lower emission intensity. In contrast, the emission at 800 nm, a spectral region where Ru-A has no absorption, still remained. (Figure 2b). This result proved efficient absorption of the upconverted blue light by Ru-A. When irradiating a dispersion of UCNPs and Ru-A with NIR light, the absorption

band of Ru-A decreased and red shifted (Figure 2c). This spectral change was identical to that observed for Ru-A which was directly photocleaved using blue light (Figure S1, ESI). Thus, Ru-A was photocleaved by NIR light irradiation. The exposure of Ru-A to NIR light in the absence of UCNPs did not change the absorption spectrum (Figure S2, ESI), proving the photocleavage of Ru-A was induced by the photon upconversion process.

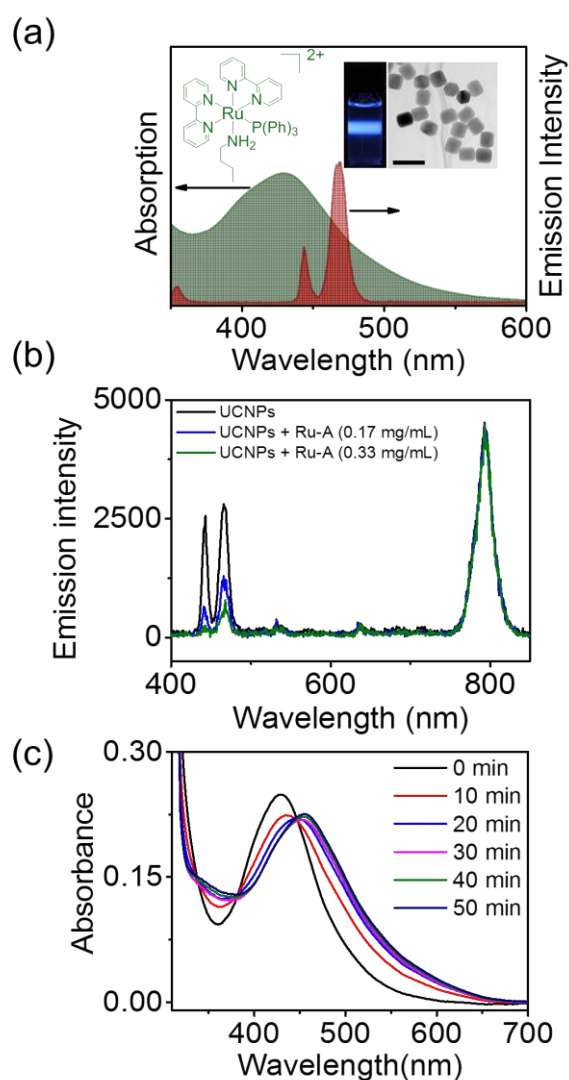


Fig. 2 (a) Absorption spectrum of Ru-A and emission spectrum of UCNPs under excitation by 974 nm light (5.5 W/cm^2). Insets: TEM image of UCNPs (scale bar 100 nm) and photograph of UCNPs under 974 nm light exposure; (b) Upconversion luminescence spectra of UCNPs (1 mg/mL) and UCNPs/Ru-A excited by 974 nm light. The concentrations of Ru-A were 0.17 (blue line) and 0.33 mg/mL (green line), respectively; (c) UV/Vis absorption spectra of the dispersion of UCNPs (0.15 mg/mL) and Ru-A (0.05 mg/mL) in acetone/water mixture (0.5/99.5, V/V) upon 974 nm light exposure (5.5 W/cm^2).

To demonstrate a NIR-induced pH increase, an aqueous dispersion of UCNPs was prepared by ultrasonic treatment of UCNPs in water (Figure S3 and Video 1, ESI). Afterward, Ru-A was introduced into the UCNPs dispersion. The UCNP/Ru-A dispersion was placed into an ice bath and irradiated with NIR light. The NIR light-induced pH change of the UCNP/Ru-A dispersion was measured (Figure 3a). The initial pH of the UCNP/Ru-A dispersion was 5.2, which did not change in the dark. However, exposure to NIR light (5.5 W cm^{-2}) changed the pH from 5.23 to 6.80 (Figure 3a). NIR light irradiation can induce the release of n-butylamine from Ru-A (Figure 2). The coordinated n-butylamine in Ru-A does not act as a base because its electron pair is strongly coordinated with Ru^{2+} . However, the released free n-butylamine is a relatively strong base with pK_a 10.77.³⁸ Thus, the NIR light-induced pH change was attributed to the released n-butylamine from Ru-A. As a control experiment, exposure of Ru-A in the absence of UCNPs to NIR light in an ice bath showed no pH change (Figure S4, ESI), which further confirmed the pH change was due to the photon upconversion process. In addition, NIR light irradiation also changed the color of the dispersion because the absorption spectra of Ru-A and Ru-aqua photoproduct ($\text{Ru-H}_2\text{O}$, Figure 1a) are different. Moreover, the ratio of UCNPs and Ru-A was tuned to investigate its influence on pH change of the solution. The concentration of UCNPs was fixed. As the concentration of Ru-A increased, pH change was larger (Figure 3b). The larger pH change was because more n-butylamine can be released from Ru-A with a higher concentration. Thus, the ratio of UCNPs and Ru-A can be used to adjust the range of pH change.

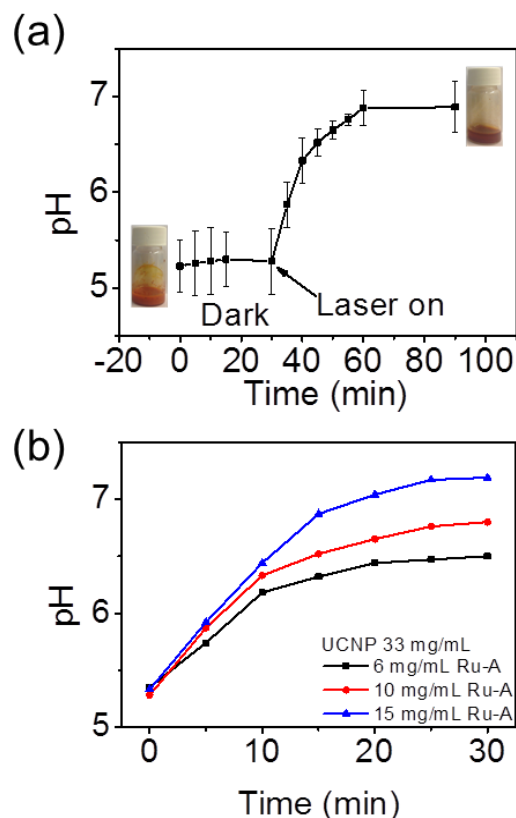


Fig. 3 (a) pH change of a dispersion of UCNPs (33 mg/mL) and Ru-A (10 mg/mL) in acetone/water mixture (6/94, V/V) upon NIR light irradiation (5.5 W cm^{-2}) in an ice bath. Inset: Photos of the dispersion before and after NIR light irradiation; (b) pH change of a dispersion of UCNPs (33 mg/mL) and Ru-A with different concentrations in acetone/water mixture (6/94, V/V) upon NIR light irradiation (5.5 W cm^{-2}) in an ice bath.

Subsequently, the NIR-manipulated pH increase was used to control deformation of a pH-sensitive hydrogel. A nanocomposite hydrogel was prepared by cross-linking PAA in the presence of Ru-A and UCNPs. Upconverted luminescence was observed from the nanocomposite hydrogel upon irradiation with NIR light (Figure 4a), which further confirmed UCNPs were incorporated inside the hydrogel. A nanocomposite hydrogel with the volume of 0.28 cm^3 was immersed in an aqueous solution (pH 3.5) and irradiated with NIR light for 15 min in an ice bath. NIR irradiation was conducted in an ice bath because an ice bath can prevent overheating problems of NIR irradiation and heat-induced side effects (Figure S5, S6).^{33, 43} After irradiation, the volume of the hydrogel increased to 0.37 cm^3 , which was 32% larger than the hydrogel before irradiation (Figure 4b, left). In addition, the

color of the hydrogel changed from orange to brown upon NIR light irradiation, which is identical to the color change observed in the dispersion of UCNPs and Ru-A upon NIR irradiation (Figure 3a). Thus, the swelling was attributed to deprotonation of PAA by the released n-butylamine from Ru-A. In a control experiment, the hydrogel without irradiation did not change size or color (Figure 4b, right). In another two control experiments, hydrogels with only Ru-A or UCNPs were prepared. The hydrogel with Ru-A and without UCNPs did not show any color or volume change upon NIR irradiation in an ice bath (Figure S7, ESI). The hydrogel only incorporating UCNPs also was unresponsive to NIR irradiation (Figure S8, ESI). These results further confirmed the swelling of the hydrogel was due to the released n-butyl amine upon NIR irradiation.

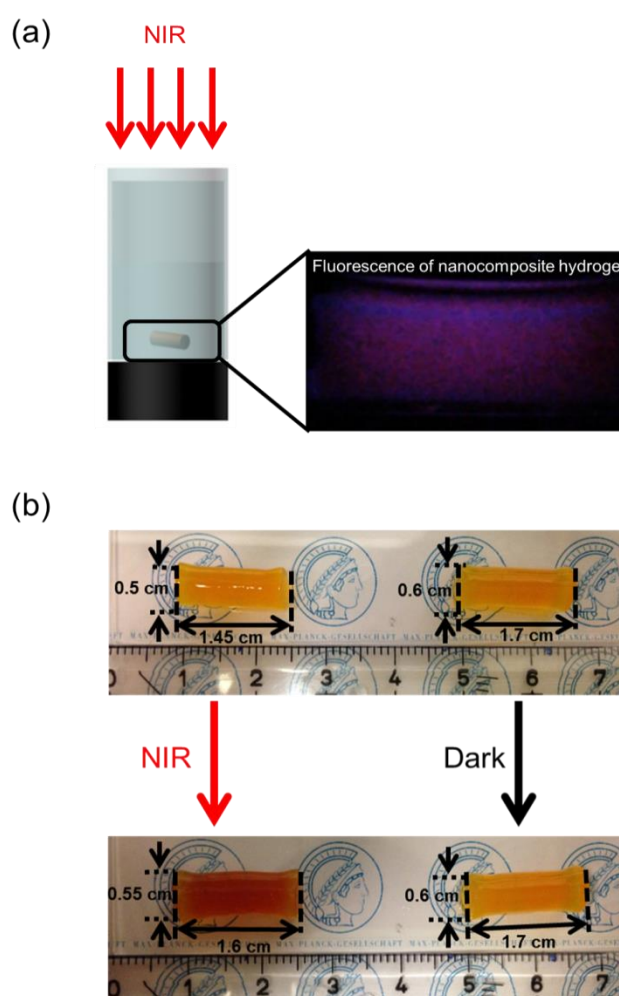


Fig. 4 (a) Schematic illustration of the set up for NIR-controlled swelling of nanocomposite hydrogel (with UCNPs, 33 mg/mL and Ru-A, 10 mg/mL). (b) Nanocomposite hydrogel before and after NIR light irradiation (5.5 W/cm², 15 min) (left) and in the dark (right). The samples were placed in an ice bath during irradiation.

4.5 Conclusion

In conclusion, we demonstrated that NIR light can increase the pH under the assistance of UCNPs and the photobase Ru-A. UCNPs converted NIR light to blue light, which triggered the release of n-butylamine from Ru-A. The released n-butylamine can further deprotonate PAA. The strategy of photon upconversion pH manipulation was further developed to control the swelling of pH-sensitive PAA hydrogels. Not only Ru-A but also many other photoacids/photobases can alter solution pH after light irradiation. Thus, the concept “photon upconversion pH manipulation” reported in this work is a general approach to control pH by NIR light. Also, photon upconversion pH manipulation can not only induce swelling of pH-sensitive hydrogels but can also stimulate other pH-responsive materials, such as micelles, capsules, and supramolecules. Thus, photon upconversion pH manipulation is a new and general way to control pH-responsive materials with high spatiotemporal resolution for various applications.

4.6 Acknowledgements

Z.C. and Y.X. were supported by the CSC program. R.E. is a member of CONICET. We thank H. Menges for measuring the upconverting luminescence spectra. This work was partly supported by the Deutsche Forschungsgemeinschaft (DFG, WU 787/2-1).

4.7 Notes and references

- 1 H. Sohn, S. Létant, M. J. Sailor and W. C. Trogler, *J. Am. Chem. Soc.*, 2000, **122**, 5399.
- 2 Y. Bae, S. Fukushima, A. Harada and K. Kataoka, *Angew. Chem., Int. Ed.*, 2003, **42**, 4640.
- 3 M. Shirai and M. Tsunooka, *Prog. Polym. Sci.*, 1996, **21**, 1.
- 4 Z. Shi, P. Peng, D. Strohecker and Y. Liao, *J. Am. Chem. Soc.*, 2011, **133**, 14699.
- 5 S. Haghghat, S. Ostresh and J. M. Dawlaty, *J. Phys. Chem. B*, 2016, **120**, 1002.
- 6 C. Fu, J. Xu and C. Boyer, *Chem. Commun.*, 2016, **52**, 7126.
- 7 J. Vázquez, M. A. Romero, R. N. Dsouza and U. Pischel, *Chem. Commun.*, 2016, **52**, 6245.
- 8 N. Abeyrathna and Y. Liao, *J. Am. Chem. Soc.*, 2015, **137**, 11282.
- 9 M. Shirai and H. Okamura, *Prog. Org. Coat.*, 2009, **64**, 175.
- 10 W. Feng, W. Zhou, S. Zhang, Y. Fan, A. Yasin and H. Yang, *Rsc Adv*, 2015, **5**, 81784.
- 11 A. Chemtob, F. Courtecuisse, C. Croutxé-Barghorn and S. Rigolet, *New J. Chem.*, 2011, **35**, 1803.
- 12 V. K. Johns, P. Peng, J. DeJesus, Z. Wang and Y. Liao, *Chem. -Eur. J.*, 2014, **20**, 689.
- 13 Z. Z. Wang, V. K. Johns and Y. Liao, *Chem.-Eur. J.*, 2014, **20**, 14637.
- 14 P. Juzenas, A. Juzeniene, O. Kaalhus, V. Iani and J. Moan, *Photoch Photobio Sci*, 2002, **1**, 745.
- 15 R. Wang and F. Zhang, *J. Mater. Chem. B*, 2014, **2**, 2422.
- 16 C. Li, D. Yang, P. Ma, Y. Chen, Y. Wu, Z. Hou, Y. Dai, J. Zhao, C. Sui and J. Lin, *Small*, 2013, **9**, 4150.
- 17 J. Hodak, Z. Chen, S. Wu and R. Etchenique, *Anal. Chem.*, 2016, **88**, 1468.
- 18 E. Ruggiero, A. Habtemariam, L. Yate, J. C. Mareque-Rivas and L. Salassa, *Chem. Commun.*, 2014, **50**, 1715.
- 19 Z. Chen, W. Sun, H. J. Butt and S. Wu, *Chem.-Eur. J.*, 2015, **21**, 9165.
- 20 B. Yan, J.-C. Boyer, D. Habault, N. R. Branda and Y. Zhao, *J. Am. Chem. Soc.*, 2012, **134**, 16558.
- 21 B. Yan, J.-C. Boyer, N. R. Branda and Y. Zhao, *J. Am. Chem. Soc.*, 2011, **133**, 19714.
- 22 J. C. Boyer, C. J. Carling, B. D. Gates and N. R. Branda, *J. Am. Chem. Soc.*, 2010, **132**, 15766.

- 23 W. Wu, L. M. Yao, T. S. Yang, R. Y. Yin, F. Y. Li and Y. L. Yu, *J. Am. Chem. Soc.*, 2011, **133**, 15810.
- 24 Y. M. Yang, Q. Shao, R. R. Deng, C. Wang, X. Teng, K. Cheng, Z. Cheng, L. Huang, Z. Liu, X. G. Liu and B. G. Xing, *Angew. Chem., Int. Ed.*, 2012, **51**, 3125.
- 25 J. Shen, G. Chen, T. Y. Ohulchanskyy, S. J. Kesseli, S. Buchholz, Z. Li, P. N. Prasad and G. Han, *Small*, 2013, **9**, 3213.
- 26 M. L. Viger, M. Grossman, N. Fomina and A. Almutairi, *Adv. Mater.*, 2013, **25**, 3733.
- 27 S. Beyazıt, S. Ambrosini, N. Marchyk, E. Palo, V. Kale, T. Soukka, B. T. S. Bui and K. Haupt, *Angew. Chem., Int. Ed.*, 2014, **53**, 8919.
- 28 A. Stepuk, D. Mohn, R. N. Grass, M. Zehnder, K. W. Krämer, F. Pellé, A. Ferrier and W. J. Stark, *Dent Mater.*, 2012, **28**, 304.
- 29 P. Lederhose, Z. J. Chen, R. Müller, J. P. Blinco, Si Wu, and C. Barner-Kowollik, *Angew. Chem. Int. Ed.*, 2016, DOI: 10.1002/anie.201606425.
- 30 D. Yang, P. Ma, Z. Hou, Z. Cheng, C. Li and J. Lin, *Chem. Soc. Rev.*, 2015, **44**, 1416.
- 31 X. G. Liu, C. H. Yan and J. A. Capobianco, *Chem. Soc. Rev.*, 2015, **44**, 1299.
- 32 Z. Y. Cheng and J. Lin, *Macromol. Rapid. Comm.*, 2015, **36**, 790.
- 33 S. Wu and H. J. Butt, *Adv. Mater.*, 2016, **28**, 1208.
- 34 A. E. Pierri, P.-J. Huang, J. V. Garcia, J. G. Stanfill, M. Chui, G. Wu, N. Zheng and P. C. Ford, *Chem. Commun.*, 2015, **51**, 2072.
- 35 P. T. Burks, J. V. Garcia, R. GonzalezIrias, J. T. Tillman, M. Niu, A. A. Mikhailovsky, J. Zhang, F. Zhang and P. C. Ford, *J. Am. Chem. Soc.*, 2013, **135**, 18145.
- 36 C. Wang, X. Li and F. Zhang, *Analyst*, 2016, **141**, 3601.
- 37 J. Zhou, Z. Liu and F. Li, *Chem. Soc. Rev.*, 2012, **41**, 1323.
- 38 O. Filevich, G. Carrone, V. A. Pavlovsky and R. Etchenique, *Anal. Chem.*, 2012, **84**, 5618.
- 39 S. Bonnet, B. Limburg, J. D. Meeldijk, R. J. M. K. Gebbink and J. A. Killian, *J. Am. Chem. Soc.*, 2011, **133**, 252.
- 40 A. Bahreman, B. Limburg, M. A. Siegler, R. Koning, A. J. Koster and S. Bonnet, *Chem.-Eur. J.*, 2012, **18**, 10271.
- 41 J. D. Knoll and C. Turro, *Coord. Chem. Rev.*, 2015, **282-283**, 110.
- 42 S. Q. He, K. Krippes, S. Ritz, Z. J. Chen, A. Best, H. J. Butt, V. Mailänder and S. Wu, *Chem. Commun.*, 2015, **51**, 431.
- 43 J.Y. Dong and J. I. Zink, *Small*, 2015, **11**, 4165.

4.8 Supporting information

Materials

Ytterbium(III) acetate hydrate (99.9%), thulium(III) acetate hydrate (99.9%), yttrium(III) acetate hydrate (99.9%), 1-octadecene (technical grade, 90%), oleic acid (technical grade, 90%), ammonium fluoride (99.99%), ruthenium(III) chloride trihydrate (technical grade), 2,2'-biquinoline (98%), acrylic acid (99%), N,N'-methylenebisacrylamide (99%) were purchased from Sigma-Aldrich. All solvents and other chemicals were purchased from Sigma-Aldrich or Fisher Scientific.

Characterization

UV-vis absorption spectra were collected using an Agilent Cary 4000 spectrometer. pH was measured using a Mettler Toledo pH meter. TEM images were collected on a JEOL JEM1400 transmission electron microscope. The upconversion photoluminescence was measured using a Spex Fluorolog II (212) spectrometer. A diode laser with a wavelength of 974 nm (type P976MF, PhotonTec Berlin GmbH) coupled with a 105- μm (core) fiber was used as the excitation light source. The diode laser was equipped with an adjustable fiber collimator (Changchun New Industries Optoelectronics Technology). The output power of the diode laser was controlled by a tabletop laser driver (device type ds11-la12v08-pa08v16-t9519-254-282, OsTech GmbH i.G.). The output power density of the diode laser was measured using an optical power meter (model 407A, Spectra-Physics Corp.) and a NIR indicator (Newport, model F-IRC1).

Synthesis

The synthesis of $\beta\text{-NaYF}_4\text{:0.5 mol\% Tm}^{3+}$, 30 mol% $\text{Yb}^{3+}/\beta\text{-NaYF}_4$ core/shell UCNPs was reported in our previous work.^[1] The details are provided below.

Synthesis of $\beta\text{-NaYF}_4\text{: 0.5 mol\% Tm}^{3+}$, 30 mol% Yb^{3+} core nanoparticles. The $\text{NaYF}_4\text{:TmYb}$ core nanoparticles were synthesized according to $\text{Y}(\text{CH}_3\text{COO})_3 \cdot x\text{H}_2\text{O}$ (372 mg, 1.4 mmol), $\text{Yb}(\text{CH}_3\text{COO})_3 \cdot x\text{H}_2\text{O}$ (210 mg, 0.6 mmol) and $\text{Tm}(\text{CH}_3\text{COO})_3 \cdot x\text{H}_2\text{O}$ (3.5 mg, 0.01 mmol) were added to a 100 mL threeneck round-bottom flask containing octadecene (30 mL) and oleic acid (12 mL). The solution was stirred magnetically and heated to 120 °C under vacuum (heating rate: 3 °C/min) to form the lanthanide oleate complexes. The solution was degassed at 120 °C for 15 min to remove residual water, acetic acid and oxygen. The

temperature of the solution was then lowered to 50 °C and the reaction flask was placed under a gentle flow of Ar. During this time, a solution of ammonium fluoride (296 mg, 8.0 mmol) and sodium hydroxide (200 mg, 5.0 mmol) dissolved in methanol (20 mL) was prepared via sonication. Once the reaction mixture reached 50 °C, the methanol solution was added to the reaction flask and the resulting cloudy mixture was stirred for 30 min at 50 °C. The reaction temperature was then increased to ~70 °C and degased for 15 min to remove methanol in the reaction flask. Then, the reaction flask was placed under a gentle flow of Ar. Subsequently, the reaction temperature was increased to 300 °C (heating rate: 20 °C/min) under the Ar flow and kept at this temperature of 90 min. During this time the reaction mixture became progressively clearer until a completely clear, slightly yellowish solution was obtained. The mixture was allowed to cool to room temperature naturally. The nanoparticles were precipitated by the addition of ethanol (~80 mL), and isolated via centrifugation at 5000 rpm. The resulting pellet was dispersed in a minimal amount of hexane (5-10 mL) and precipitated with excess ethanol (~60 mL). The nanoparticles were isolated via centrifugation at 5000 rpm and then dispersed in hexane (10–15 mL) for the subsequent shell growth procedure.

Synthesis of β -NaYF₄: 0.5 mol% Tm³⁺, 30 mol% Yb³⁺ / β -NaYF₄ core/shell nanoparticles.

Y(CH₃COO)₃•xH₂O (479 mg, 1.8 mmol) was added to a 100 mL threeneck round-bottom flask containing octadecene (30 mL) and oleic acid (12 mL). The solution was stirred magnetically and heated to 120 °C under vacuum (heating rate: 3 °C/min) and maintain at 120 °C for 15 min. The temperature of the reaction flask was lowered to 80 °C and the reaction flask was placed under a gentle flow of Ar. Then, the dispersion of NaYF₄: 0.5 mol% Tm³⁺, 30 mol% Yb³⁺ core nanoparticles in hexane, which was synthesized by the procedure shown above, was added to the flask. The resulting solution was heated to 110 °C (heating rate: 5 °C/min) and degased for 15 min to remove hexane in the reaction flask. The reaction mixture was cooled to 50 °C and the flask was place under a gentle flow of Ar. Then, a solution of ammonium fluoride (259 mg, 7.0 mmol) and sodium hydroxide (175 mg, 4.4 mmol) in methanol (20 mL) was added. The resulting cloudy mixture was stirred at 50 °C for 30 min. The reaction temperature was then increased to ~70 °C and degased for 15 min to remove methanol in the reaction flask. Then, the reaction flask was placed under a gentle flow of Ar. Subsequently, the reaction temperature was increased to 300 °C (heating rate: 20 °C/min) and kept at this temperature for 90 min under the Ar flow. The mixture was allowed to cool to room temperature naturally. The nanoparticles were precipitated by the

addition of ethanol (~80 mL) and isolated via centrifugation at 5000 rpm. The resulting pellet was dispersed in a minimal amount of hexane (5-10 mL) and precipitated with excess ethanol (~60 mL). The nanoparticles were isolated via centrifugation at 5000 rpm and then dried in the vacuum oven.

Synthesis of [Ru(bpy)₂(PPh₃)(BuNH₂)] (Ru-A)

The synthesis of Ru-A was according to the previous work of one of the authors.^[2] The details are shown below.

Synthesis of Ru(bpy)₂Cl₂. The synthesis of Ru(bpy)₂Cl₂ is according to the literature.^[3] RuCl₃•3H₂O (807.4 mg), 962.5 mg (6.2 mmol) of 2,2'-bipyridine, and 0.9 g LiCl were dissolved in 7 mL of DMF. The solution is refluxed for 8 h and cooled to room temperature. After adding 35 mL of acetone, the solution was kept in a freezer overnight. The crystalline product was filtered and washed with cool water and dried in the vacuum oven at room temperature.

Synthesis of Ru(bpy)₂(PPh₃)Cl. The synthesis of Ru(bpy)₂(PPh₃)Cl is according to the literature.^[4] Ru(bpy)₂Cl₂ (682 mg, 1.3 mmol) was dissolved in methanol (45 mL). Triphenylphosphine (410 mg, 1.5 mmol) was added, and the mixture was stirred until complete dissolution. After this, water (20 mL) was added, and the mixture was heated at reflux for 2 h. Once the reaction was complete, the solution was concentrated by rotary evaporation. The solid was resuspended in acetone (50 mL), which first produced the dissolution of [Ru(bpy)₂Cl]⁺ and then the precipitation of [Ru(bpy)₂Cl]Cl. The solution was kept at 0 °C for one hour before filtration. The red solid was washed with cold acetone and diethyl ether.

Synthesis of [Ru(bpy)₂(PPh₃)(BuNH₂)] (Ru-A). A total of 200 mg of [Ru(bpy)₂(PPh₃)Cl]Cl was dissolved in 20 mL of water and heated to 80 °C. The formation of the [Ru(bpy)₂(PPh₃)-(H₂O)]²⁺ complex was determined by its absorption band at 425 nm which moves to 450 nm at pH > 12. After formation of the aquo complex, a mixture of 20 equiv of n-butylamine (BuNH₂) and 5 equiv of p-toluenesulfonic acid previously dissolved in 5 mL of water was added. The solution was heated at 80 °C in a sealed tube and monitored by UV-Vis during about 4 h, until no further spectral changes were observed. All the following procedures were

done in darkness. The solution was filtered to remove any insoluble particles and the EtOH and the excess of BuNH₂ were removed under vacuum. The aqueous solution was precipitated with saturated KPF₆. Ru-A is non-fluorescent.

NIR-Controlled pH change of the dispersion of UCNPs and Ru-A

Ru-A (30 mg) was dissolved in 0.2 mL acetone. UCNPs (100 mg) were dispersed in 3 mL water with the assistance of ultrasonic treatment (Figure S3, see the process in Video S1). The acetone solution of Ru-A was added to the dispersion of UCNPs to prepare the dispersion of UCNPs and Ru-A. The pH change was measured while irradiating the suspension with CW 974 nm laser with the working power densities fixed at 5.5 W cm⁻² with magnetic stirring. The temperature of the system was controlled by an ice bath to exclude the influence of photothermal effect caused by NIR irradiation.

Preparation of hydrogel containing UCNPs and Ru-A

A solution containing 200 mg/mL AA, 0.5 mg/mL MBA, 3 mL H₂O, 33 mg/mL UCNPs, 10 mg/mL Ru-A, and 33 mg/mL APS was bubbled with nitrogen for 30 mins. Then, the precursor solution was added to the tubes which were subsequently sealed and kept at the room temperature for 12 h. The resulting hydrogels were removed from the glass tubes and soaked in distilled water for half an hour to remove the unreacted monomer. The hydrogel was stored in a sealed bottle in dry condition in the dark until use.

Preparation of hydrogel containing Ru-A or UCNPs Only

The procedure and amount were the identical to the preparation of hydrogel containing both UCNPs and Ru-A except excluding either UCNPs or Ru-A.

NIR-controlled swelling of hydrogel in ice bath

Before the NIR irradiation experiment, the nanocomposite hydrogel was equilibrated in water (pH = 3.5) for 4 h. The temperature of the system was held constant by an ice bath to exclude the influence of heating caused by NIR laser. As a control experiment, the hydrogel was left in the water solution (1.5 mL, pH = 3.5) for an additional 15 mins without NIR irradiation.

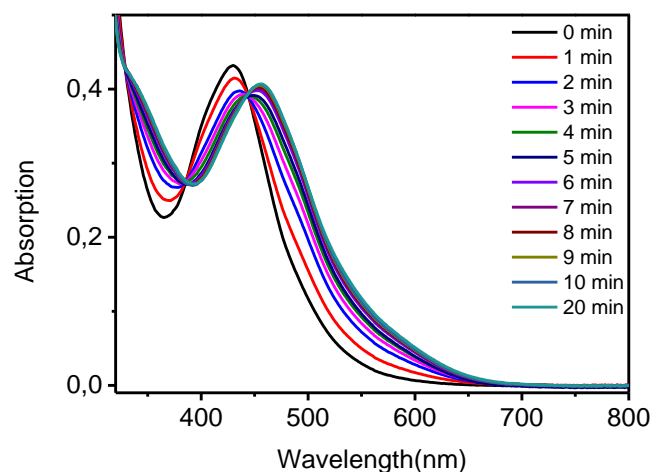


Figure S1. UV/Vis absorption spectra of Ru-A (0.1 mg/mL, 0.5/99.5 acetone/water) upon 470 nm light exposure (1 mW cm^{-2}). The spectral change shows 470 nm light efficiently triggered the release of n-butylamine.^[2]

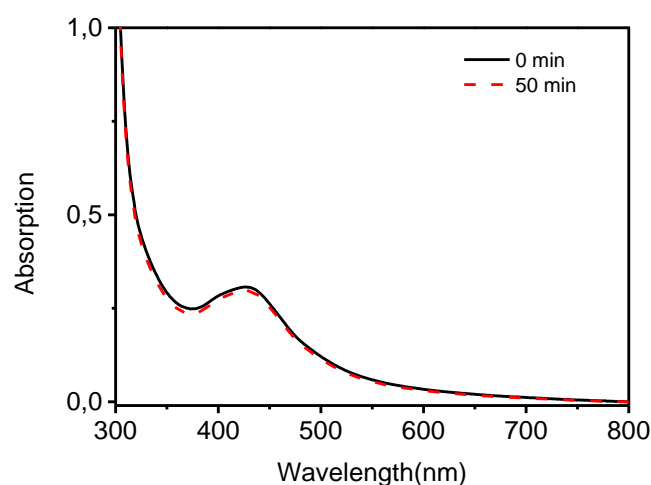


Figure S2. UV/Vis absorption spectra of Ru-A (0.1 mg/mL, 0.5/99.5 acetone/water) upon NIR light exposure (5.5 W cm^{-2}).

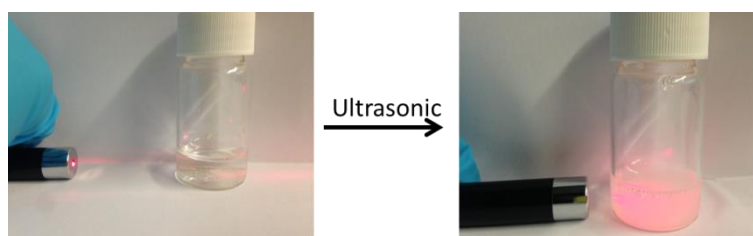


Figure S3. An aqueous dispersion of UCNPs (33 mg/mL) prepared by ultrasonic treatment. Before ultrasonic treatment (left), nearly no scattering was observed, which indicates UCNPs were not dispersed in water. After ultrasonic treatment, strong scattering was observed which indicates UCNPs were dispersed in water.

The sample preparation process was also shown in Video S1. In the preparation process, water (3 mL) was added to dry upconverting nanoparticles (100 mg). The nanoparticles were then dispersion in water by ultrasonic treatment.

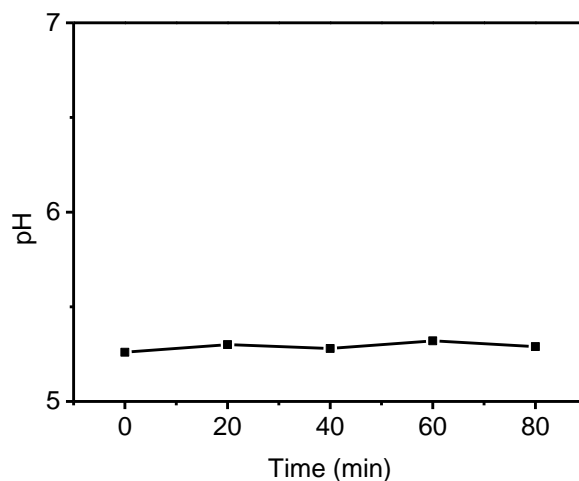


Figure S4. (a) pH change of a dispersion of Ru-A (10 mg/mL) in acetone/water mixture (6/94, V/V) upon NIR light irradiation (5.5 W cm⁻²) in an ice bath.

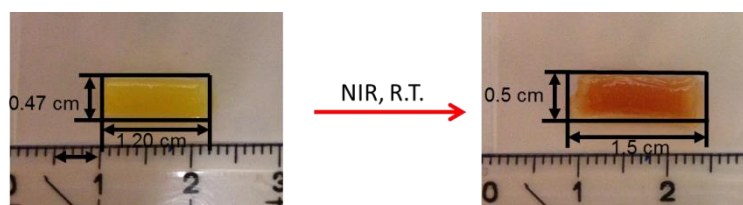


Figure S5. Nanocomposite hydrogel in the water solution (1.5 mL, pH = 3.5) before and after NIR light irradiation (5.5 W/cm², 15 min) at room temperature.

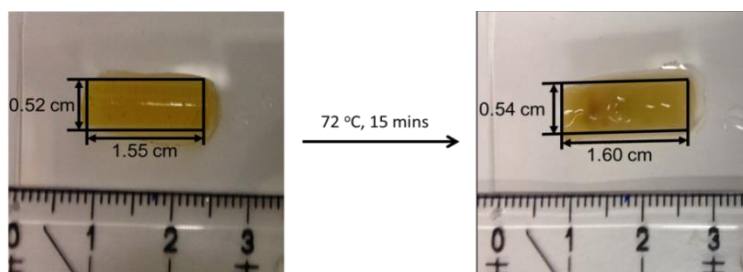


Figure S6. Nanocomposite hydrogel (1.5 mL, pH = 3.5) before and after heating at 72 °C for 15 min in an aqueous solution.

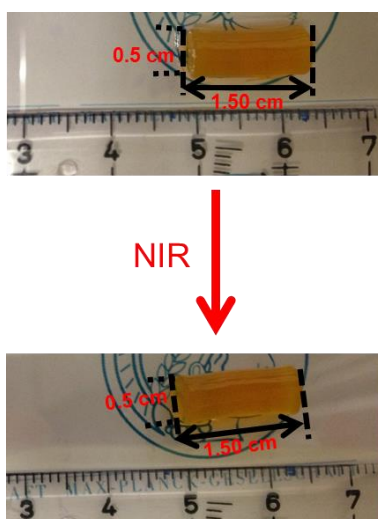


Figure S7. Hydrogel only incorporated with Ru-A (10 mg/mL) before and after NIR light exposure (5.5 W cm^{-2}). The sample in an aqueous solution was placed in an ice bath and irradiated by NIR light.

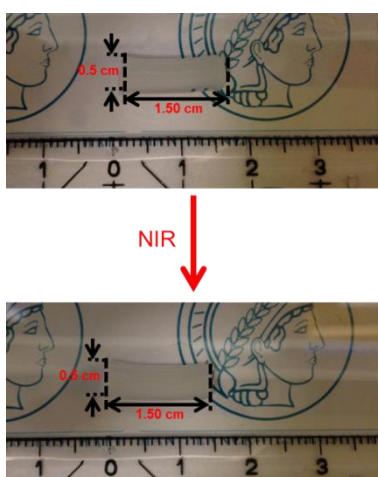


Figure S8. Hydrogel only incorporated with UCNPs (33 mg/mL) before and after NIR light exposure (5.5 W cm^{-2}). The sample in an aqueous solution was placed in an ice bath and irradiated by NIR light.

Video 1: Preparation of an aqueous dispersion of UCNPs

UCNPs (100 mg) were put in a vial. Water (3 mL) was then added to the vial. Nearly no light scattering was observed. The vial was put into an ultrasonic bath for 15 min. After that, a dispersion of UCNPs in water was obtained. Strong light scattering can be observed.

References

- [1] S. Q. He, K. Krippes, S. Ritz, Z. J. Chen, A. Best, H. J. Butt, V. Mailänder, S. Wu, *Chem. Commun.*, **2015**, *51*, 431-434.
- [2] O. Filevich, G. Carrone, V. A. Pavlovsky, R. Etchenique, *Anal. Chem.*, **2012**, *84*, 5618-5624.
- [3] Z. Assefa, D. M. Stanbury, *J. Am. Chem. Soc.*, **1997**, *119*, 521-530.
- [4] L. Zayat, M. G. Noval, J. Campi, C. I. Calero, D. J. Calvo, R. Etchenique, *ChemBioChem.*, **2007**, *8*, 2035-2038.

Chapter 5: Near-infrared photoinhibition of enzyme activities in living cells enabled by upconverting nanoparticles

Zhijun Chen, Raweewan Thiramanas, Volker Mailänder, and Si Wu*

Max Planck Institute for Polymer Research, Ackermannweg 10, D-55128, Mainz (Germany)

Submitted.

5.1 Statement of contribution

Si Wu conceived the idea and led the chemical part. Volker Mailänder led the biological part. Zhijun CHEN synthesized all the materials and characterized the materials.

Raweewan Thiramanas did all the biological experiments.

Zhijun CHEN and Raweewan Thiramanas contributed equally to this work.

5.2 Introduction

Enzymes are important macromolecular biological catalysts that enable chemical reactions in biological systems. Controlling the activities of enzymes can regulate metabolism, manipulate cell functions, kill pathogens, and treat diseases.^[1] Due to the great importance of enzymes in biological systems, the use of external stimuli, such as pH,^[2] temperature,^[3] ATP,^[4] cations,^[5] and light,^[6] to control enzyme activity has been developed. Among these stimuli, light provides high spatiotemporal resolution for controlling enzyme activities. UV or visible light can control photoresponsive compounds, such as photocages and photoswitchable molecules.^[7] The photoproducts from these photoresponsive compounds can then regulate enzyme activities.^[6a,6c,8] However, UV light may damage biological systems. Additionally, both UV and visible light cannot penetrate deeply into tissue. In contrast, near-infrared (NIR) light can penetrate deeply into tissue and cause less photodamage to biological systems.^[9] NIR light has been applied for controlling enzyme activities based on two-photon absorption.^[8a,10] However, two-photon absorption requires high-intensity pulsed lasers (typical pulse intensity: $>10^6 \text{ W cm}^{-2}$)^[11] and is inefficient even when femtosecond lasers are employed. Two-photon absorption only occurs at the laser focus. Because the laser defocuses as it passes through tissue, the two-photon absorption strategy is impractical for deep tissue applications. Additionally, controlling enzyme activities in a macroscopic system using two-photon absorption is a time-consuming and spot-by-spot process.

Recently, NIR light-triggered photoreactions based on lanthanide-doped upconverting nanoparticles (UCNPs) have been developed.^[9b,12,13] UCNPs can convert NIR light into UV and visible light. Then, the upconverted UV or visible emission can trigger photoreactions of traditional UV- or visible light-responsive compounds. This process is referred to as UCNP-assisted photochemistry.^[9b,14] UCNP-assisted photochemistry can be triggered by continuous wave laser diodes with intensities that are several orders of magnitude lower than that required for two-photon absorption.^[9b,15] UCNPs have assisted different photoreactions including photoisomerization,^[14e,16] photocleavage,^[17] photopolymerization,^[14d,18] and photocoupling reactions.^[19] These UCNP-assisted photoreactions have been applied to NIR-controlled drug delivery,^[14c,15b] biointerfaces,^[15a,16] uncaging enzymes,^[17c] catalysis,^[20] pH,^[21] and actuators.^[14e] However, inhibition of enzyme activity using NIR light assisted by UCNPs has not been investigated.

Here, we use NIR light for enzyme inhibition via UCNP-assisted photochemistry (**Figure 1**). We refer to this new method as photon upconversion enzyme inhibition (PUEI). To construct a platform for PUEI, a NaYF₄:TmYb@NaYF₄ UCNP and caged enzyme inhibitors (RuEI) are encapsulated in a hollow mesoporous silica nanoparticle (hmSiO₂) (**Figure 1b**). RuEI can be activated by blue light to release the enzyme inhibitor (EI). Our group^[9b,15,21,22] and other groups^[14f] have demonstrated that NIR light can efficiently uncage Ru complexes similar to RuEI with the assistance of UCNPs. With RuEI&UCNP@hmSiO₂ in this study, UCNPs can convert NIR light to blue light, which can uncage EI from RuEI (**Figure 1**). After NIR photoactivation, the released EI can inhibit the activities of the cathepsin K enzyme (**Figure 1b**). Cathepsin K is an important enzyme that is critical for osteoclastic bone resorption, macrophage invasion, and tumor growth.^[23] Cathepsin K is involved in the resorption of bone tissue in osteoclasts and therefore responsible for the remodeling of bone.^[24] Resorption of bone should be inhibited under some circumstances, such as bone loss in elderly patients or during the regeneration of new bone after a fracture. For the treatment of cancers and tumor metastases, cathepsin K is a key factor that affects the invasiveness of tumors into healthy tissue.^[25] Therefore, the inhibition of cathepsin K is important. NIR photoinhibition of the activity of cathepsin K allows for new routes for manipulating cell functions, regenerative medicine and treating the spread of malignant diseases in deep tissue. PUEI also provides a general platform for photoinhibition of enzyme activities in deep tissue.

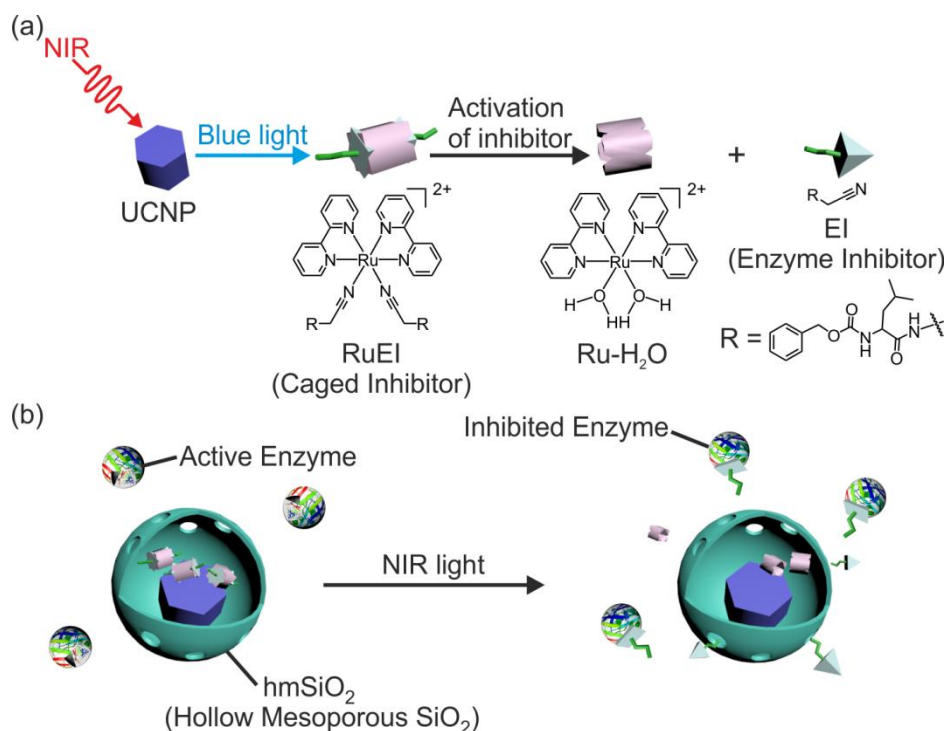


Figure 1. Schematic illustration of photon upconversion enzyme inhibition (PUEI). (a) Activation of the enzyme inhibitor using near-infrared (NIR) light with the assistance of UCNPs. UCNPs convert NIR light to blue light, which induces the cleavage of the caged inhibitor (RuEI) and activation of the enzyme inhibitor (EI). (b) NIR irradiation of RuEI&UCNP@hmSiO₂ activates EI, which inhibits enzyme activity.

5.3 Results and discussion

NaYF₄:TmYb@NaYF₄ UCNPs, which have an average diameter of 50 nm, were synthesized according to our previously published protocol (**Figure 2a, left**).^[15] UCNP@hmSiO₂ was synthesized using a modified soft template method (Supporting Information). In UCNP@hmSiO₂, the UCNP core was surrounded by an hmSiO₂ shell with an average diameter of ~100 nm (**Figure 2a, right**). The nitrogen adsorption-desorption analysis determined that the Brunauer-Emmett-Teller (BET) surface area of UCNP@hmSiO₂ was 167 m²/g (**Figure S1**). In comparison to traditional UCNPs with a mesoporous SiO₂ shell, the hollow mesoporous shell in UCNP@hmSiO₂ contains a large cavity, which enhanced the loading capacity for cargo. RuEI&UCNP@hmSiO₂ was prepared by loading RuEI into UCNP@hmSiO₂. The loading efficiency of RuEI, which was measured by UV-Vis absorption spectroscopy, was as high as 18.3 wt% (**Figure S2**).

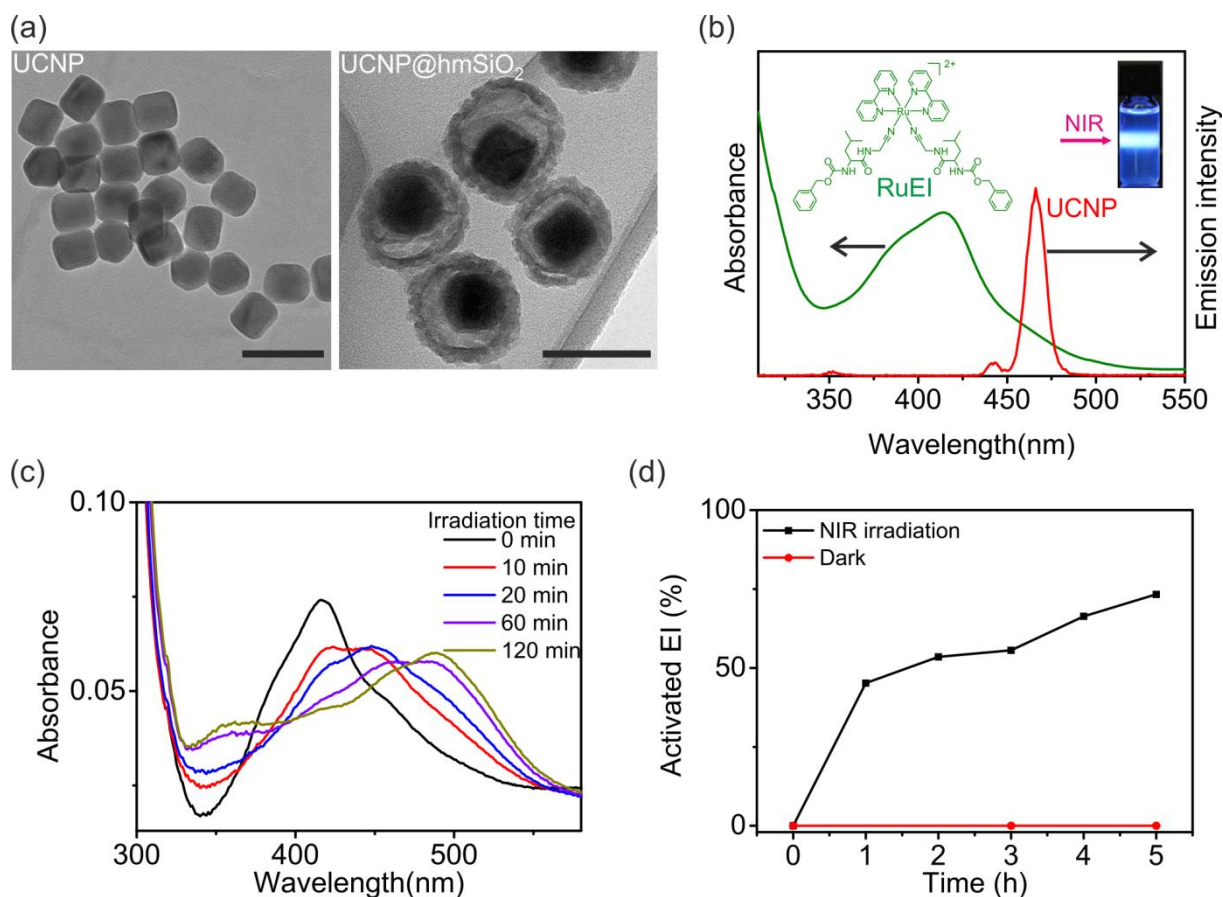


Figure 2. (a) TEM images of UCNPs (left) and UCNP@hmSiO₂ (right). The scale bars represent 100 nm. (b) UV-Vis absorption spectrum of RuEI and emission spectrum of UCNP under excitation by 974 nm light (2 W/cm²). (c) UV-Vis absorption spectra of RuEI&UCNP@hmSiO₂ (0.05 mg/mL, DMSO/H₂O = 1/99) upon 974 nm light exposure (1 W/cm²) for different time periods. (d) Percentage of activated EI released from RuEI&UCNP@hmSiO₂ when the nanoparticles were irradiated using 974 nm light (1 W/cm²) and in the dark. The content of the activated EI was measured using HPLC.

The absorption band of RuEI in the blue light region overlaps the blue emission band of the UCNP (Figure 2b). Therefore, RuEI can efficiently absorb the upconverted blue light. To confirm if the upconverted blue light can induce photocleavage of RuEI, RuEI-loaded UCNP@hmSiO₂ (RuEI&UCNP@hmSiO₂) were irradiated with NIR light (974 nm, 1 W/cm²). The NIR irradiation induced a redshift in the absorption band of RuEI in RuEI&UCNP@hmSiO₂ (Figure 2c). This spectral change was identical to that observed for the RuEI solution, which was exposed to blue light to directly trigger photocleavage (Figure S3). As shown in the control experiment, the exposure of RuEI to NIR light in the absence of

UCNPs did not result any changes to the UV-Vis spectrum (**Figure S4**). These results indicated that the RuEI loaded in UCNP@hmSiO₂ was photocleaved by the photon upconversion process. In addition, the amount of the activated enzyme inhibitor (EI) was quantified using high-performance liquid chromatography (HPLC). Activated EI was not detected in the absence of NIR irradiation (**Figure 2d, S5**). After RuEI&UCNP@hmSiO₂ was irradiated by NIR at 1 W/cm² for 5 hours, approximately 75% of the EI was activated (**Figure 2d, S5**).

RuEI&UCNP@hmSiO₂ provides a platform for NIR photoinhibition of enzyme activity in deep tissues (**Figure 3a**). The half maximal inhibitory concentration (IC₅₀) of the activated EI was only 1/6 of that of the caged inhibitor RuEI for the inhibition of cathepsin K (**Figure S6**). Therefore, photoactivation of EI can efficiently inhibit cathepsin K. NIR irradiation of cathepsin K in the presence of RuEI&UCNP@hmSiO₂ significantly inhibited its activity (**Figure 3b, blue bars**). Irradiation for 7, 15, and 30 min reduced the enzyme activity to 30%, 17%, and 13%, respectively (**Figure 3b, blue bars**). For comparison, control experiments in the absence of RuEI&UCNP@hmSiO₂ after NIR irradiation (**Figure 3b, black bars**) and the presence of RuEI&UCNP@hmSiO₂ without NIR irradiation (**Figure 3b, red bars**) were performed. Enzyme activities in these control samples did not decrease. These results demonstrated that the inhibition of enzyme activity was caused by activation of the EI using NIR light. Moreover, the feasibility of using NIR light to inhibit enzyme activity after passing through tissue was investigated, which is important for clinical applications in the future. A piece of chicken tissue was placed between the NIR light and the sample. The NIR light passed through the tissue and inhibited the enzyme activity (**Figure 3b, magenta bars**).

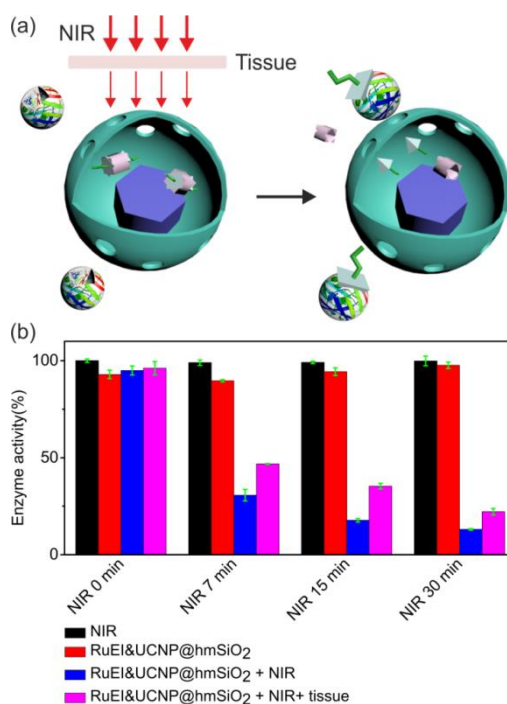


Figure 3. (a) Schematic illustration of NIR photoinhibition of enzyme activity using RuEI&UCNP@hmSiO₂. (b) NIR photoinhibition of the activity of cathepsin K. Black bars: activities of cathepsin K in the absence of RuEI&UCNP@hmSiO₂ under NIR irradiation; Red bars: activities of cathepsin K in the presence of RuEI&UCNP@hmSiO₂ without irradiation; Blue bars: activities of cathepsin K in the presence of RuEI&UCNP@hmSiO₂ under NIR irradiation. Magenta bars: activities of cathepsin K in the presence of RuEI&UCNP@hmSiO₂ under NIR irradiation through a piece of 1 mm thick tissue. The concentration of RuEI&UCNP@hmSiO₂ was 10 $\mu\text{g/mL}$, and the intensity of the 974 nm laser was 1 W/cm^2 .

Encouraged by the successful *in vitro* enzyme activity inhibition, we studied NIR-controlled enzyme activity in living cells. LNCaP, PC3 cells (prostate cancer cell lines) and SAOS-2 cells (osteosarcoma cell line) were used in our study. These cell lines were chosen because they have a high cathepsin K expression rate for their invasiveness, which results in metastases in the prostate cancer cell lines and the osteosarcoma cell line. RuEI&UCNP@hmSiO₂ was compatible to all three cell lines. Only a minor decrease in the cell viability was observed in the presence of a high concentration (150 $\mu\text{g/mL}$) of RuEI&UCNP@hmSiO₂ (**Figure S7**). NIR irradiation (1 W/cm^2) on all three cell lines in the presence or absence of RuEI&UCNP@hmSiO₂ (150 $\mu\text{g/mL}$) did not decrease the cell viability (**Figure S8**). These results suggested that RuEI&UCNP@hmSiO₂ provides a biocompatible platform for NIR photoinhibition of enzyme activity in living cells.

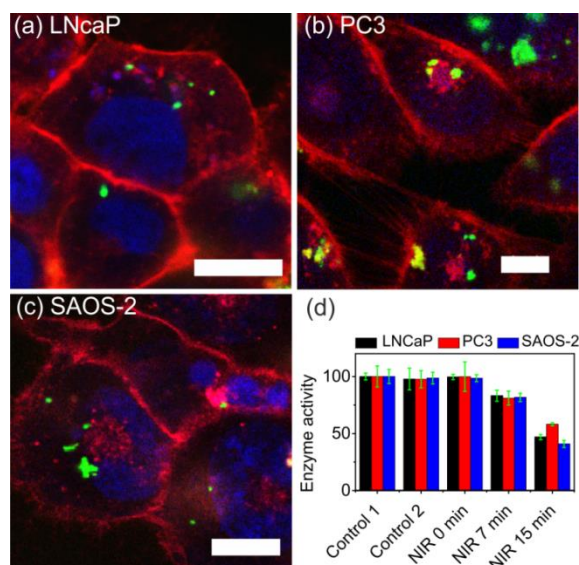


Figure 4. Confocal laser scanning microscopy images: fluorescence-labeled UCNP@hmSiO₂ was taken up by (a) LNCaP, (b) PC3, and (c) SAOS-2 cells. The scale bars represent 10 μ m. The plasma membranes were stained with CellMask™Orange (red), the DNA was stained with Draq@5 (blue), and UCNP@hmSiO₂ was stained with FITC (green). (d) Photoinhibition of the cathepsin K activity in living LNCaP, PC3, and SAOS-2 cells using 974 nm light (1 W/cm²) in the presence of RuEI&UCNP@hmSiO₂ (150 μ g/mL). Control 1: cells in the absence of RuEI&UCNP@hmSiO₂ without NIR irradiation. Control 2: cells in the absence of RuEI&UCNP@hmSiO₂ after NIR irradiation for 15 min.

All three cell lines used in this study exhibited cathepsin K activity (**Figure S9**). EI can efficiently inhibit the activity of cathepsin K derived from these cell lines (**Figure S10**). In cellular studies, fluorescence-labeled UCNP@hmSiO₂ was separately incubated with LNCaP, PC3 and SAOS-2 cells. The confocal laser scanning microscopy images indicated that UCNP@hmSiO₂ was taken up by the LNCaP, PC3, and SAOS-2 cells (**Figure 4a-c**). NIR irradiation of the LNCaP, PC3, and SAOS-2 cells, which were incubated with RuEI&UCNP@hmSiO₂ (150 μ g/mL) for 1 h, significantly inhibited the activities of cathepsin K in the cells (**Figure 4d, NIR 7 min and NIR 15 min**). For comparison, control experiments in the absence of RuEI&UCNP@hmSiO₂ without NIR irradiation (**Figure 4d, Control 1**), the absence of RuEI&UCNP@hmSiO₂ after NIR irradiation for 15 min (**Figure 4d, Control 2**), and the presence of RuEI&UCNP@hmSiO₂ without NIR irradiation (**Figure 4d, NIR 0 min**) were performed. The intracellular enzyme activities in these control samples did not decrease. These experiments demonstrated that RuEI&UCNP@hmSiO₂ enabled NIR photoinhibition of the enzyme activities in living cells.

5.4 Conclusion

In conclusion, we developed a new method (i.e., PUEI) that inhibits enzyme activities using NIR light. In PUEI, UCNP converted NIR light to blue light, which activated enzyme inhibitors. The activated enzyme inhibitors can inhibit enzyme activity in living cells. Due to the use of NIR light, PUEI is useful for deep tissue biomedical applications. NIR light may uncage different photocaged enzyme inhibitors via UCNP-assisted photochemistry. Therefore, RuEI and many other photocaged enzyme inhibitors can be combined with UCNP for NIR-controlled enzyme activity in deep tissue. Therefore, this novel PUEI is a general approach for controlling the activities of different types of enzymes. Controlling enzyme activities by NIR light provides a novel platform for regulating metabolism, manipulating cell functions, and treating diseases in deep tissue.

Supporting Information

Supporting Information is available from the Wiley Online Library or from the author.

5.5 Acknowledgements

Z.C. and R.T. contributed equally to this work. Z.C. was supported by the CSC program. R.T. was supported by the National Nanotechnology Center, Thailand and the Royal Thai government scholarship. We thank H. Menges for measuring the upconversion luminescence spectra. This work was supported by the Fonds der Chemischen Industrie (FCI, No. 661548) and the Deutsche Forschungsgemeinschaft (DFG, WU 787/2–1). V.M. and S.W. are the senior authors for the biology and chemistry parts, respectively.

5.6 References

- [1] J. M. Berg, J. L. Tymoczko, L. Stryer, *Biochemistry*, W.H. Freeman, New York, USA **2002**.
- [2] T. Stoisser, M. Brunsteiner, D. K. Wilson, B. Nidetzky, *Sci. Rep.* **2016**, *6*, 27892.
- [3] M. E. Peterson, R. M. Daniel, M. J. Danson, R. Eisenthal, *Biochem. J.* **2007**, *403*, 615.
- [4] K. Okuro, M. Sasaki, T. Aida, *J. Am. Chem. Soc.* **2016**, *138*, 5527.
- [5] M. Wiechen, I. Zaharieva, H. Dau, P. Kurz, *Chem. Sci.* **2012**, *3*, 2330.
- [6] a) P. R. Westmark, J. P. Kelly, B. D. Smith, *J. Am. Chem. Soc.* **1993**, *115*, 3416; b) I. Willner, S. Rubin, A. Riklin, *J. Am. Chem. Soc.* **1991**, *113*, 3321; c) A. Leonidova, C. Mari, C. Aebbersold, G. Gasser, *Organometallics* **2016**, *35*, 851; d) H. Kaufman, S. M. Vratsano, B. F. Erlanger, *Science* **1968**, *162*, 1487; e) T. Respondek, R. N. Garner, M. K. Herroon, I. Podgorski, C. Turro, J. J. Kodanko, *J. Am. Chem. Soc.* **2011**, *133*, 17164.
- [7] a) E. Blasco, B. V. K. J. Schmidt, C. Barner-Kowollik, M. Pinol, L. Oriol, *Macromolecules* **2014**, *47*, 3693; b) E. Blasco, M. Pinol, L. Oriol, B. V. K. J. Schmidt, A. Welle, V. Trouillet, M. Bruns, C. Barner-Kowollik, *Adv. Funct. Mater.* **2013**, *23*, 4011; c) N. Abeyrathna, Y. Liao, *J. Am. Chem. Soc.* **2015**, *137*, 11282; d) S. Bonnet, B. Limburg, J. D. Meeldijk, R. J. M. K. Gebbink, J. A. Killian, *J. Am. Chem. Soc.* **2011**, *133*, 252.
- [8] a) H. J. Montgomery, B. Perdicakis, D. Fishlock, G. A. Lajoie, E. Jervis, J. G. Guillemette, *Bioorgan. Med. Chem.* **2002**, *10*, 1919; b) T. Respondek, R. Sharma, M. K. Herroon, R. N. Garner, J. D. Knoll, E. Cueny, C. Turro, I. Podgorski, J. J. Kodanko, *ChemMedChem* **2014**, *9*, 1306.
- [9] a) R. T. Xing, K. Liu, T. F. Jiao, N. Zhang, K. Ma, R. Y. Zhang, Q. L. Zou, G. H. Ma, X. H. Yan, *Adv. Mater.* **2016**, *28*, 3669; b) S. Wu, H.-J. Butt, *Adv. Mater.* **2016**, *28*, 1208; c) N. Zhang, F. Zhao, Q. Zou, Y. Li, G. Ma, X. H. Yan, *Small* **2016**, *12*, 5936.
- [10] P. Anstaett, V. Pierroz, S. Ferrari, G. Gasser, *Photochem. Photobiol. Sci.* **2015**, *14*, 1821.
- [11] a) M. Álvarez, A. Best, S. Pradhan-Kadam, K. Koynov, U. Jonas, M. Kreiter, *Adv. Mater.* **2008**, *20*, 4563; b) M. Álvarez, A. Best, A. Unger, J. M. Alonso, A. del Campo, M. Schmelzeisen, K. Koynov, M. Kreiter, *Adv. Funct. Mater.* **2010**, *20*, 4265.

- [12] B. Yan, J.-C. Boyer, D. Habault, N. R. Branda, Y. Zhao, *J. Am. Chem. Soc.* **2012**, *134*, 16558.
- [13] a) C.-J. Carling, J.-C. Boyer, N. R. Branda, *J. Am. Chem. Soc.* **2009**, *131*, 10838; b) Z. Y. Cheng, J. Lin, *Macromol. Rapid Comm.* **2015**, *36*, 790.
- [14] a) Y. M. Yang, Q. Shao, R. R. Deng, C. Wang, X. Teng, K. Cheng, Z. Cheng, L. Huang, Z. Liu, X. G. Liu, B. G. Xing, *Angew. Chem. Int. Ed.* **2012**, *51*, 3125; b) M. L. Viger, M. Grossman, N. Fomina, A. Almutairi, *Adv. Mater.* **2013**, *25*, 3733; c) D. Yang, P. Ma, Z. Hou, Z. Cheng, C. Li, J. Lin, *Chem. Soc. Rev.* **2015**, *44*, 1416; d) S. Beyazıt, S. Ambrosini, N. Marchyk, E. Palo, V. Kale, T. Soukka, B. T. S. Bui, K. Haupt, *Angew. Chem. Int. Edit.* **2014**, *53*, 8919; e) W. Wu, L. Yao, T. Yang, R. Yin, F. Li, Y. Yu, *J. Am. Chem. Soc.* **2011**, *133*, 15810; f) E. Ruggiero, A. Habtemariam, L. Yate, J. C. Mareque-Rivas, L. Salassa, *Chem. Commun.* **2014**, *50*, 1715; g) P. T. Burks, J. V. Garcia, R. GonzalezIrias, J. T. Tillman, M. Niu, A. A. Mikhailovsky, J. Zhang, F. Zhang, P. C. Ford, *J. Am. Chem. Soc.* **2013**, *135*, 18145; h) J. A. Liu, W. B. Bu, L. M. Pan, J. L. Shi, *Angew. Chem. Int. Ed.* **2013**, *52*, 4375; i) J. Shen, G. Y. Chen, T. Y. Ohulchansky, S. J. Kesseli, S. Buchholz, Z. P. Li, P. N. Prasad, G. Han, *Small* **2013**, *9*, 3213.
- [15] a) Z. J. Chen, S. Q. He, H.-J. Butt, S. Wu, *Adv. Mater.* **2015**, *27*, 2203; b) S. Q. He, K. Krippes, S. Ritz, Z. J. Chen, A. Best, H.-J. Butt, V. Mailander, S. Wu, *Chem. Commun.* **2015**, *51*, 431.
- [16] W. Li, J. Wang, J. Ren, X. Qu, *J. Am. Chem. Soc.* **2014**, *136*, 2248.
- [17] a) B. Yan, J.-C. Boyer, N. R. Branda, Y. Zhao, *J. Am. Chem. Soc.* **2011**, *133*, 19714; b) L. Z. Zhao, J. J. Peng, Q. Huang, C. Y. Li, M. Chen, Y. Sun, Q. N. Lin, L. Y. Zhu, F. Y. Li, *Adv. Funct. Mater.* **2014**, *24*, 363; c) H. D. Gao, P. Thanasekaran, C. W. Chiang, J. L. Hong, Y. C. Liu, Y. H. Chang, H. M. Lee, *ACS Nano* **2015**, *9*, 7041.
- [18] A. Stepuk, D. Mohn, R. N. Grass, M. Zehnder, K. W. Kramer, F. Pelle, A. Ferrier, W. J. Stark, *Dent. Mater.* **2012**, *28*, 304.
- [19] P. Lederhose, Z. J. Chen, R. Muller, J. P. Blinco, S. Wu, C. Barner-Kowollik, *Angew. Chem. Int. Ed.* **2016**, *55*, 12195.
- [20] Z. Chen, L. Zhou, W. Bing, Z. Zhang, Z. Li, J. Ren, X. Qu, *J. Am. Chem. Soc.* **2014**, *136*, 7498.
- [21] Z. Chen, Y. Xiong, R. Etchenique, S. Wu, *Chem. Commun.* **2016**, in press, DOI: 10.1039/C6CC05287H.

- [22] Z. Chen, W. Sun, H.-J. Butt, S. Wu, *Chem. Eur. J.* **2015**, *21*, 9165.
- [23] K. D. Brubaker, R. L. Vessella, L. D. True, R. Thomas, E. Corey, *J. Bone. Miner. Res.* **2003**, *18*, 222.
- [24] L. J. Raggatt, N. C. Partridge, *J. Biol. Chem.* **2010**, *285*, 25103.
- [25] M. M. Mohamed, B. F. Sloane, *Nat. Rev. Cancer* **2006**, *6*, 764.

5.7 Supporting information

Materials

Ytterbium(III) acetate hydrate (99.9%) and sodium hydroxyl pellets (98%) were purchased from Alfa Aesar. Thulium(III) acetate hydrate (99.9%), yttrium(III) acetate hydrate (99.9%), 2,2'-bipyridine (98%), 1-octadecene (technical grade, 90%), oleic acid (technical grade, 90%), ammonium fluoride ($\geq 99.99\%$), ruthenium(III) chloride trihydrate (technical), silver tetrafluoroborate (98%), tetraethyl orthosilicate (98%), tetrabutylammonium chloride (97%), lauryl sulfonate betaine (99%), sodium dodecyl benzenesulfonate (99%), Z-Leu-OH (98%), N-methylmorpholine (98%), isobutyl chloroformate (97%), and aminoacetonitrile sulfate (99%) were purchased from Sigma-Aldrich. All other solvents were purchased from Sigma-Aldrich or Fisher Scientific. All the chemical materials were purchased from Sigma-Aldrich or Alfa Aesar. Milli-Q water was used to prepare all the aqueous solutions. The enzyme cathepsin K was purchased from Enzo life. Z-Gly-Pro-Arg(GPR)-AMC was purchased from Enzo Life Sciences. Abz-HPGGPQ-EDDnp was purchased from Anaspec.

Characterization

The UV-Vis absorption spectra were measured using a Lambda 900 spectrometer (Perkin Elmer). Transmission electron microscopy (TEM) images were obtained using a JEOL JEM1400 transmission electron microscope. Nitrogen adsorption-desorption isotherms were obtained at 77 K on a TriStar 3020 accelerated surface area and pore size analyzer. Upconversion photoluminescence measurements were performed on a Spex Fluorolog II (212) spectrometer. A diode laser at 974 nm (type P976MF, Photon tec Berlin GmbH) coupled with a 105 μm (core) fiber was employed as the excitation source. The diode laser was equipped with an adjustable fiber collimator (Changchun New Industries Optoelectronics Technology). The output power of the diode laser was controlled by a tabletop laser driver (device type ds11-la12v08-pa08v16- t9519-254-282, OsTech GmbH i.G. electro-optical-instruments). The output power density of the diode laser was measured by an optical power meter (Model

407A, Spectra-Physics Corporation) and an NIR indicator (Newport, Model F-IRC1). HPLC was performed using Rheodyne, Injection valve 7725i with a 20 μ L loop, Agilent Technologies Series 1200 degasser, quaternary gradient pump, column oven, photodiode array-detector Varian ELSD-Detector 385-LC, and Macherey-Nagel Polactec column (length: 125 mm, diameter: 4 mm, particle size: 5 μ m, flowrate: 1 mL/min, temperature: 20 $^{\circ}$ C). The gradient started with CH₃CN/Water+0.1%TFA 10/90%, which changed to 100/0% in 10 min. Live cell images were recorded with a commercial setup (LSM SP5 STED Leica Laser Scanning Confocal Microscope, Leica, Germany) that consisted of an inverse fluorescence microscope DMI 6000 CS equipped with a multi-laser combination and five detectors operating in the 400-800 nm range. An HCX PL APO CS 63 x 1.4 oil objective was used in this study.

Methods

Synthesis of RuEI and NaYF₄:Yb,Tm@NaYF₄ nanoparticles (UCNPs)

The synthesis of RuEI was performed according to a previously published protocol.^[1] The synthesis of UCNPs was reported in our previous study.^[2]

Synthesis of UCNP@hmSiO₂

The UCNP@hmSiO₂ was synthesized according to a previously reported protocol with minor modification. Prior to the synthesis, the oleic acid ligand on the surfaces of the UCNPs was removed. The UCNPs (40 mg) were dispersed in an aqueous solution (6 mL), and the pH was adjusted to 1.5 by adding a 0.5 M HCl solution. The obtained ligand-free UCNPs were recovered by centrifugation and redispersed in a mixed solution (20 mL) consisting of surfactant lauryl sulfonatebetaine (LSB)/sodium dodecyl benzenesulfonate (SDBS) (5 mmol for each surfactant) to form a stock solution. The stock solution (20 mL) was maintained in an oil bath at 40 $^{\circ}$ C for 30 min. Then, triethanolamine (50 μ L), APS (47 μ L), and TEOS (320 μ L) were successively added to the resulting solution. The mixture was stirred for an additional 1 h. The product was collected by centrifugation, washed with acetic acid/ethanol solution (1/20, v/v) five times to remove the surfactants. The obtained product (UCNP@hmSiO₂) was maintained in ethanol prior to use.

Synthesis of RuEI&UCNP@hmSiO₂

The RuEI (10 mg) was dissolved in dichloromethane (DCM) (10 mL) and mixed with UCNP@hmSiO₂ (10 mg). After being stirred at 25 °C for 24 h in the dark, the RuEI&UCNP@hmSiO₂ was separated by centrifugation, gently washed with DCM three times to remove the remaining unloaded RuEI, and dried under vacuum at room temperature.

Synthesis of fluorescently labeled UCNP@hmSiO₂

Fluorescein isothiocyanate (FITC, 1 mg) was dissolved in ethanol (10 mL) and mixed with UCNP@hmSiO₂ (7 mg). After being stirred at 25 °C for 24 h in the dark, the fluorescently labeled UCNP@hmSiO₂ was separated by centrifugation, gently washed with ethanol three times to remove the remaining FITC, and dried under vacuum at room temperature.

Activation of EI in RuEI&UCNP@hmSiO₂ by NIR light

RuEI&UCNP@hmSiO₂ (40 µg/mL) was dispersed in an aqueous solution (DMSO/H₂O = 1:99) in a cylindrical glass bottle. The RuEI&UCNP@hmSiO₂ suspension was irradiated with a 974 nm laser (1 W/cm²) from the side of the bottle. The solution was withdrawn at a given time interval and centrifuged at 5500 rpm for 10 min. The upper transparent solution was used for HPLC analysis after centrifugation.

Cathepsin K Inhibition Assay with EI and RuEI

The cathepsin K activity assay was performed in a 96-well plate at a total volume of 100 µL and incubated at 37 °C. Recombinant human cathepsin K (Enzo Life Sciences, USA) with a final concentration of 2 nM was used to study the catalytic activity of 100 µM Z-Gly-Pro-Arg(GPR)-AMC, which is a fluorogenic substrate specific for cathepsin K, (Enzo Life Sciences, USA) with or without EI. Commercial cathepsin K was diluted from a stock solution to 8 nM as the working concentration with enzymatic assay buffer containing 100 mM sodium acetate buffer (pH 5.5), 8 mM DTT, 4 mM EDTA, 0.01% Triton X-100, and 1% DMSO. The enzyme solution (25 µL) and additional buffer (15 µL) were activated at 37 °C for 15 min prior to the addition of the substrate and/or EI. EI (MW 303 g/mol) or RuEI (MW 1015 g/mol) at concentrations ranging from 0.001 to 10 µM were prepared in reaction buffer (50 mM sodium acetate buffer pH 5.5, 2.5 mM DTT, 2.5 mM EDTA) containing 10% DMSO.

Then, the EI solution (10 μL) was added to the activated enzyme solution to obtain a final DMSO concentration of 1%. Finally, the Z-GPR-AMC substrate, which was dissolved in the enzymatic assay buffer (200 μM , 50 μL), was added to the mixture and gently mixed. The fluorescent signals were kinetically measured every 3 min for 30 min by a plate reader with excitation at 365 nm and emission at 440 nm. The fluorescent intensities were converted to the percentage of enzyme activity by setting the signal obtained from the control experiment without EI as 100%. The IC_{50} values were calculated at a reaction time of 15 min by fitting a curve with non-linear regression using the GraphPad program. The inhibition assays of commercial cathepsin K with EI and RuEI are shown in Figure S6.

NIR photoinhibition of cathepsin K *in vitro*

To use the NIR-controllable platform, the enzyme solution was activated as previously described. RuEI&UCNP@hmSiO₂ was prepared in a reaction buffer containing 10% DMSO. Then, the RuEI&UCNP@hmSiO₂ suspension (10 μL) was added to the activated enzyme solution to obtain a final concentration of 10 $\mu\text{g}/\text{mL}$. The samples were irradiated with an NIR laser at 974 nm (1 W/cm^2) without or through a slice of chicken tissue (1 mm thickness) at various exposure times (i.e., 0, 7, 15 and 30 min). The plate was placed in a cold water bath during irradiation. Finally, the Z-GPR-AMC substrate (200 μM , 50 μL) was added, and the fluorescent signal was kinetically measured every 3 min for 30 min as previously mentioned. The enzyme activity is expressed as percentage of activity. The percentage of activity at 100% was calculated from the control experiment without the nanoparticles and NIR treatment, which were performed in parallel.

Cell culture

Three different cell lines used in this study including LNCaP, PC3 and SAOS-2 were obtained from DSMZ (Deutsche Sammlung von Mikroorganismen und Zellkulturen, Germany). They were cultured in Dulbecco's Modified Eagle's Medium (DMEM, Gibco, USA) complete medium containing 10% fetal bovine serum (FBS, Gibco, USA), 1% L-glutamine (Gibco, USA) and 1% penicillin/streptomycin (Gibco, USA) and incubated at 37 °C in CO₂-incubator with 95% humidity and 5% CO₂ (C200, Labotect, Germany). To dissociate adherent cells, the cells were trypsinized with 0.25% trypsin (Gibco, USA) for 3 min as general procedure. The cell pellet was collected by centrifugation at 130 g for 3 min, resuspended in DMEM

complete medium and used for further assays. Viable cells was determined by trypan blue exclusion method and counted by using TC10™ automated cell counter (Bio-Rad, USA).

Cell toxicity

To study cytotoxicity test, all cell lines resuspended in DMEM complete medium were seeded at a density of 5,000 cells/well in a 96-well plate for 48 h. To study effects of nanoparticle concentrations, then, the cells were treated with RuEI&UCNP@hmSiO₂ from 50 to 300 µg/mL and incubated at 37°C in CO₂-incubator for 24 h. To study effects of NIR irradiation, RuEI&UCNP@hmSiO₂ and the cleavage products, the cells were exposed to 974 nm light at 1 W/cm² (L4-9897510-100M, JDS Uniphase Corporation) for 0, 15 and 30 min with and without RuEI&UCNP@hmSiO₂ at a concentration of 150 µg/mL and incubated at 37 °C in CO₂-incubator for 24 h. Samples without NIR treatment were covered with black plate. For each cell type, all control and treatments were performed in the same plate. Sample without any treatment was used as a negative control and calculated as 100% cell viability, while 20% DMSO added sample was used as a positive control. After that, cell viability was evaluated by MTS assay using CellTiter 96® aqueous one solution cell proliferation assay (Promega, USA) according to the manufacturer's protocol. This assay is based on NADPH or NADH produced by dehydrogenase enzymes in metabolically active cells that can reduce MTS tetrazolium compound [3-(4,5-dimethylthiazol-2-yl)-5-(3-carboxymethoxyphenyl)-2-(4-sulfophenyl)-2H-tetrazolium,inner salt] into a soluble-colored formazan product which can be detected at 490 nm by plate reader (Infinite® M1000, Tecan, Germany). Cell viability assays are shown in Figures S7 and S8.

Cathepsin K Activity Assay of Lysate and Live Cells

For preparation of cell lysate, 1 mL of approximately 10⁶ cells/mL culture was centrifuged, resuspended in 1 mL of cold reaction buffer containing 1% Triton X-100 and incubated on ice for 10 min. After centrifugation at 13,000 g at 4 °C for 10 min, the supernatant was collected. Then, 100 µL of lysate or live cells (2-days culture starting from approximately 10⁶ cells/mL per well) were incubated with 5 µM of Abz-HPGGPQ-EDDnp, a highly cathepsin K specific fluorogenic substrate (Anaspec) at 37 °C in 96-well plate. Abz-HPGGPQ-EDDnp substrate was dissolved in dimethylformamide at a concentration of 1 mM stock solution, kept at -20 °C until used and diluted to 0.1 mM working substrate solution in the reaction buffer. The

fluorescent signals of enzymatic hydrolysis were monitored until 24 h. The cathepsin K activity assay of lysate and live cells is shown in Figure S9.

Cathepsin K Inhibition Assay of Lysate with EI

Cell lysate was prepared from lysis of LNCaP, PC3 and SAOS-2 cells as previous described. Protein concentration in lysate was determined by Pierce™ 660nm protein assay reagent using BSA as standard curve. Then, 1 µg of lysate protein was used as a source of cathepsin K instead of the commercial one. The reaction was carried out in the absence or presence of EI at concentration in a range of 0.1-1000 µM in the reaction buffer containing 1 % DMSO. The inhibition was allowed to occur for 1 h at 37 °C before adding Abz-HPGGPQ-EDDnp substrate at final concentration of 5 µM. After that, the fluorescent signals were measured at 5 h of incubation. The IC₅₀ values were calculated at 15 min of reaction time by fitting a curve with non-linear regression using GraphPad Program. The cathepsin K inhibition assay of lysate is shown in Figure S10.

Cell imaging by confocal laser scanning microscopy (CLSM)

For cellular uptake study, three cell lines were seeded at a density of 5×10^4 cells/well in µ-Slide 8 well with a glass coverslip bottom (Ibidi, Germany) and cultured for 72 h in DMEM complete medium (Phenol red free). After removing of old medium, the cells were incubated for 1 h with FITC-labeled UCNP@hmSiO₂ resuspended in DMEM at a concentration of 150 µg/mL. Subsequently, the cells were washed twice with DMEM to remove the remaining nanoparticles outside of the cells, stained subcellular organs with fluorescent dyes and finally suspended in DMEM. The excitation and detection conditions in a sequential mode were described as follows: Fluorescent nanoparticles were excited with an Ar laser (488 nm), detected at 510-540 nm and pseudocolored in green; The cell membrane was stained with CellMask™Orange (5 µg/mL, Life technologies, USA), excited with a DPSS laser (561 nm), detected at 570-600 nm, pseudocolored in red; The cell nucleus was stained with DraQ[®]5 (5 µM, Cell signaling technology, USA), excited with a HeNe laser (633 nm), detected at 650-710 nm and pseudocolored in blue. The CLSM images are shown in Figure 4a-c.

NIR photoinhibition of cathepsin K in live cells

To perform NIR-controlled inhibition assay in cellular system, all cell lines resuspended in DMEM complete medium were seeded at a density of 5,000 cells/well in 96-well plate for 72

h. After medium removal, the reaction was carried out in the absence or presence of RuEI&UCNP@hmSiO₂ at a concentration of 150 µg/mL in the reaction buffer containing 1 % DMSO. The nanoparticles and cells were incubated for 1 h at 37 °C prior to treatment with NIR at 0, 7, and 15 min. The inhibition was then allowed to occur for 1 h at 37 °C before adding Abz-HPGGPQ-EDDnp substrate at final concentration of 5 µM. The fluorescent signals were measured at 3 h after incubation. Enzyme activity was exhibited as percentage of activity. The percentage of activity at 100% was calculated from the control experiment without the NPs and NIR treatment which were performed in parallel. The NIR-controlled inhibition assay of cellular cathepsin K is shown in Figure 4d.

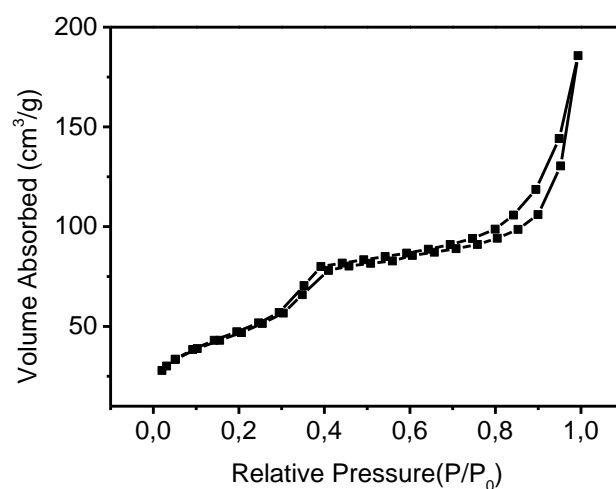


Figure S1. N₂ adsorption-desorption isotherm of UCNP@hmSiO₂. The average BET surface area was ~167 m²/g.

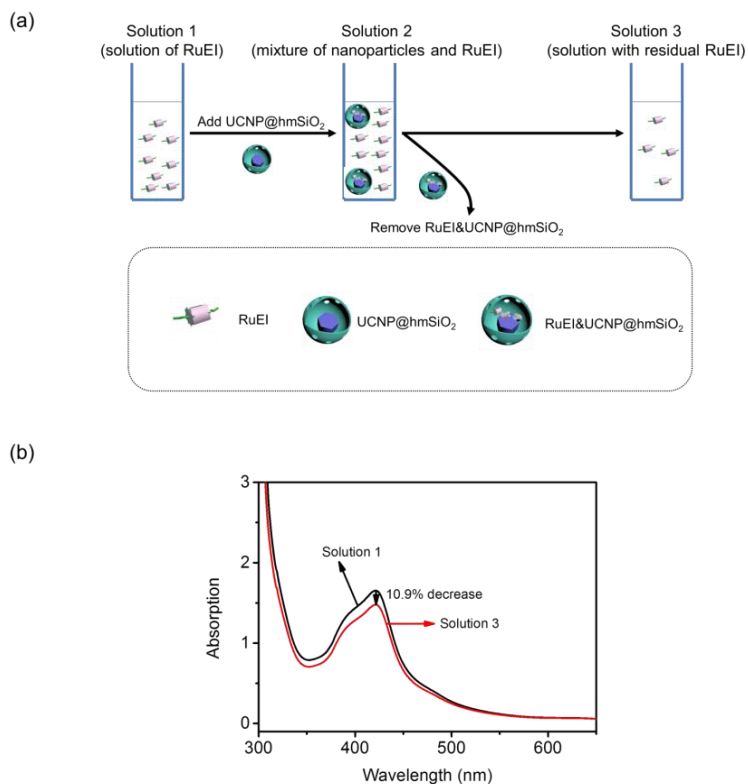


Figure S2. Procedure to determine the loading efficiency of RuEI in UCNP@hmSiO₂. (a) Schematic illustration of the procedure. (b) UV-Vis absorption spectra of Solution 1 and Solution 3. The RuEI loading efficiency measured using UV-Vis absorption spectroscopy was 18.3 wt%. There was ~0.11 mg RuEI loaded in 0.6 mg UCNP@hmSiO₂.

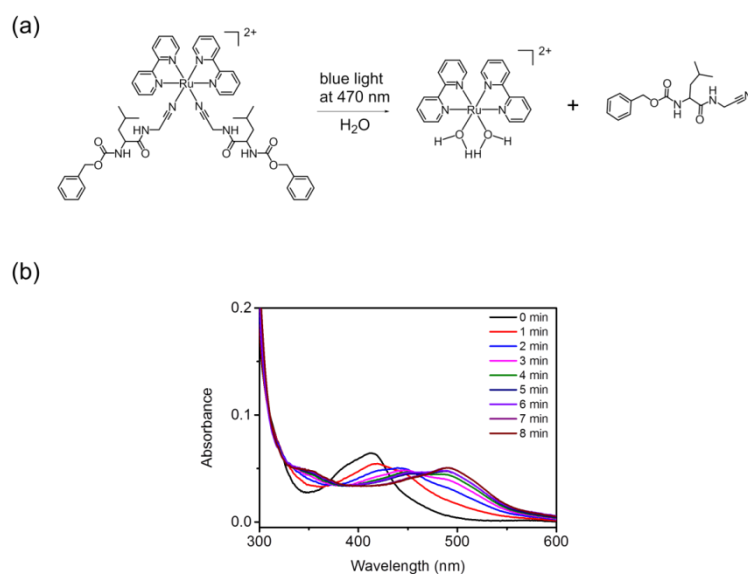


Figure S3. (a) The photoreaction of RuEI induced by blue light. (b) UV-Vis absorption spectra of RuEI (0.0075 mg/mL, DMSO/H₂O = 1/99) upon 470-nm light irradiation (1

mW/cm²). The metal-to-ligand charge transfer band shifted to longer wavelength, which indicates the cleavage of the RuEI complex.^[1]

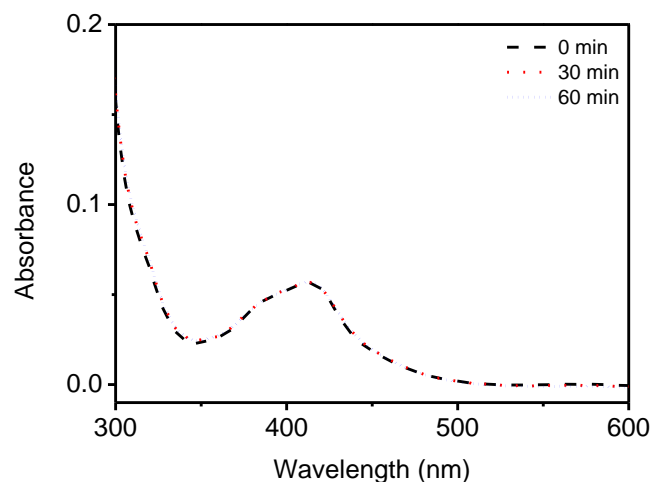


Figure S4. UV-Vis absorption spectrum of RuEI (0.0075 mg/mL, DMSO/H₂O = 1/99) upon 974-nm light irradiation (1 W cm⁻²) in the absence of UCNP@hmSiO₂. This result indicates that RuEI in the absence of UCNP@hmSiO₂ cannot be cleaved by 974 nm light directly.

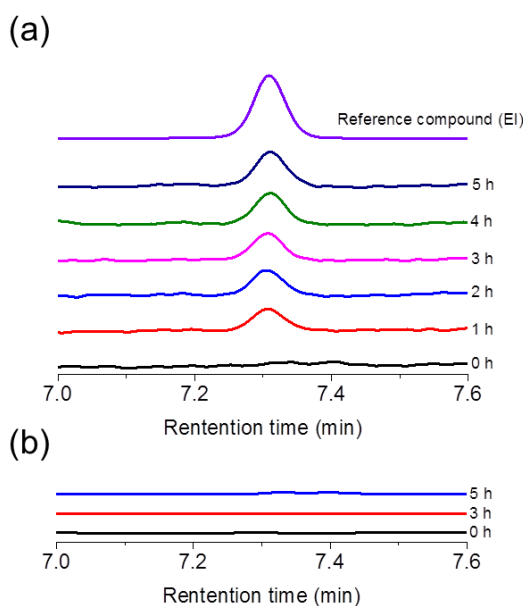


Figure S5. (a) HPLC traces of the dispersion of RuEI&UCNP@hmSiO₂ nanoparticles in solution (DMSO/H₂O = 1/99) upon irradiation of NIR light. (b) HPLC traces of the dispersion of RuEI&UCNP@hmSiO₂ nanoparticles in solution (DMSO/H₂O = 1/99) in the dark. THF/CH₃CN/water+0.1% TFA was used as eluent and a 220 nm UV detector was employed.

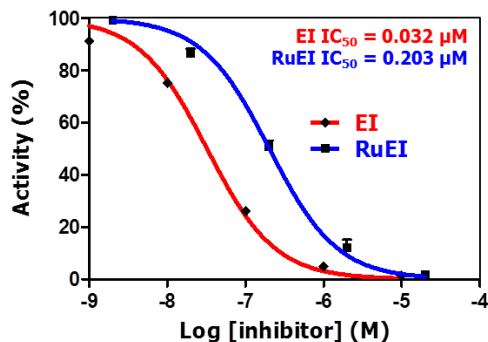


Figure S6. Cathepsin K inhibition assay of commercial enzyme in the presence of EI or RuEI determined with hydrolysis of the fluorogenic substrate Z-GPR-AMC. The IC₅₀ of EI and RuEI were 0.032 and 0.203 μM, respectively. This result indicates EI generated by photoactivation of RuEI can efficiently inhibit the activity of cathepsin K.

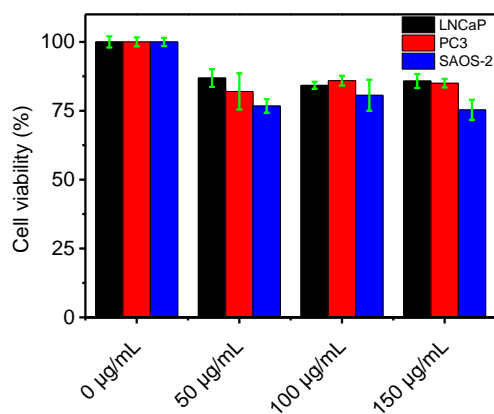


Figure S7. Cytotoxicity of RuEI&UCNP@hmSiO₂ in LNCaP, PC3, and SAOS-2 cells. Cell viability was determined by MTS assay after treatment for 24 h. The results indicate that RuEI&UCNP@hmSiO₂ has good biological compatibility with these cells.

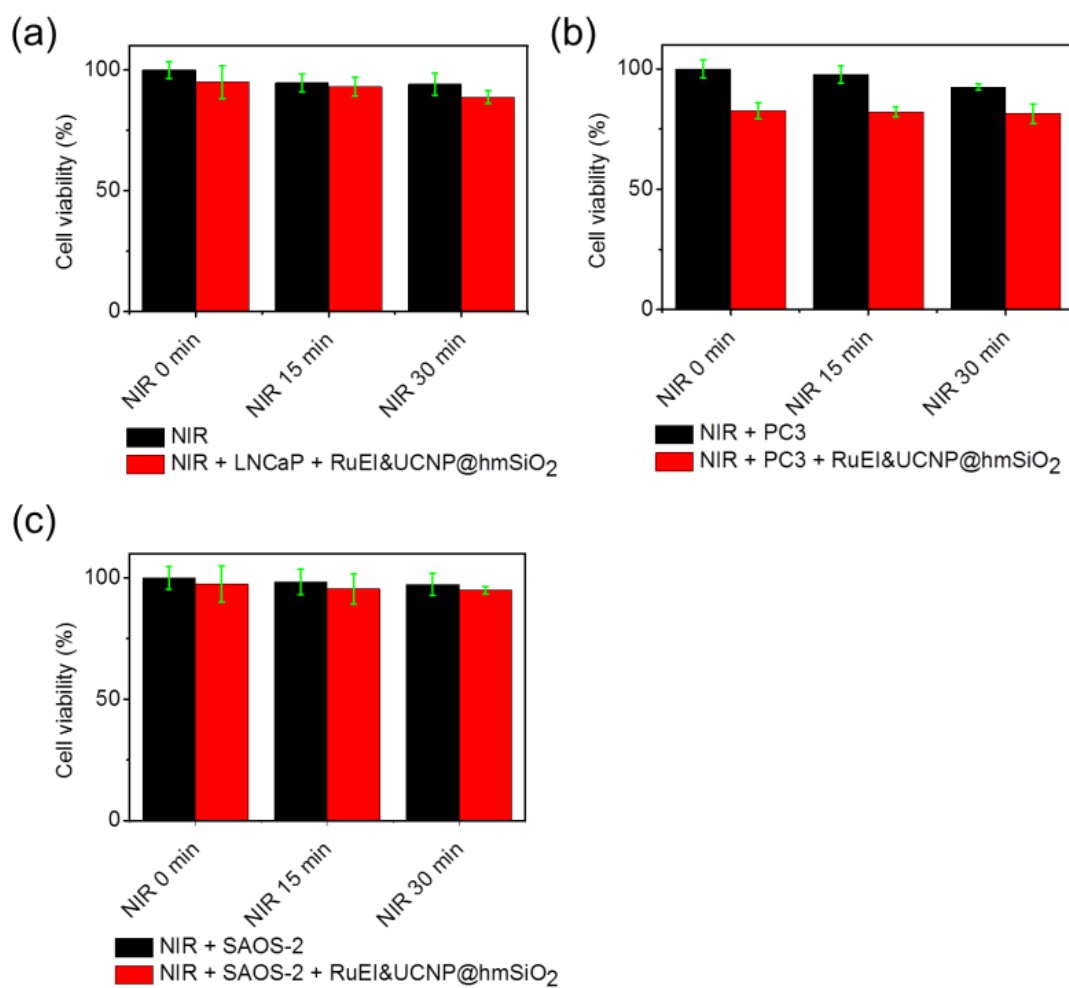


Figure S8. Viability of LNCaP, PC3 and SAOS-2 cells in the absence and presence of RuEI&UCNP@hmSiO₂ under NIR irradiation for different time periods. Cell viability was determined by MTS assay after treatment for 24 h. NIR irradiation with or without RuEI&UCNP@hmSiO₂ did not decrease cell viability.

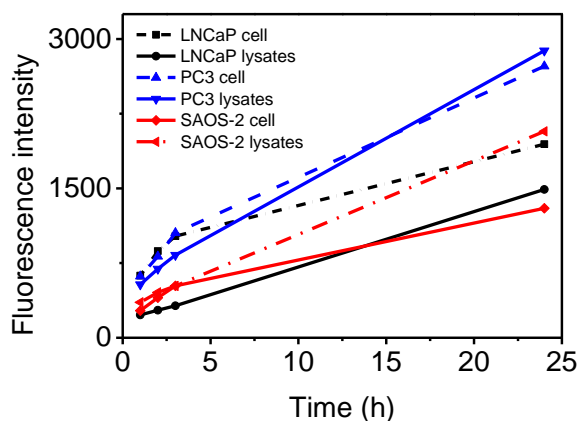


Figure S9. Cathepsin K activity assay of LNCaP, PC3 and SAOS-2 lysate and live cells determined with hydrolysis of cathepsin K fluorogenic substrate Abz-HPGGPQ-EDDnp. The presence of cathepsin K activity was identical to previous reports.^[3]

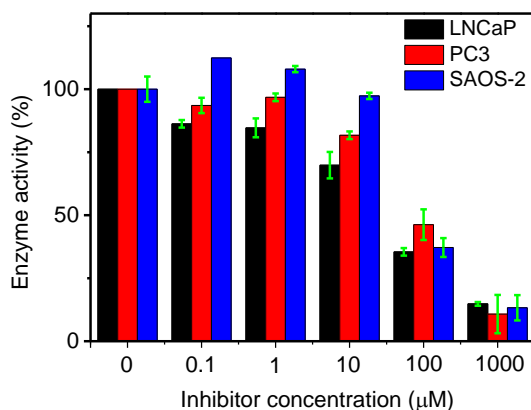


Figure S10. Cathepsin K inhibition assay of LNCaP, PC3 and SAOS-2 lysate in the presence of EI determined with hydrolysis of cathepsin K fluorogenic substrate Abz-HPGGPQ-EDDnp. This experiment shows that IC_{50} of cathepsin K in lysates of LNCaP, PC3, and SAOS-2 were 76.6 μ M, 34.9 μ M, and 72.8 μ M, respectively.

Reference

- [1] T. Respondek, R. Sharma, M. K. Herroon, R. N. Garner, J. D. Knoll, E. Cueny, C. Turro, I. Podgorski, J. J. Kodanko, *ChemMedChem*. **2014**, *9*, 1306.
- [2] S. Q. He, K. Krippes, S. Ritz, Z. J. Chen, A. Best, H. J. Butt, V. Mailänder, S. Wu, *Chem. Commun.* **2015**, *51*, 431.
- [3] K. D. Brubaker, R. L. Vessella, L. D. True, R. Thomas, E. Corey, *J. Bone. Miner. Res.* **2003**, *18*, 222.

Chapter 6: Near infrared photoinduced coupling reactions assisted by upconversion nanoparticles

Paul Lederhose,^{[‡], b, c, d} Zhijun Chen,^{[‡], a} Rouven Müller,^{c, d} James P. Blinco,^{*, b, c, d} Si Wu,^{*, a}
and Christopher Barner-Kowollik^{*, b, c, d}

Published in *Angew. Chem. Int. Ed.* **2016**, *55*, 12195-12199.

Reproduced from *Angew. Chem. Int. Ed.* **2016**, *55*, 12195-12199 with permission from WILEY-VCH Verlag GmbH & Co. KGaA.

6.1 Statement of contribution

Christopher Barner-Kowollik, James P. Blinco and Si Wu led the project.

Paul Lederhose synthesized organic molecules and conducted MS analysis.

Zhijun CHEN performed synthesis of UCNPs, laser experiments and HPLC analysis.

Rouven Müller synthesized the organic molecules.

[‡]Authors contributed equally to this work.

^aMax-Planck-Institut für Polymerforschung, Ackermannweg 10, 55128 Mainz, Germany.

^bSchool of Chemistry, Physics and Mechanical Engineering, Science and Engineering Faculty, Queensland University of Technology (QLD), 2 George St, Brisbane, Queensland 4001, Australia.

^cPreparative Macromolecular Chemistry, Institut für Technische Chemie und Polymerchemie, Karlsruhe Institute of Technology (KIT), Engesserstr. 18, 76131 Karlsruhe, Germany.

^dInstitut für Biologische Grenzflächen, Karlsruhe Institute of Technology (KIT), Hermann-von-Helmholtz-Platz 1, 76344 Eggenstein-Leopoldshafen, Germany.

Keywords: Photoinduced cycloaddition, Upconversion, Polymer ligation, NITEC, Infrared Irradiation.

6.2 Abstract: We report nitrile imine-mediated tetrazole-ene cycloadditions (NITEC) in the presence of upconversion nanoparticles (UCNPs), constituting a powerful coupling tool requiring only near infrared light as a stimulus. When a pyrene aryl tetrazole derivative ($\lambda_{\text{abs, max}} = 346 \text{ nm}$) and UCNPs are irradiated with a low energy light source at 974 nm, rapid conversion of the tetrazole to a reactive nitrile imine occurs. In the presence of an electron-deficient-ene, quantitative conversion to a pyrazoline cycloadduct occurs under ambient

reaction conditions. The combination of NITEC and UCNP technology is exploited for small molecule cycloadditions, polymer end-group modification and the formation of block copolymers from functional macromolecular precursors, constituting the first example of a NIR-induced cycloaddition. As the technique is attractive for potential *in vivo* applications, through-tissue experiments in the presence of a biologically relevant biotin coupling species were carried out. Quantitative cycloadditions and retention of biological activity of the biotin units are possible at 974 nm irradiation.

6.3 Introduction

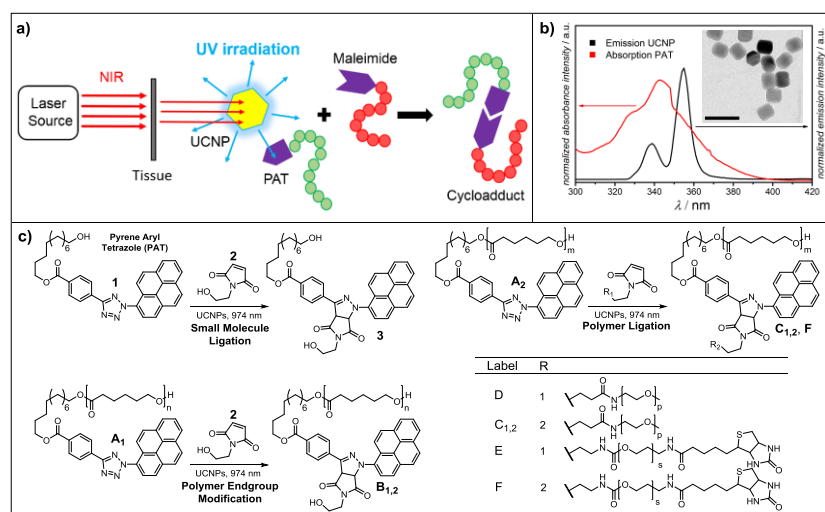
Light induced reactions are an important tool in the field of contemporary chemical synthesis as they afford spatial^[1] and temporal reaction control.^[2] A large number of functionalities can be found in literature which are labelled photo-sensitive *i.e.* having the capability of undergoing a light stimulated elimination, participate in a chemical reaction.^[3] The most ideal of these reactions also fulfil the criteria required for a click reaction, namely equimolarity, full reagent conversion, exclusive product formation, short reaction times, functional group orthogonality and mild reaction conditions.^[4] This class of reactions have been termed as ‘photo-click’ reactions.^[2,5] While a number of these photo-click reactions have been reported, they almost exclusively require UV-light as a trigger. The use of such high-energy UV photons can be detrimental to a large proportion of organic, inorganic and biological species which are sensitive to UV irradiation, leading to unwanted side-reactions. Thus, efficient photo-reactions triggered by substantially lower energy photons (e.g. wavelengths in the visible or infrared regime) are highly sought.^[6] This wavelength regime is of critical importance for *in vivo* biological applications as tissue is more optically transparent in this region, allowing for overall deeper light penetration. One example of a photo-click moiety that has been applied in polymer chemistry,^[7] for the modification of surfaces^[8] or in the field of biological-ligation^[9] is the diaryl tetrazole. Triggered *via* a light stimulus, the tetrazole undergoes a rapid elimination of nitrogen to yield a reactive nitrile imine intermediate, which will undergo a subsequent equimolar cycloaddition with a dipolarophile in quantitative yields. Recently, some of us have reported that the inclusion of a pyrene chromophore at the N-aryl moiety of the tetrazole substantially red-shifted the wavelength at which the formation of the nitrile imine was triggered.^[10] Block copolymers *via* polymer NITEC coupling were achieved through irradiation with an LED at 410 - 420 nm, constituting a shift of over 70 nm compared with the diaryl tetrazole system. To date this is the longest

wavelength single-photon triggering of a NITEC reaction. Two photon excitation has also been successfully applied in the literature with naphthalene-based tetrazoles efficiently activated by a 700 nm femtosecond pulsed laser.^[11] However, two-photon absorption requires high-intensity pulsed lasers (typical pulse intensity: $>10^6 \text{ W} \cdot \text{cm}^{-2}$)^[12] and is of low efficiency even when femtosecond lasers are employed. Two-photon absorption only occurs at the laser focus. As the femtosecond laser will defocus while passing through the tissue, the two-photon absorption strategy is impractical for deep tissue trials.

Recently, upconversion nanoparticles (UCNPs) were used as upconverters to efficiently assist various NIR-induced photoreactions, including photolysis, photoisomerization and photopolymerization.^[6b, 13] UCNPs consist of a crystalline host matrix (e.g., NaYF_4 , LaF_3 , Y_2O_3) doped with lanthanide sensitizer ions (e.g., Yb^{3+}) and activators (e.g., Er^{3+} , Tm^{3+}). Upon NIR irradiation, the sensitizer ion absorbs and transfers NIR energy to the activator ion, resulting in multiple luminescence emissions at various wavelengths, including UV, blue, green, red, and NIR. The required light intensity to induce photoreactions using upconversion (hundred $\text{mW} \cdot \text{cm}^{-2}$ to some hundred $\text{W} \cdot \text{cm}^{-2}$) is several orders of magnitude lower than those using two-photon absorption.^[6b] In the current study, we introduce a new type of reaction, i.e. UCNP-assisted photoinduced coupling chemistry, triggered with 974 nm light by combining upconversion and NITEC reactions. To the best of our knowledge, the technique described herein is the only example of a photoinduced coupling reaction using a near-infrared source at such a long wavelength, providing an efficient and rapid linkage method. Especially in the field of biology, the method has significant potential due to the deep tissue penetration ability of the employed light source. Furthermore, the formed pyrazoline cycloadduct exhibits near-infrared fluorescence, allowing for potential theranostic applications by *in vivo* imaging/tracking of the ligated species. In the current study, the concept of upconversion photoinduced coupling chemistry is applied for small molecule ligation, polymer end group modification and block copolymer formation *via* functional polymer block linkage (refer to Scheme 1). Further to demonstrate *in vivo* penetration upconversion photoinduced coupling reactions induced by NIR light were carried out with a tissue spacer placed between the reaction vessel and irradiation source. In addition to demonstrate the bioorthogonality of the upconversion photoinduced coupling chemistry, photoinduced coupling experiments in the presence of a biotin derivative were performed and the retained bio-activity confirmed.

6.4 Results and discussion

The synthesis and applications of the UCNP and the pyrene aryl tetrazole (PAT) have both been previously described.^[10, 14] For efficient NITEC reaction to occur, sufficient overlap between the emission of UCNP and the absorbance of the PAT must be ensured, leading to nitrile imine formation. As shown in Scheme 1, when NaYF₄:TmYb@NaYF₄ upconversion nanoparticles (UCNPs) are employed, there is significant overlap in the region of 330 - 370 nm. Although the PAT species has been reported to undergo 410-420 nm light triggered cycloadditions, it can also be activated in UV wavelength regime. Thus, the observed joint activation region has the potential for near-infrared light triggering of NITEC systems.



Scheme 1 a) Schematic illustration of near infrared photoinduced coupling reactions assisted by upconversion nanoparticles. Tissue was optionally placed between the beam and reaction vessel to demonstrate the penetration capability of the near-infrared light. b) Magnification of the 300 - 420 nm region of the emission spectra of UCNP (black line), absorption spectra of PAT (red line) and transmission electron microscopy image of UCNP. c) Synthetic path for near infrared photoinduced coupling reactions to form small molecule cycloadduct **3**, endgroup modified PCL **B₁** (no tissue used) / **B₂** (tissue used), block copolymers **C₁** (no tissue used) / **C₂** (tissue used) and biotin functional block copolymer PCL-*b*-PEG **F**. Refer to SI Section 2,5 for the reaction details.

Initially, model experiments were undertaken involving small molecules **1** (1.0 eq.) and **2** (1.1 eq.) in order to validate the concept of upconversion photoinduced coupling chemistry, as well as to quantify the efficiency of the reaction compared to established photoligations *via*

NITEC.^[10, 15] Therefore, photo-active PAT **1** and hydroxyl-functional maleimide **2** were dissolved in acetonitrile (MeCN) in the presence of UCNPs and irradiated at 974 nm (refer to Scheme 1). The kinetics of the NITEC reaction were monitored using fluorescence spectroscopy *via* the emission of the generated pyrazole at 570 nm (refer to the SI, Section 3). The resulting product stream was investigated *via* HPLC without any further purification (refer to Figure 1). Full conversion of PAT **1** and exclusive formation of the desired pyrazoline cycloadduct under NIR irradiation was observed. Only very minimal side reactions were detected in the crude NIR-irradiated reaction mixture. Trace (1) shows the tetrazole signal before irradiation eluting at 9.2 min. A shift of the signal to 8.2 min was observed in trace (2), indicating full conversion of the tetrazole species and exclusive formation of the desired cycloadduct. Trace (3) shows the purified cycloadduct **3**, synthesized according to the literature,^[10] and employed as a reference. The structure of the formed pyrazoline **3** was confirmed by ESI-MS (refer to the SI, Section 2). The corresponding control experiment in the absence of UCNPs did not yield any of the desired cycloadduct (refer to the SI, Figure S2). After the successful upconversion photoinduced coupling chemistry for small molecules, the concept was extended as a tool for macromolecular end group modification and block copolymer formation. The NITEC reaction was carried out in the presence of poly(ϵ -caprolactone) (PCL) and polyethylene glycol (PEG) polymers since both species are relevant in the field of biology due to their non-toxicity and biocompatibility.^[16]

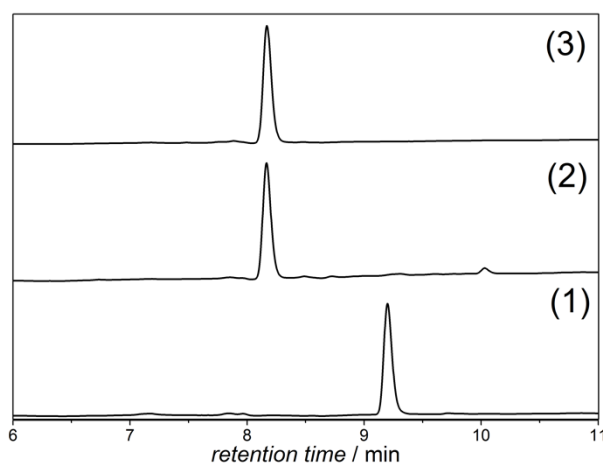


Figure 1. Normalized HPLC traces of PAT **1** (1), crude reaction mixture of PAT **1**, hydroxyl functionalized maleimide **2** and UCNPs, irradiated at 974 nm in MeCN for 30 min (2) and reference sample of cycloadduct **3** synthesized according to the literature in the absence of UCNPs (3) (refer to Scheme 1 for the reaction details); THF/MeCN/H₂O + 0.1 % trifluoroacetic acid was used as eluent and a 220 nm UV detector was employed.

In the first approach, a PAT from which a PCL chain had been polymerized, **A**₁, was employed for end group modification. The tetrazole-containing polymer (1.0 eq.) was irradiated in the presence of maleimide **2** (1.5 eq.) in MeCN at 974 nm for 40 min (refer to Scheme 1). Experiments both with direct irradiation, **B**₁, and in the presence of a tissue-shielded light source, **B**₂, were carried out. The resulting reaction mixtures were investigated *via* ESI-MS (refer to Figure 2). Full conversion of the PAT end capped polymer and exclusive formation of the cycloadducts **B**_{1,2} under the employed conditions was observed. For the tissue shielded **B**₂ experiment, a prolonged reaction time (60 min) was necessary due to the strength of the irradiation stimulus being reduced by tissue absorbance. However, the presence of the tissue had no significant influence on the final level of conversion or the products formed by the coupling. The structures of the modified polymers, **B**_{1,2}, were confirmed by ¹H NMR (refer to the SI, Figures S4 and S7). Interestingly, the fluorescence excitation of the pyrazoline containing PCL formed *via* NITEC can potentially be excited by infrared light, as long as the UCNP are in close proximity. Combination of the fluorescence properties of the cycloadduct revealing a strong tail into the near-infrared region and UCNP provides the opportunity of fluorophore excitation and fluorescence detection involving near-infrared light only.

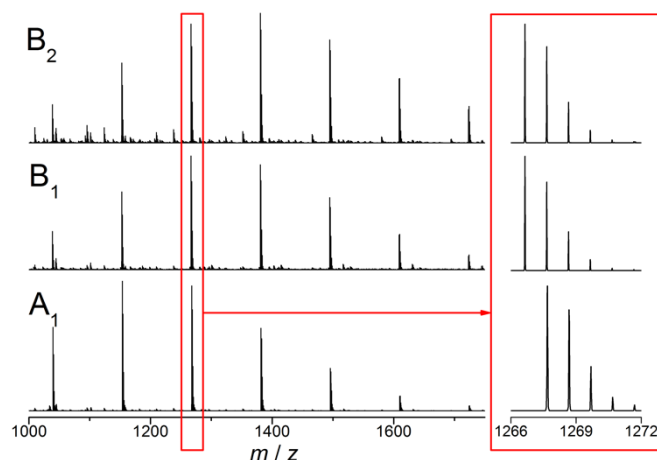


Figure 2. Magnified view in the region of 1000 - 1750 m/z of the high resolution ESI-MS spectrum of PAT end-capped poly(ϵ -caprolactone) (PCL) **A**₁ and the cycloadducts **B**₁ (no tissue used) and **B**₂ (tissue used). Inset: magnified view of the isotopic patterns for **A**₁ and **B**_{1,2}. Refer to Scheme 1 for the structures of formed cycloadducts **B**_{1,2} and the reaction conditions; refer to the SI, Table 2 for the exact theoretical and experimental masses of the depicted polymer species **A**₁ and **B**_{1,2}. Note that only a shift of approx. 1 Da results.

Subsequently, upconversion assisted polymer-polymer coupling was attempted. PAT functional PCL **A**₂ (1.0 eq.) was irradiated in the presence of a maleimide functional PEG (1.5 eq.) and UCNPs at 974 nm for 60 min to form PCL-*b*-PEG block copolymer **C**₁ (refer to Scheme 1). Again, both standard NIR irradiation (cycloadduct **C**₁) and a tissue-shielded irradiation (cycloadduct **C**₂) were attempted, to mimic differences between an *in vitro* and *in vivo* experiment. The corresponding reaction mixtures were analyzed by size exclusion chromatography (SEC) (refer to Figure 3). Inspection of Figure 3 indicates that full conversion of the tetrazole-terminated PCL and exclusive formation of the block copolymer is observed. For both experiments (**C**₁ and **C**₂) a significant shift to lower retention times combined with a decrease of *D* were observed. The structures of the formed cycloadducts were confirmed by ¹H NMR (refer to the SI, Figures S10 to S12). Similar to the end group modification experiments, prolonged irradiation times were necessary for the coupling reaction in the presence of the tissue shield to proceed to full conversion. However, the extended reaction times did not result in the formation of additional side products, *e.g.* due to the decomposition of the cycloadduct formed. To demonstrate the feasibility of upconversion photo-induced coupling chemistry for the preparation of block copolymers carrying a photosensitive, bioactive species, a polymer functionalized with a biotin terminus was used. PCL **A**₂ was irradiated at 974 nm in the presence of UCNPs and a bifunctional biotin/maleimide PEG for 60 min under ambient conditions (refer to Scheme 1). Again, tissue was placed between the irradiation source and the reaction vessel to demonstrate the penetration ability of the NIR light. The conversion of the PAT moiety ($\lambda_{em} = 431$ nm) and formation of the pyrazoline containing block copolymer **F** ($\lambda_{em} = 571$ nm) was detected by fluorescence spectroscopy from the crude reaction mixture after removing the UCNPs (refer to Figure 4). Full conversion of the PAT moiety and formation of the desired cycloadduct was observed. The fluorescence band of the tetrazole species (black line) vanishes, while a new band associated with the cycloadduct appears (blue line). Importantly, the biotin retains its bioactivity after the upconversion photoinduced coupling reaction with 88% of the block copolymer **F** found to undergo non-covalent bonding with avidin protein (refer to the SI, Section 5).

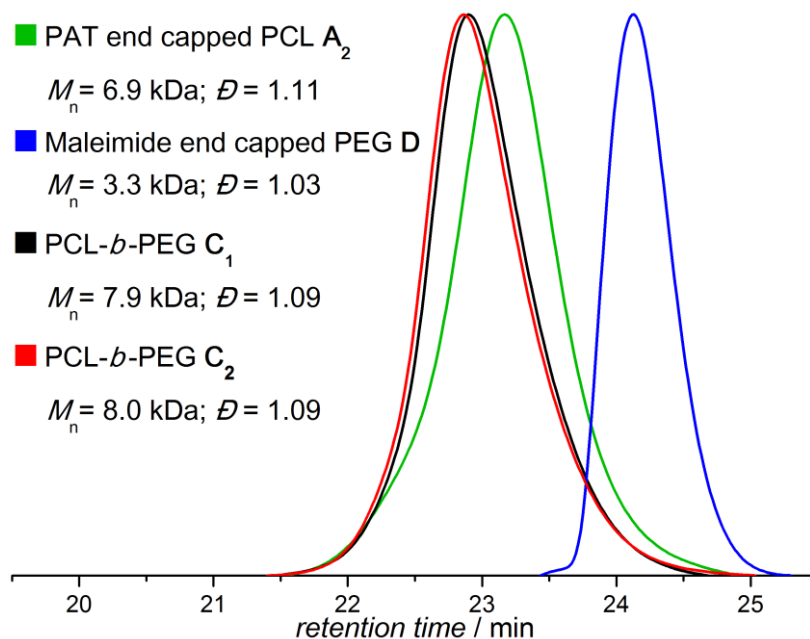


Figure 3. Normalized SEC traces of PAT functional PCL A_2 (green line), maleimide functional PEG (blue line) and block copolymers C_1 (no tissue used, black line) and C_2 (tissue used, red line) formed by upconversion photoinduced coupling reactions, respectively. M_n and D were determined by SEC in THF using poly(styrene) calibration standards.

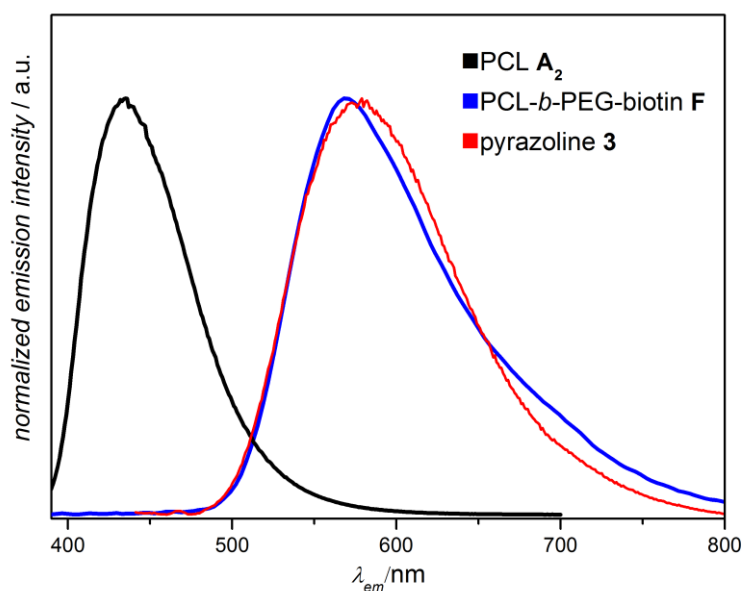


Figure 4. Normalized fluorescence spectra of PCL A_1 , PCL-*b*-PEG-biotin F and pyrazoline 3 .

6.5 Conclusion

In summary, we introduce a mild, efficient, rapid, photoinduced coupling strategy at 974 nm. The methodology was shown to be suitable for small molecule ligation, polymer end group modification, as well as polymer-polymer linkage. For all performed reactions, full conversion of the photo-active tetrazole species was observed, leading to the exclusive formation of the desired cycloadduct and no visible side-reactions. In addition, the formed cycloadducts display strong fluorescence reaching into the near-infrared region. Our current report constitutes the first example of a NITEC reaction and, more broadly, a photoinduced coupling reaction that can be triggered by NIR light, offering a new tool for bio-orthogonal labelling.

6.6 Acknowledgements

J.B. and C.B.-K. acknowledge the DAAD/ATN for funding, facilitating a research stay of P. L. at the Karlsruhe Institute of Technology (KIT). C.B.-K. acknowledges the Sonderforschungsbereich 1176 (project B4) funded by the German Research Council (DFG) for support. P. L. acknowledges the Queensland University of Technology (QUT) and the KIT for funding his PhD studies. C.B.-K. acknowledges continued support from the KIT in the context of the Helmholtz STN and BIFTM programs. Z.C.'s PhD studies were supported by a CSC scholarship. S. W. acknowledges the DFG (WU 787/2-1) and the Fonds der Chemischen Industrie (FCI, No. 661548) for financial support.

6.6 References

- [1] R. G. Wylie, S. Ahsan, Y. Aizawa, K. L. Maxwell, C. M. Morshead, M. S. Shoichet, *Nat. Mater.* **2011**, *10*, 799-806.
- [2] B. J. Adzima, Y. Tao, C. J. Kloxin, C. A. DeForest, K. S. Anseth, C. N. Bowman, *Nat. Chem.* **2011**, *3*, 256-259.
- [3] M. A. Tasdelen, Y. Yagci, *Angew. Chem. Int. Ed.* **2013**, *52*, 5930-5938.
- [4] C. Barner-Kowollik, F. E. Du Prez, P. Espeel, C. J. Hawker, T. Junkers, H. Schlaad, W. Van Camp, *Angew. Chem. Int. Ed.* **2011**, *50*, 60-62.
- [5] a) W. Xi, M. Krieger, C. J. Kloxin, C. N. Bowman, *Chem. Commun.* **2013**, *49*, 4504-4506; b) T. Gruending, K. K. Oehlenschlaeger, E. Frick, M. Glassner, C. Schmid, C. Barner-Kowollik, *Macromol. Rapid Commun.* **2011**, *32*, 807-812.
- [6] a) T. P. Yoon, M. A. Ischay, J. Du, *Nat. Chem.* **2010**, *2*, 527-532; b) S. Wu, H.-J. Butt, *Adv. Mater.* **2016**, *28*, 1208-1226.
- [7] a) C. J. Dürr, P. Lederhose, L. Hlalele, D. Abt, A. Kaiser, S. Brandau, C. Barner-Kowollik, *Macromolecules* **2013**, *46*, 5915-5923; b) J. O. Mueller, D. Voll, F. G. Schmidt, G. Delaittre, C. Barner-Kowollik, *Chem. Commun.* **2014**, *50*, 15681-15684.
- [8] a) M. Dietrich, G. Delaittre, J. P. Blinco, A. J. Inglis, M. Bruns, C. Barner-Kowollik, *Adv. Funct. Mater.* **2012**, *22*, 304-312; b) E. Blasco, M. Piñol, L. Oriol, B. V. K. J. Schmidt, A. Welle, V. Trouillet, M. Bruns, C. Barner-Kowollik, *Adv. Funct. Mater.* **2013**, *23*, 4011-4019.
- [9] W. Song, Y. Wang, J. Qu, M. M. Madden, Q. Lin, *Angew. Chem. Int. Ed.* **2008**, *47*, 2832-2835.
- [10] P. Lederhose, K. N. R. Wuest, C. Barner-Kowollik, J. P. Blinco, *Chem. Commun.* **2016**, *52*, 5928-5931.
- [11] Z. Yu, T. Y. Ohulchanskyy, P. An, P. N. Prasad, Q. Lin, *J. Am. Chem. Soc.* **2013**, *135*, 16766-16769.
- [12] a) M. Álvarez, A. Best, S. Pradhan-Kadam, K. Koynov, U. Jonas, M. Kreiter, *Adv. Mater.* **2008**, *20*, 4563-4567; b) M. Álvarez, A. Best, A. Unger, J. M. Alonso, A. del Campo, M. Schmelzeisen, K. Koynov, M. Kreiter, *Adv. Funct. Mater.* **2010**, *20*, 4265-4272.
- [13] Z. Cheng, J. Lin, *Macromol. Rapid Commun.* **2015**, *36*, 790-827.
- [14] a) Z. J. Chen, S. Q. He, H. J. Butt, S. Wu, *Adv. Mater.* **2015**, *27*, 2203-2207; b) S. Wu, H. J. Butt, *Adv. Mater.* **2016**, *28*, 1208-1226; c) S. Beyazit, S. Ambrosini, N. Marchyk, E. Palo, V. Kale, T. Soukka, B. T. S. Bui, K. Haupt, *Angew. Chem. Int. Edit.* **2014**, *53*,

- 8919-8923; d) Y. M. Yang, Q. Shao, R. R. Deng, C. Wang, X. Teng, K. Cheng, Z. Cheng, L. Huang, Z. Liu, X. G. Liu, B. G. Xing, *Angew. Chem. Int. Edit.* **2012**, *51*, 3125-3129; e) D. Yang, P. Ma, Z. Hou, Z. Cheng, C. Li, J. Lin, *Chem. Soc. Rev.* **2015**, *44*, 1416-1448; f) S. Q. He, K. Krippes, S. Ritz, Z. J. Chen, A. Best, H. J. Butt, V. Mailander, S. Wu, *Chem. Commun.* **2015**, *51*, 431-434; g) X. G. Liu, C. H. Yan, J. A. Capobianco, *Chem. Soc. Rev.* **2015**, *44*, 1299-1301; h) Z. Chen, W. Sun, H. J. Butt, S. Wu, *Chem-Eur J.* **2015**, *21*, 9165-9170; i) J. C. Boyer, C. J. Carling, B. D. Gates, N. R. Branda, *J. Am. Chem. Soc.* **2010**, *132*, 15766-15772; j) B. Yan, J. C. Boyer, D. Habault, N. R. Branda, Y. Zhao, *J. Am. Chem. Soc.* **2012**, *134*, 16558-16561; k) Z. Y. Cheng, J. Lin, *Macromol. Rapid. Comm.* **2015**, *36*, 790-827.
- [15] Y. Wang, C. I. Rivera Vera, Q. Lin, *Org. Lett.* **2007**, *9*, 4155-4158.
- [16] J. Ulbricht, R. Jordan, R. Luxenhofer, *Biomaterials* **2014**, *35*, 4848-4861.

6.7 Supporting information

Materials

1-(2-Hydroxyethyl)-1H-pyrrole-2,5-dione **2** was synthesized according to the literature.^[1] 11-Hydroxyundecyl 4-(2-(pyren-1-yl)-2H-tetrazol-5-yl)benzoate (PAT) **1** and PAT end capped PCL **A**_{1,2} were synthesized according to the literature.^[2] Maleimide end capped PEG was purchased from Creative PEGWorks. The maleimide-PEG-biotin HABA avidin kit was purchased from Thermo Fisher Scientific. All other reagents including the 1 mm thick pork tissue were purchased from commercial suppliers and used without further purification.

Characterization

¹H and ¹³C NMR spectra were recorded on a 400 MHz spectrometer and referenced to the relevant solvent peak. The employed solvent is listed in the spectra descriptions. High-resolution mass spectra (HRMS) were obtained using a Q Exactive (Orbitrap) mass spectrometer (Thermo Fisher Scientific, San Jose, CA, USA) equipped with a HESI II probe. The instrument calibration was carried out in the *m/z* range 74 - 1822 using calibration solutions from Thermo Scientific. A constant spray voltage of 4.7 kV and a dimensionless sheath gas of 5 were applied. The capillary temperature and the S-lens RF level were set to 320 °C and 62.0, respectively. The samples were dissolved in a THF:MeOH mixture (volume ratio 3:2) containing 100 μmol of sodium triflate and injected with a flow of 5 μL·min⁻¹. Molecular weight determination was performed on a GPC system (PL-GPC 50 Plus, Polymer Laboratories) consisting of an auto injector, a guard column (PLgel Mixed C, 50 × 7.5 mm), three linear columns (PLgel Mixed C, 300 × 7.5 mm, 5 μm bead-size) and a differential refractive index detector using THF as the eluent at 35 °C and a flow rate of 1 mL·min⁻¹. The system was calibrated using narrow PS standards (Polymer Standard Service) ranging from 160 to 6 × 10⁶ g·mol⁻¹. Samples were injected from solutions in THF (2 mg·mL⁻¹). Absorption spectra were recorded using a 300 UV/Vis Spectrometer (Varian Cary) in MeCN (*C*_{target compound} = 20 μmol·L⁻¹). Fluorescence spectra were recorded using a Carry Eclipse fluorescence spectrometer in MeCN (*C*_{target compound} = 20 μmol·L⁻¹). HPLCs were recorded using set-up consisting of a Rheodyne injection valve 7725i with 20 μL loop, an Agilent Technologies Series 1200 degasser, a quaternary gradient pump, a column oven, a photodiode array-detector (Varian ELSD-Detector 385-LC), a Macherey-Nagel Polactec column (length: 125 mm, diameter: 4 mm, particle size: 5 μm, flow rate: 1 mL min⁻¹,

temperature: 20 °C). Gradient: starting with THF/acetonitrile/H₂O + 0.1 % trifluoroacetic acid 10/10/95 vol.% ramping within 10 min up to 80/20/20 vol.%.

Irradiation

The irradiation source was a diode laser with 974 nm emission. For all irradiation experiments, the employed setup is illustrated in Figure 1. For the tissue shielded irradiation, a piece of tissue was placed between the laser and sample solution. Details of the laser source: The diode laser was equipped with an adjustable fiber collimator (Changchun New Industries Optoelectronics Technology). The output power of the diode laser for inducing the photoreactions was fixed at 14 W, which was controlled by a tabletop laser driver (device type ds11-la12v08-pa08v16-t9519-254-282, OsTech GmbH i.G.). The output power of the diode laser was measured using an optical power meter (model 407A, Spectra-Physics Corp.).

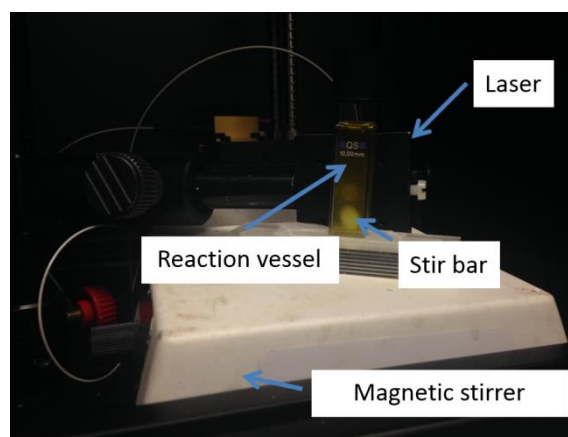
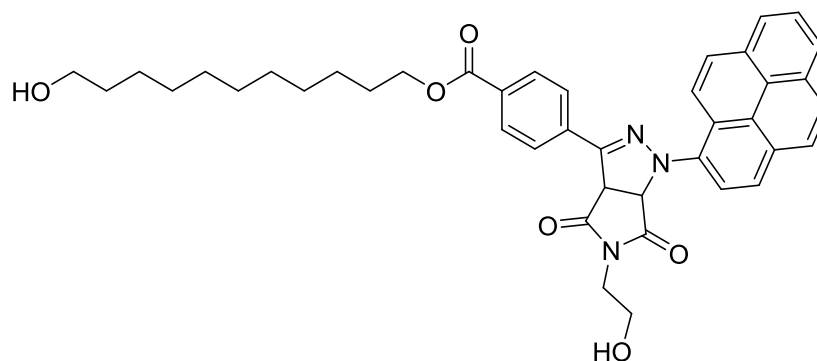


Figure S1 Experimental set up for the upconversion photoinduced coupling chemistry.

Synthesis of Cycloadducts *via* Near Infrared Upconversion Assisted NITEC

11-Hydroxyundecyl 4-(5-(2-hydroxyethyl)-4,6-dioxo-1-(pyren-1-yl)-1,3a,4,5,6,6a-hexahydropyrrolo [3,4-c]pyrazol-3-yl)benzoate (3)



The PAT molecule (0.35 mM, 1 eq.) and hydroxy functionalized maleimide (0.38 mM, 1.1 eq.) were mixed in MeCN (3 mL) containing 3.3 mg mL⁻¹ UCNPs. The mixture was magnetically stirred during irradiation by the NIR laser. HRMS [M+Na]⁺ *m/z*: calcd for C₄₁H₄₃N₃NaO₆ 696.3050, found 696.3058.

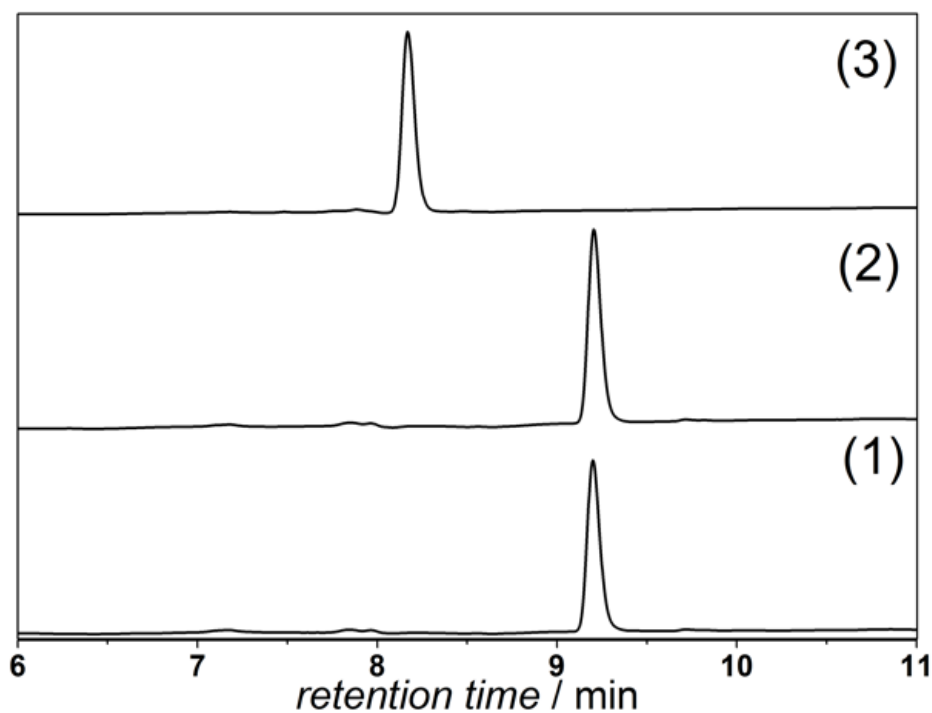
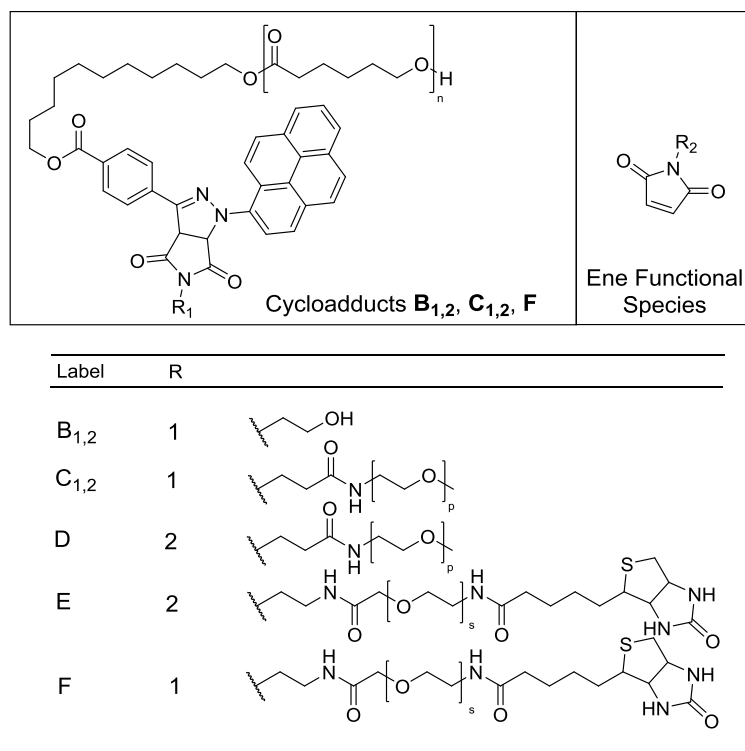


Figure S2. HPLC traces of PAT 1 (1), control experiment carried out in the absence of UCNPs under identical conditions as the small molecule ligation of PAT 1 and hydroxy functionalized maleimide 2 (2), reference pyrazole 3 synthesized according to the literature (refer to the SI, Materials) (3).

Polymer End Group Modification and Formation of Block Copolymers.

Figure S3. Overview over the structures of cycloadducts B_{1,2} and C_{1,2}. Refer to Section 5 for synthesis of F.

The PAT functional PCL was mixed with hydroxyl functionalized maleimide in MeCN (3 mL) containing UCNPs (without tissue, 33 mg mL⁻¹; with tissue, 50 mg mL⁻¹). Subsequently, the mixture was magnetically stirred during NIR irradiation. For the irradiation experiment with tissue, a pork tissue (1 mm thickness) was placed between the NIR laser and the sample. To avoid overheating, pulsed irradiation was used (5 seconds irradiation time and 3 seconds dark time). For the polymer-polymer coupling experiment, the same procedure was used. ¹H NMR (CDCl₃) **B**₁ = 8.54 - 7.96 (m, 13 H), 5.68 - 5.61 (m, 1 H), 5.12 - 5.05 (m, 1 H), 4.40 - 4.30 (m, 2 H), 4.12 - 4.04 (m, polymer backbone), 3.85 - 3.60 (m, 6 H), 2.37 - 2.25 (m, polymer backbone), 1.86 - 1.21 (m, 18 H + polymer backbone); **B**₂ = 8.53 - 7.94 (m, 13 H), 5.70 - 5.60 (m, 1 H), 5.14 - 5.05 (m, 1 H), 4.40 - 4.30 (m, 2 H), 4.12 - 4.04 (m, polymer backbone), 3.84 - 3.62 (m, 6 H), 2.39 - 2.25 (m, polymer backbone), 1.86 - 1.19 (m, 18 H + polymer backbone); **C**₁ = 8.59 - 7.97 (m, 13 H), 5.74 - 5.67 (m, 1 H), 5.15 - 5.09 (m, 1 H), 4.41 - 4.22 (m, 2 H), 4.05 - 3.85 (m, polymer back bone (PCL)), 3.72 - 3.50 (m, 6 H + polymer back bone (PEG)), 3.47 - 3.43 (m, 2 H), 3.39 - 3.31 (m, 5 H), 2.38 - 2.24 (m, polymer backbone (PCL)), 1.92 - 1.20 (m, 18 H + polymer back bone (PCL)); **C**₂ = 8.60 - 7.95 (m, 13 H), 5.74 - 5.65 (m, 1 H), 5.14 - 5.09 (m, 1 H), 4.41 - 4.21 (m, 2 H), 4.04 - 3.85 (m, polymer backbone (PCL)),

3.74 - 3.50 (m, 6 H + polymer backbone (PEG)), 3.45 - 3.43 (m, 2 H), 3.39 - 3.30 (m, 5 H), 2.38 - 2.21 (m, polymer backbone (PCL)), 1.92 - 1.21 (m, 18 H + polymer backbone (PCL)).

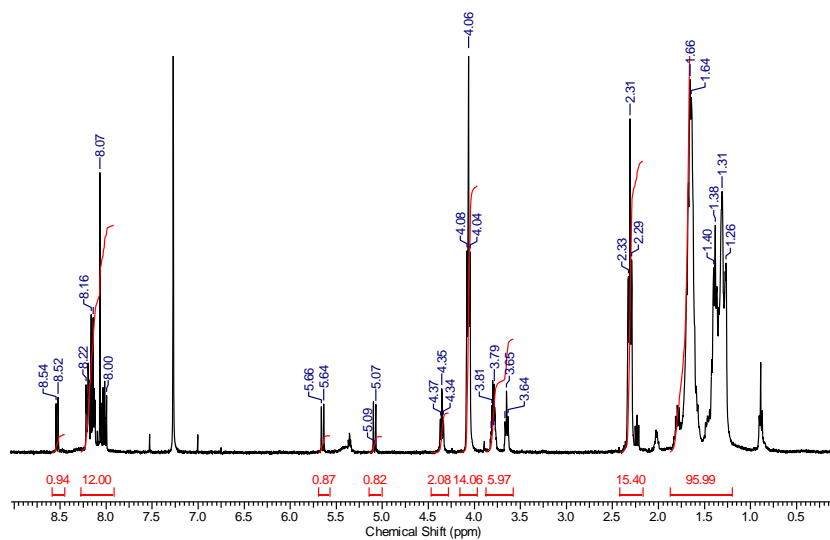
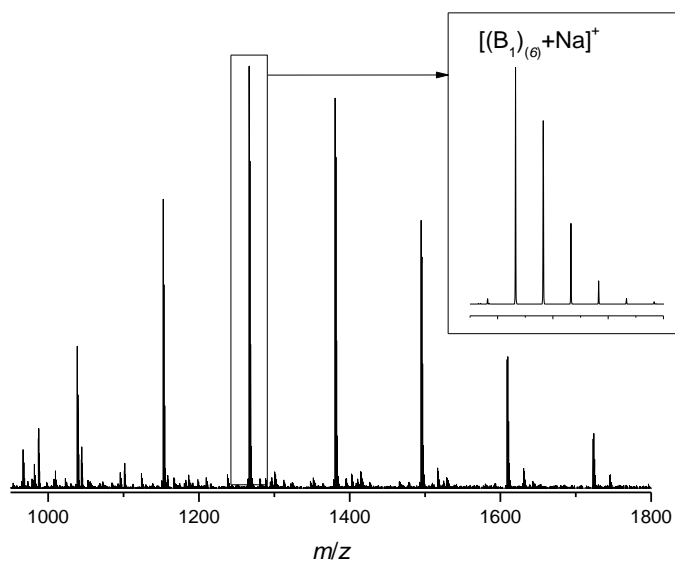
Table 1 M_n and D of PAT capped PCL $A_{1,2}$ before and after coupling with maleimide 2 or maleimide end capped PEG to form $B_{1,2}$ or $C_{1,2}$. All reactions were carried out in MeCN.

Adduct	PAT end capped PCL	c_{PCL} /mmol·L ⁻¹	c_{ene} /mmol·L ⁻¹	Ene capped polymer	D_{ene}	$M_n^{[c]}_{ene}$ /kDa	$D_{cycloadduct}$	$M_n^{[c]}_{cycloadduct}$ /kDa
$B_1^{[a]}$	A ₁	0.5	0.75	-	-	-	1.09	2.2
$B_2^{[a]}$	A ₁	0.5	0.75	-	-	-	1.09	2.2
$C_1^{[b]}$	A ₂	2.4	3.6	PEG D	1.03	3.3	1.09	7.9
$C_2^{[b]}$	A ₂	2.4	3.6	PEG D	1.03	3.3	1.09	8.0

[a] The cycloadduct was analyzed without any further purification. [b] The crude product was dissolved in ethyl acetate (50 mL) extracted with 1 M hydrochloric acid (4×100 mL) and dried over NaSO₄. Ethyl acetate was removed under reduced pressure. The residual solid was dissolved in 50 mL DCM and extracted with 1 M hydrochloric acid (1 × 100 mL). [c] M_n was determined by GPC using PS calibration standards.

Table 2 Sum formula, the exact masses of the experimentally obtained data, theoretical m/z values and the deviation of both for PAT end capped PCL A_1 and cycloadducts $B_{1,2}$.

Label	Sum formula	m/z_{exp}	m/z_{theo}	$\Delta m/z$
A₁	[C ₈₃ H ₁₁₆ N ₄ NaO ₁₉] ⁺	1495.815	1495.813	0.002
B₁	[C ₈₃ H ₁₁₃ N ₃ NaO ₂₀] ⁺	1494.787	1494.789	0.002
B₂	[C ₈₃ H ₁₁₃ N ₃ NaO ₂₀] ⁺	1494.787	1494.781	0.006

Cycloadduct B₁Figure S4. ¹H NMR (400 MHz, CDCl₃) spectrum of cycloadduct B₁.Figure S5. Magnified view into the region of 950 - 1800 *m/z* of the ESI-MS spectrum of cycloadduct B₁. Signals repeat in intervals of 114.14 Dalton. Sodium adduct of PAT end-capped PCL, [(B₁)₆ + Na]⁺.

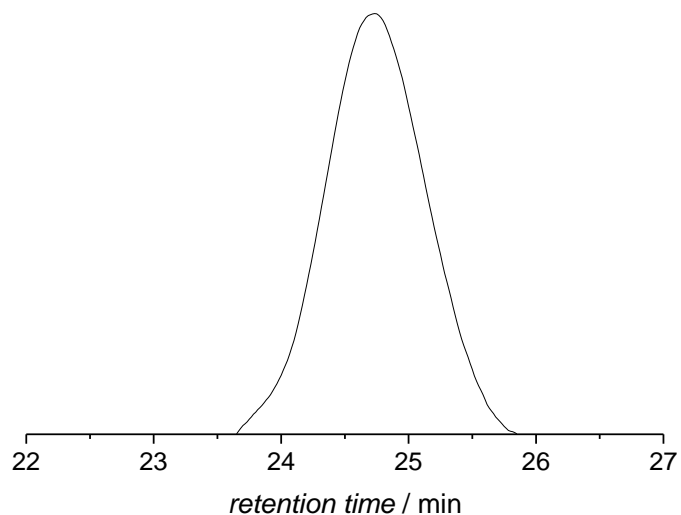


Figure S6. GPC of the cycloadduct B₁ in THF (see Table 1 for corresponding M_n and D).

Cycloadduct B₂

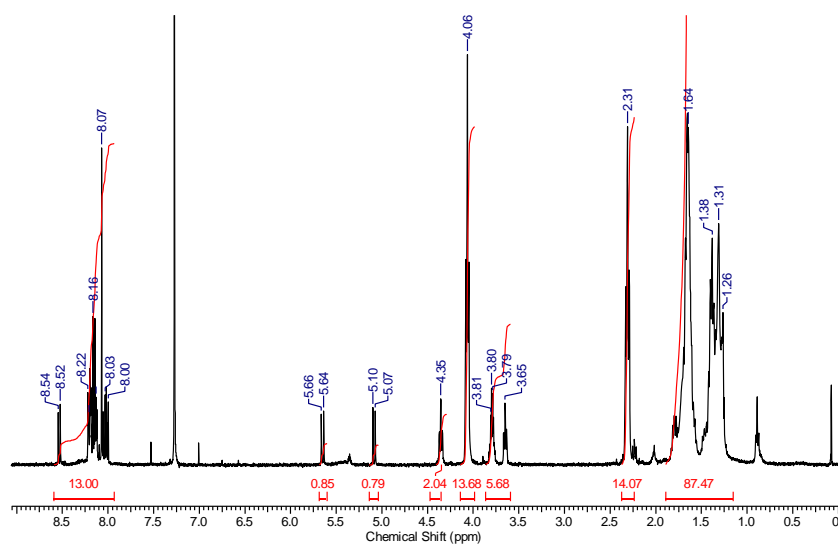


Figure S7. ¹H NMR (400 MHz, CDCl₃) spectrum of the cycloadduct B₂.

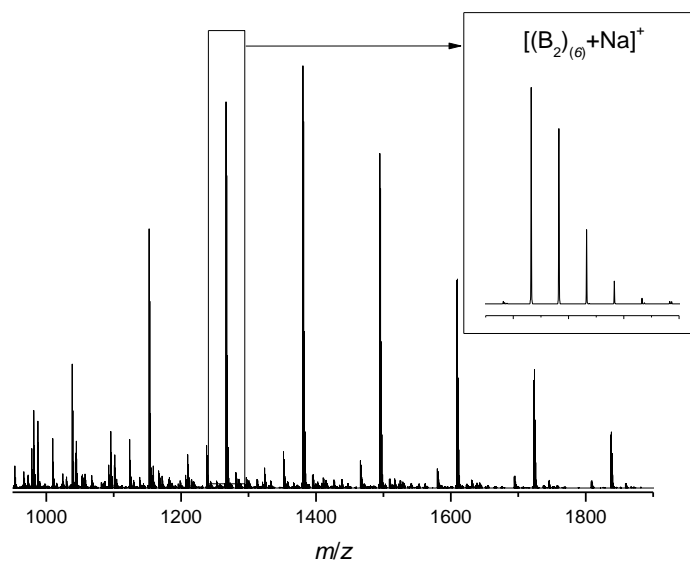


Figure S8. Magnified view into the region of 950 - 1900 *m/z* of the ESI-MS spectrum of cycloadduct B₂. Signals repeat in intervals of 114.14 Dalton. Sodium adduct of PAT end-capped PCL, $[(B_2)_{(6)} + Na]^+$.

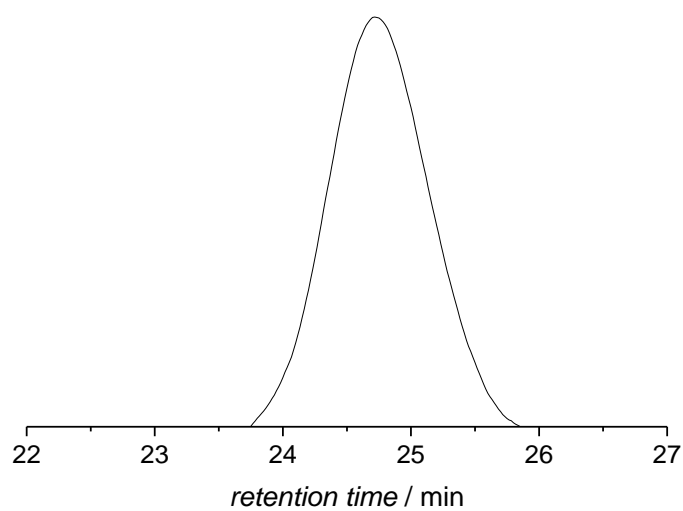


Figure S9. GPC of the cycloadduct B₂ in THF (see Table 1 for corresponding M_n and \mathcal{D}).

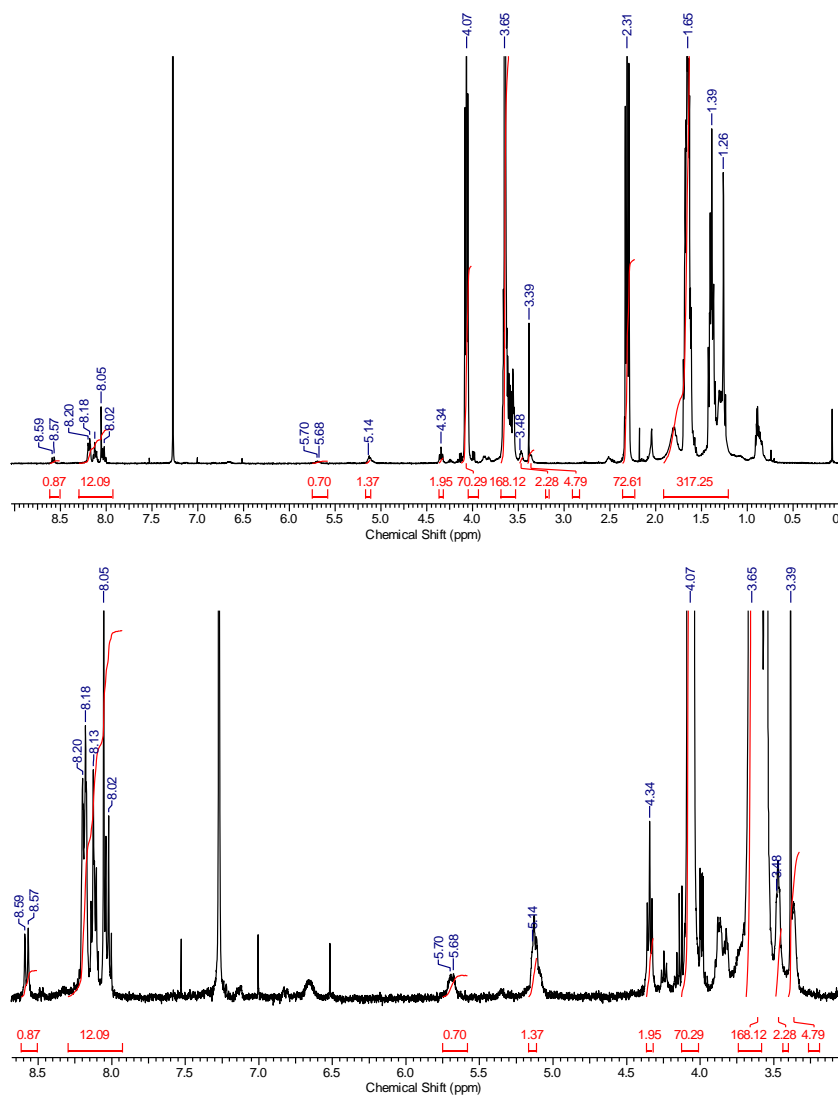
Cycloadduct C₁

Figure S10. ¹H NMR (400 MHz, CDCl₃) spectrum of the cycloadduct C₁. Full spectrum of the PCL-*b*-PEG block copolymer (top) and magnification of the 8.7 - 2.9 ppm region (bottom).

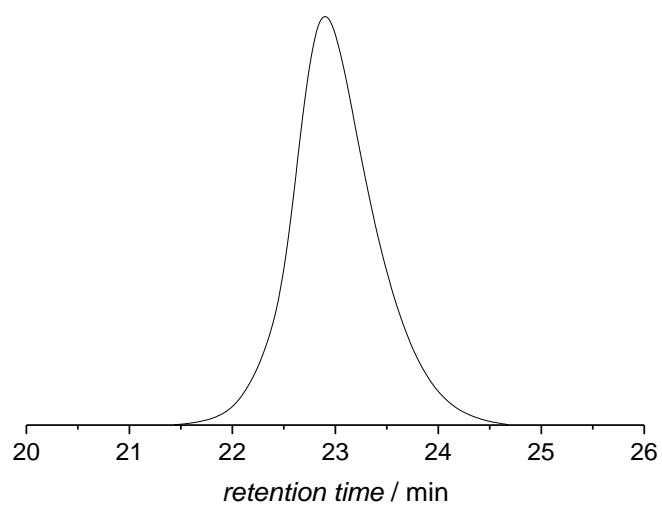


Figure S11. GPC of the cycloadduct C_1 in THF (see Table 1 for corresponding M_n and D).

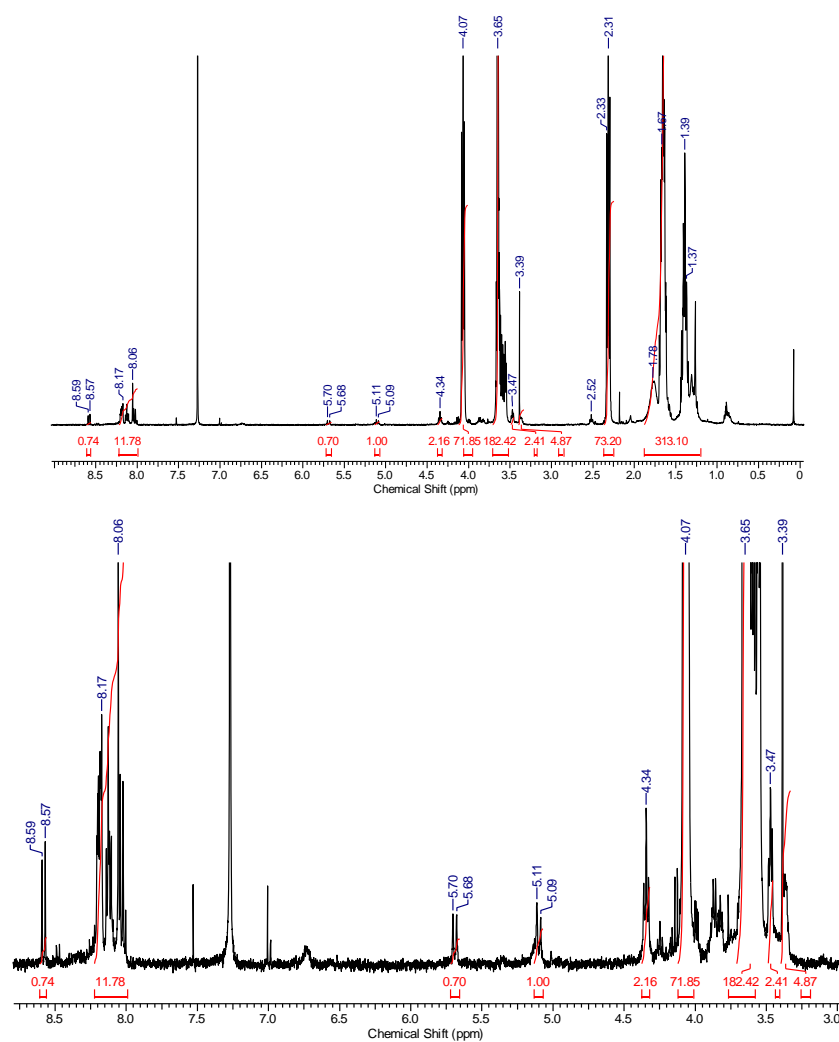
Cycloadduct C₂

Figure S12. ¹H NMR (400 MHz, CDCl₃) spectrum of the cycloadduct C₂. Full spectra of the PCL-*b*-PEG block copolymer (top) and magnification of the 8.7 - 2.9 ppm region (bottom).

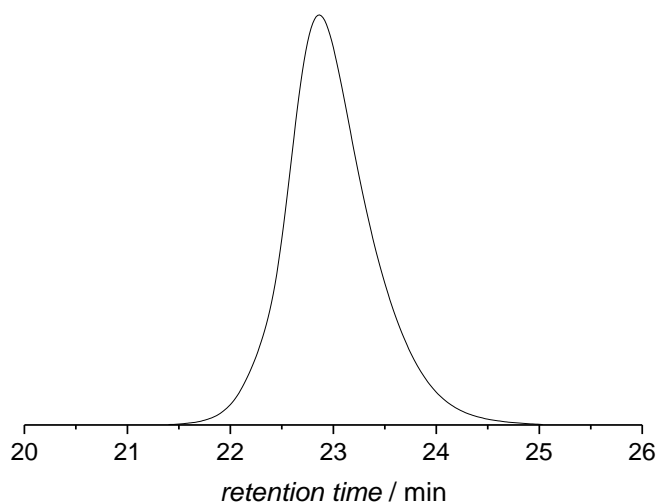


Figure S13. GPC of the cycloadduct C_2 in THF (see Table 1 for the corresponding M_n and D)

Kinetic Studies

The NITEC reaction can be followed by fluorescence spectroscopy. The PAT molecule is fluorescent at 431 nm, while the pyrazoline moiety emits at 571 nm (refer to the SI, Figure S16).

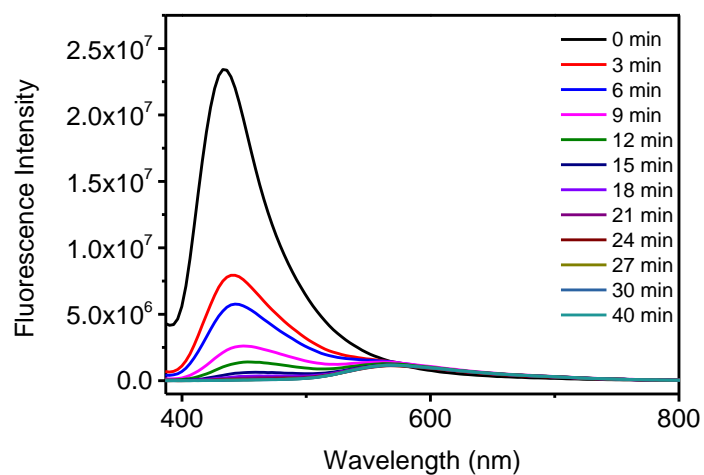


Figure S14. Fluorescence trace of the upconversion photoligation reaction of PAT 1 and hydroxy functionalized maleimide (HFM) 2 (C_{PAT} : 0.35 mM, PAT : HFM = 1:1.1, MeCN, $C_{(UCNPs)} = 3.3 \text{ mg mL}^{-1}$, $\lambda_{ex} = 365 \text{ nm}$).

Spectroscopic Data

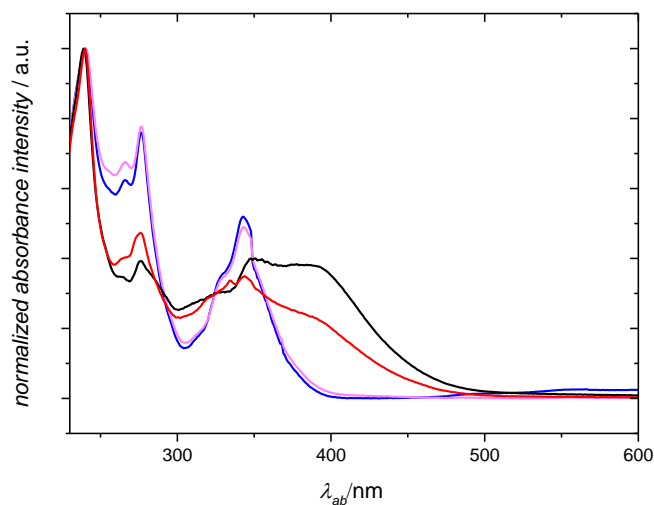


Figure S15. Normalized absorption spectra of PAT 1 (blue), pyrazoline 3 (black), PAT end-capped PCL A₂ (pink) and pyrazoline containing PCL B₁ (red) in MeCN.

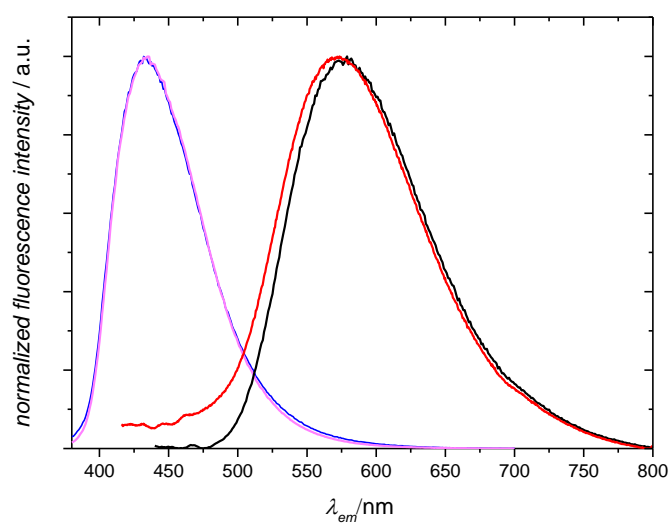


Figure S16. Normalized fluorescence spectra of PAT 1 (blue), pyrazoline 3 (black), PAT end-capped PCL A₂ (pink), pyrazoline containing PCL B₁ (red) in MeCN. $\lambda_{\text{ex}} = 365$ nm for 1 and 3, $\lambda_{\text{ex}} = 400$ nm for A₂ and B₁.



Figure S17. Fluorescence behaviour of PAT 1 (left) and pyrazoline 3 (right) irradiated with a UV hand lamp at 365 nm.

Biotin Related Studies

Preparation of the Biotin End Capped PEG-*b*-PCL Block F

PAT functional PCL **A**₂ (1 mM) was mixed with maleimide end capped, biotin functional PEG (1.5 mM) in MeCN (3 mL) containing UCNPs (50 mg mL⁻¹). The mixture was magnetically stirred during irradiation with NIR light. A 1 mm thick pork tissue was placed between the NIR source and the sample solution. NIR irradiation was pulsed (with 5 seconds on and 3 seconds off).

Measurement of Biotin Activity

The bio-activity of biotin was measured according to the instructions of the producer (Instructions, Pierce Biotin Quantification Kit, Thermo Scientific).^[3] The HABA/Avidin premix was equilibrated at ambient temperature. 100 μ L of ultrapure water was added to one microtube (standard kit from Thermo Fisher, catalogue No. 28005) of the HABA/Avidin Premix. 20 μ L of the HABA/Avidin Premix solution was added to the PBS (pH = 7.2, V = 2 mL) in a well. The well was placed on an orbital shaker. The absorbance of the solution in the well was detected. 30 μ L of biotin end capped PEG **E** or biotin end capped PEG-*b*-PCL block **F** (0.2 mM) were added to the well containing the HABA/avidin reaction mixture. The absorbance of the solution was detected again. The procedure was repeated for 0, 6 and 9 μ M solutions of biotin containing compound.

Biotin and avidin (or streptavidin) bind non-covalently with a higher binding affinity than most antigen-antibody interactions. HABA/avidin (4'-hydroxyazobenzene-2- carboxylic acid) complexes show strong absorption at 500 nm. If biotin containing species are added to the HABA/avidin complex, HABA is replaced by biotin, since biotin features a much higher binding affinity towards avidin. Therefore, the HABA absorption efficiency will decrease due

to its poor solubility in aqueous solution. Quantification of the biotin content can be achieved by recording the absorption spectra change before and after addition of biotin.

Calculation of the number of biotin moiety (activity) after the reaction

$$\text{Biotin activity} = \Delta A_{500} (\mathbf{F}) / \Delta A_{500} (\mathbf{E}) \cdot 100 \% = 0.08/0.09 \cdot 100 \% = 88 \%$$

$\Delta A_{500} (\mathbf{E})$ = Absorption value (500 nm) of HABA/avidin after addition of **E** - Absorption value (500 nm) of HABA/avidin

$\Delta A_{500} (\mathbf{F})$ = Absorption value (500 nm) of HABA/avidin after addition of **F** - Absorption value (500 nm) of HABA/avidin

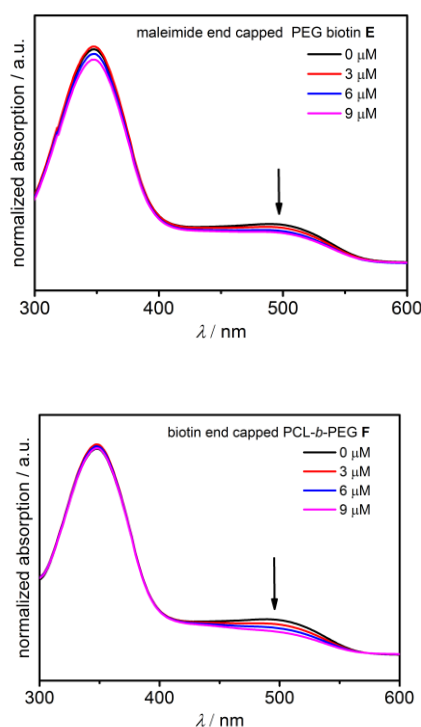


Figure S18. Absorption spectra of HABA/avidin mixtures before and after adding of biotin containing solutions E and F in concentration range 0-9 μM . The arrow illustrates the absorption band used for the biotin activity calculations.

References

- [1] W. H. Heath, F. Palmieri, J. R. Adams, B. K. Long, J. Chute, T. W. Holcombe, S. Zieren, M. J. Truitt, J. L. White, C. G. Willson, *Macromolecules* 2008, 41, 719-726.
- [2] P. Lederhose, K. N. R. Wust, C. Barner-Kowollik, J. P. Blinco, *Chemical Communications* 2016, 52, 5928-5931.
- [3] <https://www.thermofisher.com/order/catalog/product/28005> (accessed on June 30th, 2016).

Curriculum vitae

Personal information:

First name: Zhijun

Last name: Chen

Date of Birth: 12.10.1987

Nationality: China

Sexual: Male

Educational Background:

2013.09-present Max Planck Institute for Polymer research, Germany

Ph.D candidate

2010.9-2013.3 East China University of Science and Technology, China

Master of Engineering in Leather chemistry and engineering

2006.9-2010.7 Northeast Forestry University, China

Bachelor of engineering in Forestry chemistry and engineering, China

Publications:

1. **Zhijun Chen**⁺, Shuqing He⁺, Hans-Jürgen Butt, Si Wu. Photon upconversion lithography: Patterning of biomaterials using near-Infrared light. *Adv. Mater.* 2015, **27**, 2203-2206. (shared first author).
2. Paul Lederhose⁺, **Zhijun Chen**⁺, Rouven Müller, James P Blinco, Si Wu, Christopher Barner-Kowollik. Near-infrared photoinduced coupling reaction assisted by UCNPs. *Angew. Chem. Int. Ed.* 2016, **55**, DOI: 10.1002/anie.201606425. (shared first author).
3. **Zhijun Chen**, Yubing Xiong, Roberto Etchenique, Si Wu. Manipulating pH using near-infrared light assisted by upconverting nanoparticles. *Chem. Commun.* 2016, DOI: 10.1039/C6CC05287H. In press.
4. **Zhijun Chen**, Wen Sun, Hans-Jürgen Butt, Si Wu. Upconverting-nanoparticle-assisted photochemistry induced by low-Intensity near-Infrared light: how low can we go?. *Chem. Eur. J.* 2015, **21**, 9165-9170.
5. Yubing Xiong, **Zhijun Chen**, Hong Wang, Lisa-Maria Ackermann, Markus Klapper, Hans-Jürgen Butt, Si Wu. An autonomic self-healing organogel with a photo-mediated modulus. *Chem. Commun.* 2016. DOI: 10.1039/C6CC08513J, in press.

-
6. Jose Hodak, **Zhijun Chen**, Si Wu, Roberto Etchenique. Multiphoton Excitation of Upconverting Nanoparticles in Pulsed Regime. *Anal. Chem.* 2016, 88, 1468-1475.
 7. Shuqing He, Kristina Krippes, Sandra Ritz, **Zhijun Chen**, Andreas Best, Hans-Jürgen Butt, Volker Mailänder, Si Wu. Ultralow-intensity near-infrared light induces drug delivery by upconverting nanoparticles. *Chem. Commun.* 2015, 51, 431-434.
 8. **Zhijun Chen**, Raweewan Thiramanas, Volker Mailänder, Si Wu. Near-infrared photoinhibition of enzyme activities in living cells enabled by upconverting nanoparticles. *Submitted to Chem. Commun.*